To the Graduate Council:

I am submitting herewith a dissertation written by Timothy Eugene Valentine entitled "MCNP-DSP: A Neutron and Gamma Ray Monte Carlo Calculation of Source-Driven Noise-Measured Parameters". I have examined the final copy of this dissertation for form and content and recommend that it be accepted in partial fulfillment of the requirements for the degree of Doctor of Philosophy, with a major in Nuclear Engineering.

John T. Mihalczo, Major Professor

We have read this dissertation
and recommend its acceptance:

Accepted for the Council:

Associate Vice Chancellor
and Dean of The Graduate School

MCNP-DSP: A NEUTRON AND GAMMA RAY MONTE CARLO CALCULATION OF SOURCE-DRIVEN NOISE-MEASURED PARAMETERS

A Dissertation

Presented for the

Doctor of Philosophy

Degree

The University of Tennessee, Knoxville

Timothy Eugene Valentine

May 1995

DEDICATION

This dissertation is dedicated to my wife,

Jennifer S. Valentine.

ACKNOWLEDGMENTS

I wish to thank my major professor, John T. Mihalczo, for his guidance, advice, and patience. Without his contributions, this research would not have been completed. I am also grateful to V. K. Paré, E. D. Blakeman, D. J. Nypaver, and P. E. Koehler for their advice with various parts of my research. I am also grateful to R. A. Forster, R. Seamon, G. W. McKinney, and J. R. Nix of Los Alamos National Laboratory for their consultation during my research.

I am very grateful to my committee members, P. N. Stevens, W. F. Lawkins, and R. B. Perez, for their assistance and feedback on the written dissertation and oral defense.

I also thank the staff of the Oak Ridge Institute for Science and Education for the fellowship that I received to perform this research. I would also like to thank the U. S. Department of Energy for sponsoring this work and Martin Marietta Energy Systems, Inc. for giving me the opportunity to perform this research.

I appreciate the support that I have received from my family. I also would like to thank my wife's family for their encouragement.

A special "thank you" is reserved for my wife, Jennifer Valentine. Her love, patience, and support gave me the strength to complete this work. She put aside many of her own goals in order for me to complete my research. Words cannot express my gratitude for her unconditional love.

ABSTRACT

The ^{252}Cf-source-driven noise analysis (CSDNA) measurement method was developed by J. T. Mihalczo and V. K. Paré to determine the subcriticality of a fissile assembly. The technique provides measured parameters that can be used for verification of calculation models and cross section data. A certain ratio of spectral densities, $R(\omega)$, obtained from the measured spectra is independent of detection efficiency and in some cases source intensity. MCNP-DSP was developed from the Monte Carlo code MCNP4A (*MCNP is a trademark of the Regents of the University of California, Los Alamos National Laboratory*) in order to calculate the noise measured parameters, time analysis quantities such as autocorrelation and cross-correlation functions, and the time distribution of counts after ^{252}Cf fission for both neutrons and gamma rays.

Several calculations were performed to validate MCNP-DSP. MCNP-DSP successfully calculated the neutron and photon time distributions after ^{252}Cf fission for simple configurations. The data processing algorithms were validated by successfully calculating problems with known analytical solutions. In the calculations, the frequency spectra can be obtained directly by Fourier transforming the detector response or indirectly by taking the Fourier transform of the autocorrelation and cross-correlation functions. The direct and indirect Fourier processing methods were shown to produce the same frequency spectra, and the convergence of the estimates of the frequency spectra are the same. The calculated value of $R(\omega)$ was shown to be independent of detection efficiency and in some cases source intensity.

Several calculations were performed for systems that have been measured using the CSDNA technique. MCNP-DSP was able to adequately calculate the low-frequency value of $R(\omega)$ from the detector responses due to neutrons and gamma rays for the unmoderated, unreflected uranium metal cylinders using the ENDF/B-IV cross sections. These calculations also showed that the frequency dependence of the spectra obtained from the neutron detector and from the gamma ray detector responses, in this case, are the same. The ability to calculate the measured low-frequency value of $R(\omega)$ for a two tightly coupled uranium metal cylinders separated by a borated plaster disk, using detectors sensitive only to gamma rays, further demonstrated that the code could accurately calculate the detector response due to gamma rays. The code was able to adequately calculate the low-frequency value of $R(\omega)$ for a uranyl nitrate solution system at various heights. However, for some solution heights, the results of the calculations differed from the measurements. The results of the calculations were shown to be strongly dependent on the cross section data sets used in the analysis. The calculated noise parameters changed significantly when using different cross section data sets although k_{eff} changed slightly. This demonstrated the increased sensitivity in calculating the noise-measured parameters over calculating k_{eff} when validating computational methods and cross section data. This more general neutron and gamma ray treatment provides the most comprehensive calculation of the measured parameters and is useful for planning experiments and analyzing the results of measurements.

TABLE OF CONTENTS

CHAPTER PAGE

LIST OF TABLES

TABLE **PAGE**

LIST OF FIGURES

CHAPTER 1

INTRODUCTION

1.0 Background

One of the primary concerns of reactor physics is being able to characterize the behavior of neutrons in a fissile assembly. In the fission process, a neutron gets absorbed by a fissile nucleus. This results in an isotope of the nucleus that is in an excited state. The excited nucleus will de-excite by splitting into two (binary fission) or possibly three (ternary fission) fragments, causing the release of energy and the emission of neutrons and gamma rays. The neutrons from fission are capable of inducing future fissions. This process is referred to as a fission chain reaction.

The effective neutron multiplication, k_{eff}, may be defined as the ratio of the number of fissions in one generation to the number of fissions in the immediately preceding generation. If, on average, exactly one neutron from fission leads to one neutron from another fission, the fissile configuration is said to be critical, and k_{eff} is equal to unity. On the other hand, if, on average, each neutron leads to more than one neutron, the system is said to be supercritical, and k_{eff} is greater than unity. Conversely, if, on average, less than one neutron results from a previous neutron, the system is said to be subcritical, and k_{eff} is less than unity. The value of k_{eff} determines the safety margin of a given fissile configuration.

The subcriticality of a configuration of fissile materials is essential for the safe operation of facilities that produce, process, utilize or store fissile material. Several techniques can be employed to measure the subcriticality of a given fissile assembly, for

example, inverse kinetics,[1] modified source neutron multiplication,[2] break frequency noise analysis,[3] source jerk,[4] and pulse neutron methods.[5] However, these methods have difficulties that have precluded their use for practical in-plant applications. Several of these methods depend on detection efficiency, which may be more sensitive to changes in the geometry of the fissile configuration than to changes in k_{eff}. Many of the methods require a calibration near delayed critical in order to obtain a value for k_{eff}; consequently, this is not practical for in-plant situations where criticality cannot be achieved. Some of these methods also depend on the intensity of the source which can further obscure the determination of k_{eff}. To alleviate these difficulties, the ^{252}Cf-source-driven noise analysis (CSDNA) measurement technique was developed by Mihalczo and Paré.[6] This measurement technique has been proven to be very sensitive to small changes in the fissile configuration. This sensitivity (in some cases as much as a factor of 50 more sensitive than k_{eff}) has been demonstrated in various subcritical measurements and in Monte Carlo calculations of the measured data.[7]

1.1 ^{252}Cf-Source-Driven Noise Analysis (CSDNA) Measurement

The CSDNA technique is a measurement method that employs two or more particle detectors along with a ^{252}Cf source to provide measured quantities that can be directly calculated for the verification of calculational methods and cross section data sets and to determine the reactivity of a subcritical assembly. The source, which is contained within an ionization chamber, is placed in or near the subcritical fissile configuration to initiate the fission chain multiplication process. The neutron detectors are placed in or near the fissile assembly to measure particles from the fission chains induced by the spontaneous fission of the ^{252}Cf source.

This method evolved from time domain Rossi-α measurements[8] and pulsed neutron measurements.[9] In the Rossi-α measurement, the time distribution of counts in a detector after the first count in the same or another detector is measured. The pulse neutron method measures the time distribution of counts from a detector in or near the fissile assembly after a pulse of neutrons is injected into the assembly. Simultaneous measurements by both the Rossi-α and the randomly pulsed neutron method allowed elimination of the dependence on detection efficiency. To avoid limitations of source intensity and background that must be subtracted in the time domain measurements, frequency analysis measurements analogous to the time domain methods were performed. By combining these measurement techniques into one measurement, a measurement of a subcritical fissile assembly could be performed without dependence on detection efficiency, without dependence on source intensity as long as there are no intrinsic or other significant sources in the fissile configuration other than the ^{252}Cf source, and without requiring a measurement near delayed critical.

A certain ratio of spectral densities, $R(\omega)$, obtained from the measured data has these properties. The ratio of spectral densities is defined as

$$R(\omega) = \frac{G_{12}^{*}(\omega)\, G_{13}(\omega)}{G_{11}(\omega)\, G_{23}(\omega)}, \qquad (1.1)$$

where ω is the angular frequency; G_{12}^{*} is the complex conjugate of the cross-power spectral density (CPSD) of the source detector #1 and detector #2, which detects particles from fission; G_{13} is the CPSD of the source detector #1 and the particle detector #3; G_{11} is the auto-power spectral density (APSD) of the source detector; and G_{23} is the CPSD between the two particle detectors. If point kinetics is applicable, the ratio of spectral densities can be related to the neutron multiplication factor in the following manner

$$\frac{1-k}{k} = \frac{C_1 R(\omega)}{1-C_2 R(\omega)}, \qquad (1.2)$$

where C_1 and C_2 are constants that depend only on other subcritical parameters of the system and on the effect of the detector on the subsequent detection of the fission chain population. To avoid the limitation of the point kinetics model, a more generalized particle transport model was developed using Monte Carlo to obtain the subcriticality of a fissile assembly by direct calculation of the measured spectral densities. Verification of the Monte Carlo model and the cross sections with noise measured parameters for a particular application allows confidence in the prediction of the neutron multiplication factor for this application by this validated Monte Carlo model and cross sections.

The KENO-NR[10] Monte Carlo code was developed by Ficaro to calculate the spectral densities of the CSDNA measurement. KENO-NR was developed from KENO Va[11] because of the simplicity of KENO Va. However, this code is limited in that it only calculates the detector responses due to neutrons, whereas the most efficient detectors used in the measurements detect both neutrons and gamma rays. Sometimes gamma ray detectors are used exclusively in the measurements. Furthermore, the code uses group cross sections whose angular dependence of the differential scattering cross section is limited to only the first few terms of the Legendre expansion and have all the usual problems associated with group cross sections. Because of these limitations and because the code is not capable of calculating the spectral densities for all the measured subcritical assemblies, a more generalized Monte Carlo model which has continuous energy cross sections and which also includes gamma rays was needed to calculate the spectral densities.

To provide a more detailed model of the CSDNA method, the Monte Carlo code MCNP[12] was modified to calculate both the time domain detector responses and the

spectral densities of the CSDNA measurement. MCNP is a continuous energy Monte Carlo code that is capable of tracking both neutrons and photons. Several modifications were made to the neutron and photon tracking routines of MCNP such that the calculated parameters are obtained in a manner similar to the measured parameters. The structure of the code had to be modified in order to obtain the calculated parameters in the form of data blocks of detector responses, as is done in the measurement. The data blocks are time samples of detector response of typically 512 or 1024 points for a certain time period, which is determined from the sampling rate of the data analyzers. The particle weighting and biasing in MCNP were disabled in order to have a strictly analog Monte Carlo calculation that simulates the actual particle random walks. Analog Monte Carlo refers to the tracking of whole particles as they interact with the materials of the system or detectors. A dual particle source was developed which produces both neutrons and photons from the fission of ^{252}Cf. Additional evaluated measured data were incorporated into the code for certain neutron and photon interactions to treat the particles more correctly. Average quantities like $\overline{\nu}$, the average number of prompt neutrons per fission, were removed from MCNP because average quantities remove some of the statistical fluctuations from the fission chain populations. Experimental data describing the probability distribution of the number of prompt neutrons from fission were incorporated into the code where available; otherwise, the Gaussian theoretical distribution of Terrell is used. A modified Maxwellian energy distribution was included in the code to obtain the energy of prompt neutrons from the spontaneous fission of ^{252}Cf along with angular distribution data for neutrons from fission to describe the neutron direction in the laboratory system. The energy distribution of gamma rays from the spontaneous fission of ^{252}Cf and the multiplicity of these gamma rays has also been included in MCNP-DSP.

Several detector options were added to MCNP-DSP to simulate the various detectors used in the measurements. The detectors used in the calculations are capture detectors, scatter detectors, or fission detectors. A new simplified algorithm for the proper treatment of multiple scattering events in the scatter detectors was included in the code in addition to multiple scattering of particles between detectors. Data processing algorithms were also incorporated into the code to analyze the detector responses for both time and frequency analysis. The frequency spectra can be obtained by directly calculating the Fourier transforms of N point blocks of pulses from the detector and performing a complex multiplication to obtain the APSDs and the CPSDs. The APSDs and CPSDs were also obtained by Fourier transforming the autocorrelation and cross-correlation functions to evaluate a new processing concept that leads to faster processing since the fast Fourier transform is performed only once after the correlation functions are obtained. The time distribution of detector counts after ^{252}Cf fission was also calculated.

This research has produced the most complete calculation of the CSDNA method without the limitations of KENO-NR or the point kinetics model. The modified code, MCNP-DSP, provides a more general continuous energy Monte Carlo calculation of measured parameters, which includes not only prompt neutrons but also prompt gamma rays. This research has demonstrated that the calculated frequency spectra obtained from the gamma ray response agrees well with the frequency spectra obtained from the neutron response for some systems. For some systems, the calculated low frequency value of $R(\omega)$ agrees well with the measured value of $R(\omega)$. Therefore, MCNP-DSP provides a more general tool for planning experiments for criticality safety, safeguards, nondestructive assay, and arms control verification.

1.2 Organization

The purpose of Chap. 2 is to define the basic frequency analysis parameters from the measurement, provide a general description of the CSDNA measurement, relate the measured quantities to reactor physics parameters, and provide a rationale for the calculation of the CSDNA method using Monte Carlo analysis. Chapter 3 provides a description of the modifications to the neutron and photon physics of the code, outlines the program flow of the code for both the frequency analysis calculation and the analog calculation of k_{eff}, and discusses the treatment of the detection processing. Various tests are outlined in Chap. 4 which validate the code modifications, in particular, the detection of particles and the processing of the detector responses to obtain the various time distributions and frequency spectra. These include time analysis methods which directly sort the time distribution of pulses in a detector after the spontaneous fission of ^{252}Cf. In Chap. 5, a comparison of the measured and calculated detector responses are presented for several fissile configurations. Chapter 6 provides the conclusions of this research and recommendations for future work.

CHAPTER 2

^{252}Cf-SOURCE-DRIVEN NOISE ANALYSIS (CSDNA) METHOD

2.0 Background

The CSDNA method is a measurement technique that was developed by Mihalczo and Pare to determine the subcriticality of a fissile assembly. The technique also provides measured parameters that can be used for verification of calculational methods. The method is preferable over other measurements used to determine the subcriticality of a fissile assembly because the ratio of spectral densities for the ^{252}Cf measurement does not depend on detection efficiency or in some cases source intensity and does not require a measurement near delayed criticality. The measured parameters are very sensitive to small changes in the fissile configuration. This sensitivity has been demonstrated in measurements[13] and in calculations of the measured parameters.[14,15] The measurement is performed by placing the ^{252}Cf source, which is contained within an ionization chamber, near the fissile configuration along with two or more detectors to measure the particles from fission chains initiated by the source. The goal of this chapter is to provide an understanding of the parameters that are obtained from the measurement and how these parameters may be calculated.

In this chapter, some basic frequency analysis quantities are defined, and the measurement of the quantities is then discussed. To intuitively understand how the frequency analysis quantities are related to the reactor physics parameters, expressions for the probabilities of correlated detector counts in the time domain are defined.[16] Finally, the foundations of the Monte Carlo calculation are defined, and the basis of the Monte

Carlo calculation of the CSDNA method is presented.

2.1 Frequency Analysis Measured Quantities

In the CSDNA measurement, detector pulses are sampled as a function of time in order to obtain the various auto-and cross-power spectral densities. The auto-and cross-power spectral densities are defined by performing a complex multiplication of the Fourier transform of the detector signal. The auto-power spectral density (APSD) is defined as

$$G_{xx}(\omega) = X^*(\omega) X(\omega), \tag{2.1}$$

where $X(\omega)$ is the Fourier transform of the detector signal and * denotes the complex conjugate. Similarly, the cross-power spectral density (CPSD) is defined as

$$G_{xy}(\omega) = X^*(\omega) Y(\omega). \tag{2.2}$$

In the measurement, the detector signals are sampled as blocks of data that are Fourier transformed. A data block is a sample of the detector response for a certain time period which is determined from the sampling rate of the data analyzers and the number of discrete points to sample. The APSDs and CPSDs are averaged over many data blocks to obtain better and better estimates of the APSDs and CPSDs.

The auto-and cross- power spectral densities can also be defined by taking the Fourier transform of the autocorrelation and cross-correlation functions of the detector responses respectively. The autocorrelation function is defined as

$$\phi_{xx}(\tau) = \lim_{T\to\infty} \frac{1}{2T} \int_{-T}^{T} x(t)\, x(t+\tau)\, dt, \tag{2.3}$$

where $x(t)$ is the detector time response (the detector signal sampled into blocks of data). The autocorrelation function of a variable is the measure of similar information contained in the variable at time t and the correlated information contained in the variable at time

$t+\tau$. The APSD is then defined as

$$G_{xx}(\omega) = \int_{-\infty}^{\infty} \phi_{xx}(\tau)\, e^{-j\omega\tau} d\tau . \qquad (2.4)$$

The cross-correlation function between two signals is defined as

$$\phi_{xy}(\tau) = \lim_{T\to\infty} \frac{1}{2T} \int_{-T}^{T} x(t)\, y(t+\tau)\, dt. \qquad (2.5)$$

The cross-correlation function is a measure of the correlated information contained in one signal at time t and the other signal at time $t+\tau$. The CPSD is then defined as

$$G_{xy}(\omega) = \int_{-\infty}^{\infty} \phi_{xy}(\tau)\, e^{-j\omega\tau} d\tau . \qquad (2.6)$$

The coherence between two signals is the measure of the degree to which one signal depends on the other signal, is the fraction of information that is common to both signals, and varies between 0 and 1. The coherence between the detector 2 and the source detector 1 response is defined as

$$\gamma_{12}^2(\omega) = \frac{|G_{12}(\omega)|^2}{G_{11}(\omega)\, G_{22}(\omega)}, \qquad (2.7)$$

between detector 3 and the source,

$$\gamma_{13}^2(\omega) = \frac{|G_{13}(\omega)|^2}{G_{11}(\omega)\, G_{33}(\omega)}, \qquad (2.8)$$

and between both detectors,

$$\gamma_{23}^2(\omega) = \frac{|G_{23}(\omega)|^2}{G_{22}(\omega)\, G_{33}(\omega)} . \qquad (2.9)$$

The following ratio of coherences is equivalent to the magnitude of the ratio of spectral

densities (Eq. 1.1),

$$R(\omega) = \sqrt{\frac{\gamma_{12}^2(\omega)\,\gamma_{13}^2(\omega)}{\gamma_{23}^2(\omega)}}. \qquad (2.10)$$

Expressing the ratio in the form of coherences, the variance of the ratio can be determined by using the variances of the coherences. Since the coherences are real variables, the estimation of the variance in the ratio is made easier than using the variances of the ratio of spectral densities since some of the CPSDs are complex numbers.

The true coherence between two signals (γ^2) is

$$\gamma^2 = \frac{S/N}{1+S/N}, \qquad (2.11)$$

where *S/N* is the signal-to-noise ratio and is assumed to be the same for both signals. King[17] has shown that the measured coherence ($\hat{\gamma}^2$) satisfies the relation

$$\hat{\gamma}^2 = \gamma^2 + \frac{(1-\gamma^2)^2}{n}, \qquad (2.12)$$

where n is the number of data blocks. For *n* equal to one, this relationship is not true unless γ^2 is either zero or one. The measured standard deviation was shown by King to be

$$\sigma_{\hat{\gamma}^2} = \frac{\hat{\gamma}^2(1-\gamma^2)}{\sqrt{1+n\gamma^2/2}}. \qquad (2.13)$$

Since the bias, $\hat{\gamma}^2-\gamma^2$, diminishes as $1/n$, the coherences can be used to estimate the amount of data needed for the measured coherence to converge to the true coherence. The bias is known precisely and can be removed from the data. For the purpose of error

analysis, King has shown that treating the coherences as independent quantities yields a correct estimate of the uncertainty. The relative error of the ratio is expressed as

$$\epsilon_R = \frac{\sigma_R^2}{R} = \frac{[\epsilon^2_{\hat{\gamma}^2_{12}} + \epsilon^2_{\hat{\gamma}^2_{13}} + \epsilon^2_{\hat{\gamma}^2_{23}}]^{1/2}}{2}, \qquad (2.14)$$

where

$$\epsilon_{\hat{\gamma}^2} \approx \frac{\sigma_{\hat{\gamma}^2}}{\hat{\gamma}^2} = \frac{(1-\gamma^2)}{\sqrt{1+n\gamma^2/2}}. \qquad (2.15)$$

2.2 ^{252}Cf-Source-Driven Noise Analysis Measurement

As previously mentioned, the CSDNA measurement employees a ^{252}Cf source and two or more particle detectors. The detector signals are sent through discriminators to eliminate noise and small pulses from background radiation. There are two ways in which the detector pulses may be processed. The first involves directly calculating the frequency spectra of the detector responses to obtain the various APSDs and CPSDs. The second method involves the calculation of correlation functions and then calculating the frequency spectra.

In the first method, the signal pulses from the discriminator are input into a circuit that converts them into voltage pulses that have a constant area and a frequency spectrum defined by an adjustable *RC* time constant. The signals are then passed through a low-pass filter, which eliminates the upper frequency components that are greater than half the sampling rate. This prevents aliasing from occurring during the discrete Fourier processing of the signals. Aliasing is the folding of high frequencies over to the low frequency when the sampling rate is less than twice the maximum frequency of the signal. The filtered signal is digitized repeatedly by an analog-to-digital converter to provide an integer value

proportional to the voltage of the signal. The digitized data are divided into segments, termed data blocks, of typically 512 or 1024 points, and then the data are Fourier transformed. The APSDs and CPSDs are calculated for each data block by complex multiplication of the transformed data. The latest estimates are then averaged with the previous data to obtain the current APSDs and CPSDs. This process is continued until the desired convergence is reached.

The second method is to calculate the correlation functions from the digitized data. The correlation functions are calculated for each data block and averaged. After all data blocks have been calculated, the average correlation functions are Fourier transformed to obtain the average APSDs and CPSDs. After obtaining the average APSDs and CPSDs, the coherences and the ratio of spectral densities are calculated. Both methods of obtaining the frequency spectra are implemented in this work.

2.3 Probability of Correlated Counts

Some simple expressions from time domain measurements are presented to illustrate how measurements have been performed initially, that is, Rossi-α measurement and randomly pulsed neutron measurements with ^{252}Cf. In these expressions, the simplification of point kinetics is used for ease of understanding. The probability of correlated data in the time domain can be expressed by using some simplistic formulas in which basic reactor physics parameters are used. These expressions will only be presented. Since the objective of this work is to provide the most complete calculation of the frequency spectra without imposing limitations on the spatial or energy dependence of the spectra, these formulas are not included as a part of the calculation process of the code and are only provided here to state the origins of the measurement method. However, the time distribution of counts after ^{252}Cf fission is provided by the code for measurements

with simple configurations and have been used to verify parts of the code.

The probability of a spontaneous fission from the ^{252}Cf source in dt_0 about t_0 is

$$p(t_0)\,dt_0 = F_c dt_0, \tag{2.16}$$

where F_c is the spontaneous fission rate of the source. The probability of observing a count in dt_1 about t_1 due to the spontaneous fission at t_0 can be expressed as

$$p(t_1)\,dt_1 = \frac{\epsilon_1}{\bar{\nu}}\bar{\nu}_c \frac{e^{-\alpha(t_1-t_0)}}{\ell} dt_1, \tag{2.17}$$

where $\bar{\nu}_c$ is the average number of prompt neutrons for the source, $\bar{\nu}$ is the average number of prompt neutrons from induced fissions, α is the prompt neutron decay constant, ℓ is the prompt neutron lifetime, and ϵ_1 is the detection efficiency in counts per source fission. The product of these two probabilities is the probability of a correlated count in the detector from the spontaneous fission and is expressed as

$$p(t_1, t_0)\,dt_1 dt_0 = \frac{\epsilon_1}{\bar{\nu}}\bar{\nu}_c F_c \frac{e^{-\alpha(t_1-t_0)}}{\ell} dt_1 dt_0. \tag{2.18}$$

For the Rossi-α measurement, the probability of a fission in dt_0 about t_0 is

$$p(t_0)\,dt_0 = F dt_0, \tag{2.19}$$

where F is the induced fission rate of the system. The probability of observing a count in dt_1 about t_1 due to a fission at t_0 can be expressed as

$$p(t_1)\,dt_1 = \nu e^{-\alpha(t_1-t_0)} \frac{\zeta_1 dt_1}{\ell}, \tag{2.20}$$

where ζ_1 is the detector efficiency in counts per induced fission. For a detection process that removes a neutron from the system, the probability for an additional count at $t_2 > t_1$ due to the fission at t_0 is

$$p(t_2)\,dt_2 = (\nu-1)\,e^{-\alpha(t_2-t_0)}\,\frac{\zeta_2\,dt_2}{\ell}, \qquad (2.21)$$

where ζ_2 is the detection efficiency in counts per induced fission for the second detector. The (υ-1) appears because one neutron from the common ancestor fission was lost by absorption in the first detection, and thus the same neutron cannot be detected by two absorption detectors. For scattering detectors, this expression would be altered. Combining the above probabilities and integrating over all possible fissions up to time t_1 yields the probability that correlated counts will be detected by the two neutron absorbing detectors. The resulting equation is

$$p(t_1, t_2)\,dt_1 dt_2 = \int_{-\infty}^{t_1} dt_0 \frac{\zeta_1\zeta_2}{\overline{\nu}^2}\,\nu(\nu-1)\,F\frac{e^{-\alpha(t_2+t_1-2t_0)}}{\ell^2}\,dt_1 dt_2. \qquad (2.22)$$

These probabilities are used to express the measured time distributions in terms of neutron physics parameters. These equations and others may be used to obtain the neutron multiplication factor from the measured time spectra.

2.4 Monte Carlo Calculation of the CSDNA Method

To obtain the reactivity from the measured frequency spectra, a model has to be used. The Monte Carlo calculation of the CSDNA method was developed because of the limitations required in using the point kinetics models for interpretation of the spectral densities. To avoid the limitations of the point kinetics formulas, the Monte Carlo calculation is used to calculate the ratio of spectral densities and other frequency analysis parameters and to calculate the neutron multiplication factor. The Monte Carlo calculation does not impose any limitations on the spatial dependence of the calculation. The only limitation on the energy dependence is that imposed by the ENDF cross section data files and the representation of the neutron and gamma ray energy spectra from

fission.

The Monte Carlo random walk is formally based on the Integral Emergent Particle Density Equation[18]

$$\chi(\vec{r},\vec{\Omega},E,t) = S(\vec{r},\vec{\Omega},E,t) + C(\vec{r},\vec{\Omega}'\rightarrow\vec{\Omega},E'\rightarrow E)\, T(\vec{r}'\rightarrow\vec{r},\vec{\Omega}',E')\,\chi(\vec{r}',\vec{\Omega}',E',t), \tag{2.23}$$

where $\chi(\vec{r},\vec{\Omega},E,t)$ is the emergent particle density and $S(\vec{r},\vec{\Omega},E,t)$ is the source term, $T(\vec{r}'\rightarrow\vec{r},\vec{\Omega}',E')$ is the transport integral operator, and $C(\vec{r},\vec{\Omega}'\rightarrow\vec{\Omega},E'\rightarrow E)$ is the collision integral operator. The source term may be a point source or the fission source. The transport integral operator is defined as

$$T(\vec{r}'\rightarrow\vec{r},\vec{\Omega},E) \equiv \int_0^{\infty} \Sigma_t(\vec{r},E)\, e^{-\beta(\vec{r},R,\vec{\Omega})}\, dR, \tag{2.24}$$

where

$$\beta(\vec{r},R,\vec{\Omega},E) \equiv \int_0^{R} \Sigma_t(\vec{r}-R'\vec{\Omega},E)\, dR', \tag{2.25}$$

and R is the flight distance. The collision integral operator is defined as

$$C(\vec{r},\vec{\Omega}'\rightarrow\vec{\Omega},E'\rightarrow E) = \int_0^{\infty}\int_{4\pi} \frac{\Sigma_s(\vec{r},\vec{\Omega}'\rightarrow\vec{\Omega},E'\rightarrow E)}{\Sigma_t(\vec{r},E')}\, d\vec{\Omega}'dE', \tag{2.26}$$

where $\Sigma_s(\vec{r},\vec{\Omega}'\rightarrow\vec{\Omega},E'\rightarrow E)$ is the differential scattering cross section and $\Sigma_t(\vec{r},E')$ is the total cross section. Appendix A contains the relationship between the emergent particle density equation and the integro-differential Boltzmann transport equation. The random walk procedure is implemented by representing the emergent particle density, $\chi(\vec{r},\vec{\Omega},E,t)$, by a Neuman series

$$\chi(\vec{r},\vec{\Omega},E,t)=\sum_{n}\chi^{n}(\vec{r},\vec{\Omega},E,t)\,, \tag{2.27}$$

where $\chi^{n}(\vec{r},\vec{\Omega},E,t)$ is the density of particles emerging from the nth collision. The source position is determined first. The particle's flight distance is chosen from the transport kernel. The collision kernel is used to determine if the particle scatters or if it is absorbed. This process is represented as

$$\begin{aligned}\chi^{n}(\vec{r},\vec{\Omega},E,t)=\\ C(\vec{r},\vec{\Omega}'\rightarrow\vec{\Omega},E'\rightarrow E)\,T(\vec{r}'\rightarrow\vec{r},\vec{\Omega}',E')\,\chi^{n-1}(\vec{r}',\vec{\Omega}',E',t)\,,\end{aligned} \tag{2.28}$$

where $\chi^{0}(\vec{r},\vec{\Omega},E,t)=S(\vec{r},\vec{\Omega},E,t)$. The process is repeated until the particle history is terminated.

As can be seen from the Neuman series approach, the Monte Carlo method solves the transport equation by estimating the average behavior of many individual particle histories. This makes the Monte Carlo technique the logical choice to provide a calculation of the CSDNA method since the measurement technique examines the contribution of the individual fission chains to the detector responses. Fission chains are initiated by ^{252}Cf fission. These particles are transported throughout the system. The collision events and sites are probabilistically determined. The production of secondary particles is chosen from the ratio of the fission cross section to the total cross section. These subsequent particles are transported in the same manner as the source particles. When the particles have an event in the detection media, which must be specified in the calculation, a test is performed to determine if the particle contributes to the detector response. After the particles have been transported, the necessary blocks of data are calculated and the frequency spectra are determined.

CHAPTER 3

THE MODIFIED MCNP CODE

3.0 General Description of MCNP

MCNP is a multipurpose Monte Carlo N-Particle code that is used for neutron, photon, electron, and coupled neutron-photon-electron transport. MCNP has a wide array of capabilities, for example, detector tally calculations, flux estimation tallies, and eigenvalue calculations for fissile assemblies. The code uses a generalized geometry package that allows explicit modeling of a given geometry. The geometry is assembled as cells by defining the surfaces of the unit.

The materials that comprise the cells are described using the appropriate material densities along with a descriptor that indicates the cross-section data set to be used in the calculation. These cross sections can either be point-wise data or multigroup data. The cross-section data sets for neutrons contain all the reactions which have been evaluated for a particular isotope along with any known angular distributions. Cross-section data in the form of thermal $S(\alpha,\beta)$ tables are also available to account for molecular binding effects for low-energy neutrons. Secondary photon production data are also available in some evaluated data sets. For photons, the code uses cross-section data for incoherent scattering, coherent scattering, the photoelectric effect, and pair production. A continuous slowing-down model is used for the electron transport.[12]

MCNP contains several options that make it a very versatile code. Various tally options can be used to calculate the flux, current, reaction rates, etc. The source can be described in great detail. The source particle type, energy, position, and direction can

easily be specified. There are also many different variance reduction techniques that can be used if needed. Although MCNP is very versatile, several changes had to be made to the code in order to provide an accurate estimation of the various spectral densities of the CSDNA method. A dual-particle source was developed which produced both neutrons and photons. The variance reduction features were disabled in order to have strictly analog particle tracking, and the neutron and photon transport routines were modified to better represent the collision physics. Some simplified detector options were incorporated in MCNP-DSP to represent the detectors used in the measurements. Various processing routines were included in MCNP-DSP to obtain the desired time distributions, correlation functions, or frequency spectra from the data blocks of counts in the detectors.

3.1 Modified Neutron Transport

Since the CSDNA method measures the behavior of the individual fission chains in a fissile configuration, it is necessary that the calculation be able to adequately simulate the behavior of the individual fission chains. This requires replacing average parameters such as $\overline{\nu}$ with probability distributions since the spectral densities of the CSDNA method provide statistical estimates of the fission chain fluctuations and the average quantities reduce the fission chain fluctuations. The proper treatment of the angular distribution of neutrons from fission must also be included in the calculation to adequately describe the particle direction from fission for both spontaneous fission and induced fission. The selection of the energy of the neutrons from the spontaneous fission of ^{252}Cf has been modified to incorporate recent improvements in the representation of the prompt neutron energy spectrum. Implementing these changes along with analog neutron tracking allow for the correct representation of the individual fission chains.

3.1.1 Number of Prompt Neutrons from Fission

There have been various experiments performed to determine the number of prompt neutrons from fission. The average number of prompt neutrons from fission is a function of the fissioning isotope and the energy of the neutron that induces the fission. The average number of neutrons from fission is strongly dependent on the excitation energies of the fission fragments and the fragment mass yield. The fragment yield depends on the excitation energy of the compound nucleus.

The complexity of determining $P(\nu)$, the probability of obtaining ν prompt neutrons from fission, for various fissioning isotopes was simplified by Terrell.[19] Terrell suggests that the neutron multiplicities are dependent on the fission fragment properties. If a Gaussian distribution of the fission fragment excitation energies is assumed, the cumulative probability, $P(\nu)$, of observing ν prompt neutrons from fission is approximated by the Gaussian distribution[20]

$$P(\nu) = \frac{1}{\sqrt{2\pi}} \int_{-\infty}^{(\nu-\bar{\nu}+1/2+b)/\sigma} e^{-\frac{1}{2}t^2} dt, \qquad (3.1)$$

where b is a small correction factor ($< 10^{-2}$) to ensure that the ν's are positive and σ is the root-mean-square width of the initial total excitation-energy distribution ($\sigma = 1.08$).[19] Terrell has shown that this distribution function can be used to describe the emission probability for several different fissioning isotopes. In MCNP, the $\bar{\nu}$ obtained from the cross-section data sets is a function of the energy of the neutron that induces the fission. Thus the emission probability that was incorporated into MCNP-DSP is an energy dependent distribution. The Gaussian distribution is an approximation to describe the prompt neutron emission probabilities at all energies and is used unless additional

measured distribution data are included for certain isotopes when available.

An option has been added to MCNP-DSP to use the measured data analyzed by Zucker and Holden.[21] Zucker and Holden tabulated the $P(\nu)$ distributions for ^{235}U, ^{238}U, and ^{239}Pu as a function of the energy of the neutron that induces the fission. Figures 3.1, 3.2, and 3.3 show the dependence of $P(\nu)$ on the energy of the neutron obtained from the Zucker and Holden tabulated data. The tabulated data of Zucker and Holden are used by default. The probability distribution data were fit with least-square polynomials to obtain a functional representation of the energy dependence of neutron emission probabilities. The probability distribution data for the spontaneous fission of ^{252}Cf were taken from Spencer's measurements.[22] These probabilities are provided in Appendix B.

3.1.2 Angular Distribution of Prompt Neutrons from Fission

There are instances in which the angular distributions of prompt neutrons from fission may be important, such as when the ^{252}Cf source is located some distance from the fissile configuration or perhaps with interacting arrays. Hence, assuming an isotropic emission of neutrons from fission can be a poor approximation. The angular distribution of neutrons relative to the direction of the light fission fragment has been measured by Budtz-Jorgensen and Knitter for the spontaneous fission of ^{252}Cf.[23] Budtz-Jorgensen and Knitter have shown that there is angular anistoropy in the laboratory reference frame. The probability distribution function obtained from the Budtz-Jorgensen and Knitter data is shown in Fig. 3.4. As can be seen from Fig. 3.4, the angular distribution at zero energy is more isotropic; however, as the neutron energy increases, the angular distribution becomes very anisotropic.

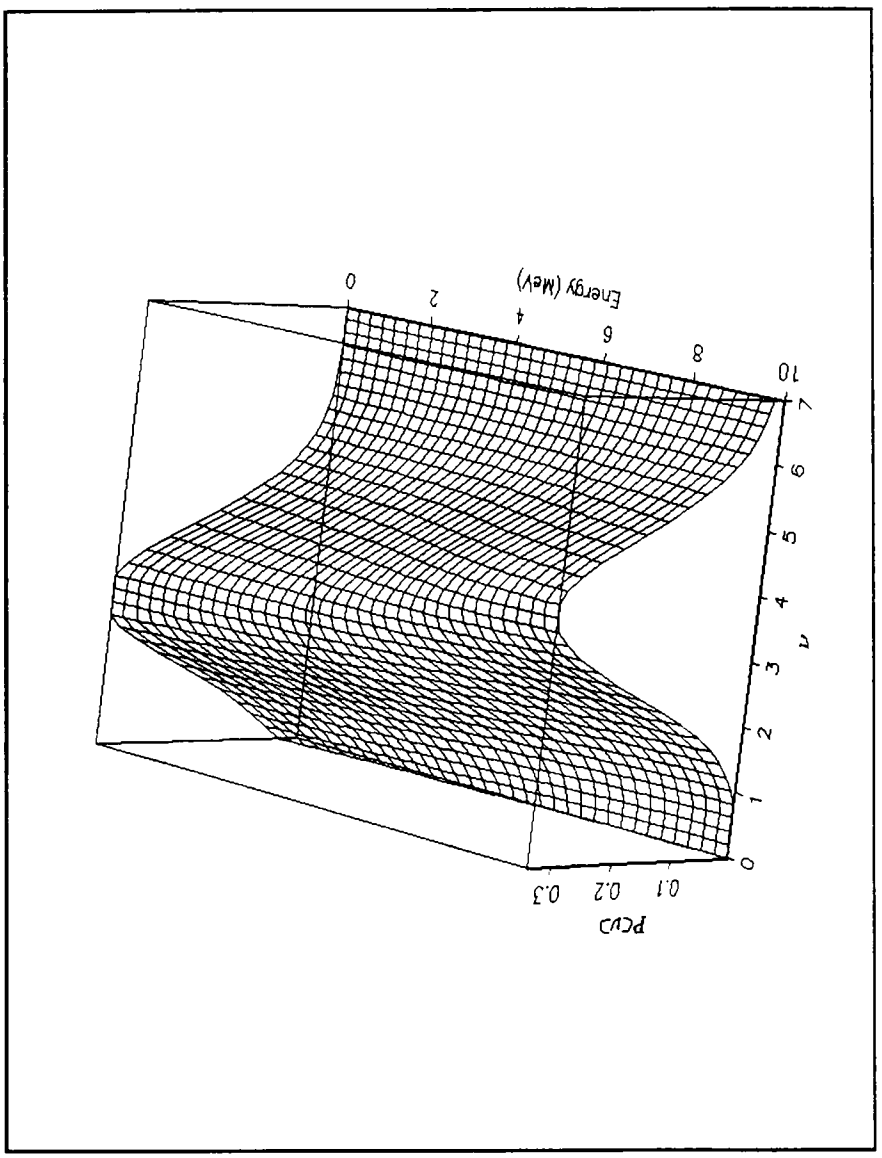

Figure 3.1 P(ν) Distribution for ^{235}U as a Function of the Energy of the Neutron Inducing Fission

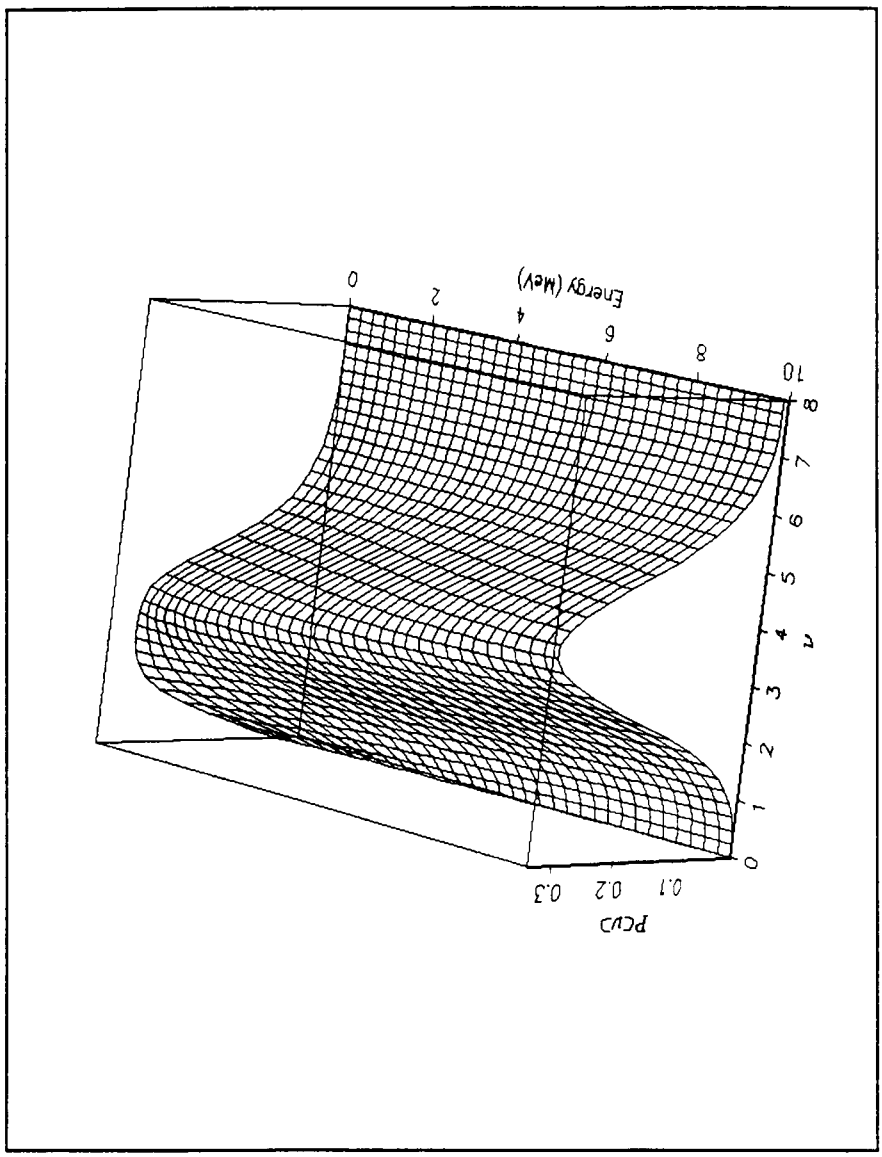

Figure 3.2 P(ν) Distribution for ^{238}U as a Function of the Energy of the Neutron Inducing Fission

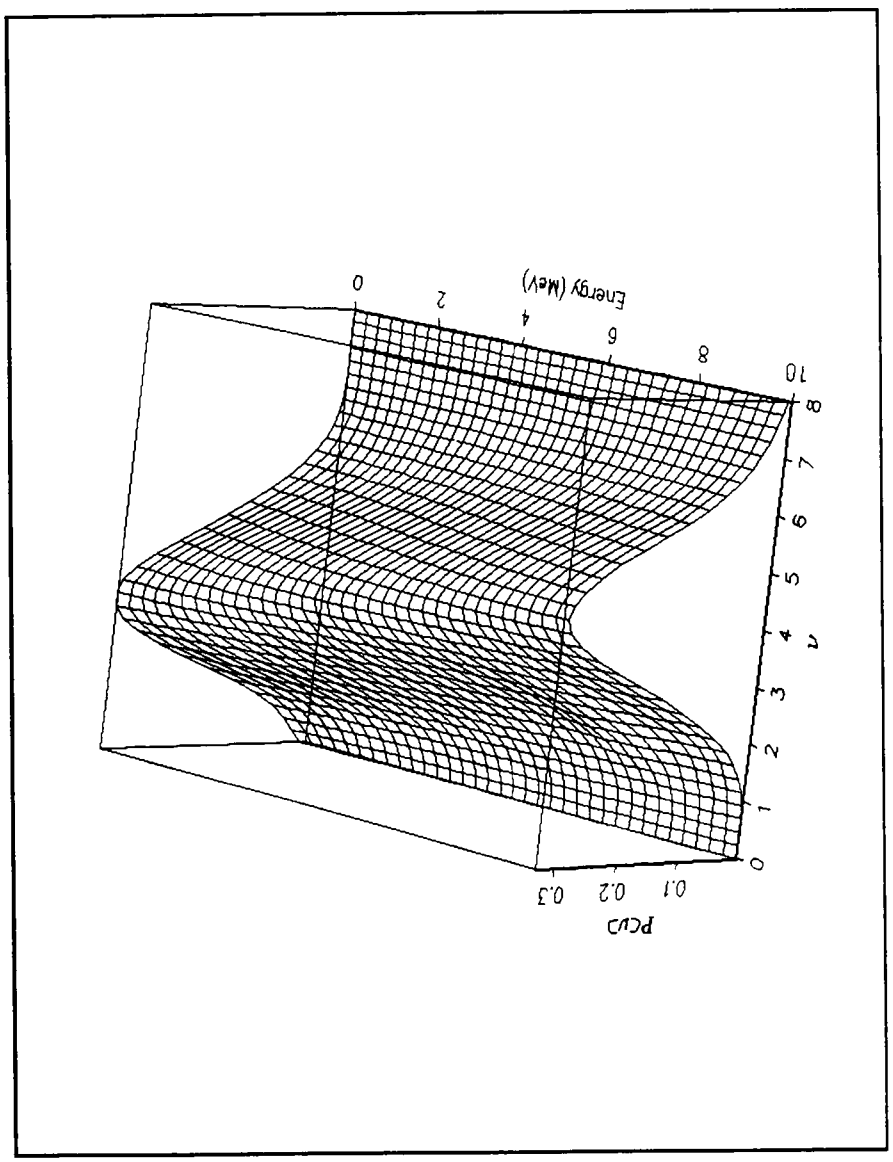

Figure 3.3 P(ν) Distribution for ^{239}Pu as a Function of the Energy of the Neutron Inducing Fission

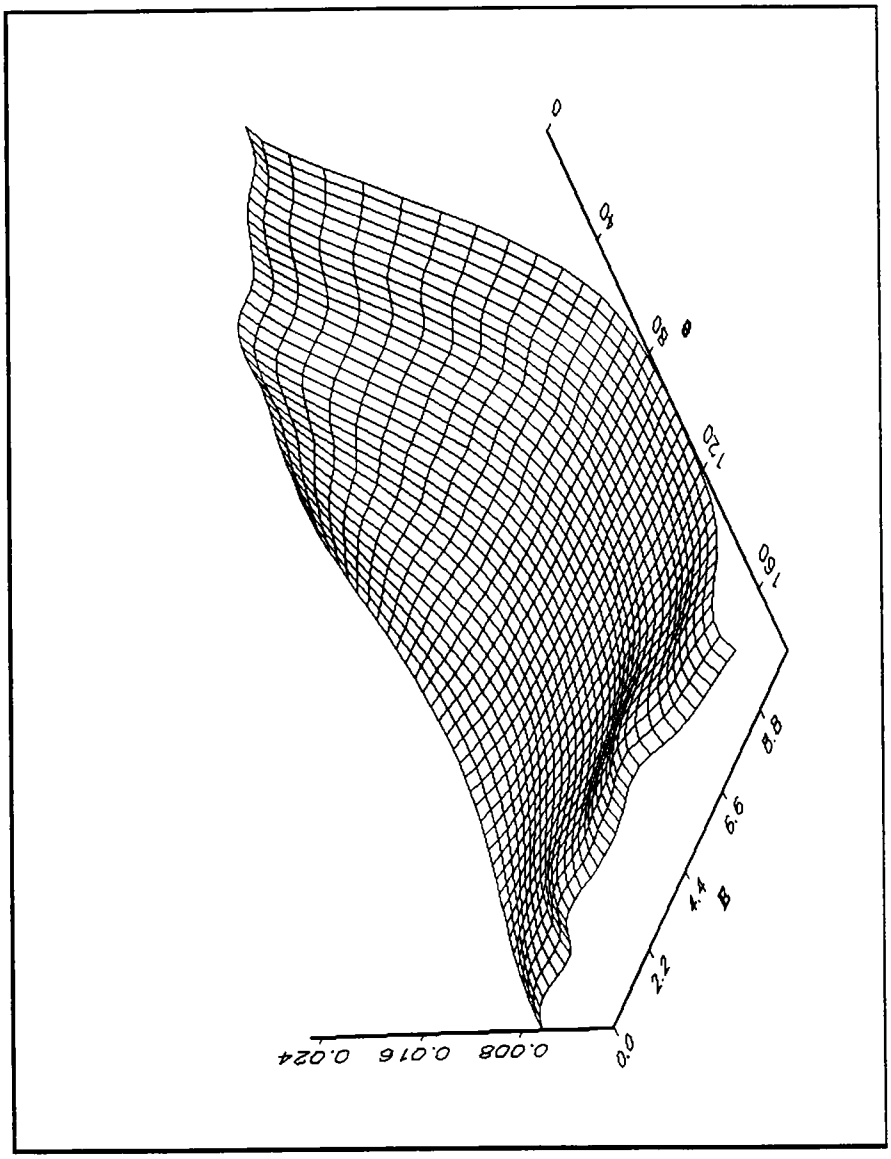

Figure 3.4 Probability Density Function for Angular Distribution (Lab System) of Neutrons from Fission with Respect to the Direction of Light Fission Fragment

These data are incorporated into MCNP-DSP by selecting the direction of the light fission fragment from an isotropic distribution. The neutron direction is then determined by sampling its azimuthal direction uniformly on the interval 0 to 2π. The polar angle of each fission neutron relative to the light fission fragment is determined from the angular probability distribution function. This process has been described by Paré[24] and is included in Appendix C. The resulting expression for the neutron's direction relative to the laboratory reference frame is given by

$$\begin{aligned}\vec{r} = &\left(\alpha\frac{uw}{\sqrt{1-w^2}} - \beta\frac{v}{\sqrt{1-w^2}} + u\mu\right)\hat{e}_x \\ &+\left(\alpha\frac{vw}{\sqrt{1-w^2}} + \beta\frac{u}{\sqrt{1-w^2}} + v\mu\right)\hat{e}_y \\ &+\left(-\alpha\sqrt{1-w^2} + w\mu\right)\hat{e}_z,\end{aligned} \tag{3.2}$$

where the coordinate directions for the light fission fragment in the laboratory reference frame are

$$\begin{aligned}u &= \sin\theta\cos\phi, \\ v &= \sin\theta\sin\phi, \\ w &= \cos\theta,\end{aligned}$$

and where

$$\begin{aligned}\alpha &= \sin\psi\cos\eta, \\ \beta &= \sin\psi\sin\eta, \\ \mu &= \cos\eta,\end{aligned}$$

are the coordinate directions for the neutron in the reference frame of the fission fragment. These data may be used for both the spontaneous fission of the ^{252}Cf source and for induced fissions in the system to investigate the effects of the angular dependence of the neutron emission. Since the majority of the neutrons are released from the fully accelerated fission fragments, the angular distribution of the neutrons relative to the direction of the fission fragments is dependent on the de-excitation of the fission

fragments. Therefore, there would be little difference between the angular distribution of spontaneous fission neutrons and the angular distribution of induced fission neutrons.[25]

3.1.3 Fission Neutron Energy Distribution for ^{252}Cf

In the Monte Carlo calculation, the energy of a neutron from fission is determined from the normalized prompt neutron energy spectrum. Typically, the prompt neutron energy spectrum, $N(E)$, can be represented by a Maxwellian

$$N(E) = \frac{2}{\sqrt{\pi}} \frac{\sqrt{E}}{T^{3/2}} e^{-E/T}, \qquad (3.3)$$

where E is the energy and T is the nuclear temperature. Consequently, many experiments have been analyzed in terms of the Maxwellian distribution. A detailed analysis of the experimental data has been performed by Mannhart[26] to obtain the relative difference between the spectrum obtained from the measured data and the Maxwellian distribution for the spontaneous fission of ^{252}Cf. Mannhart developed an energy dependent correction factor for the Maxwellian distribution. The correction factor data can be found in Appendix D. By multiplying the Maxwellian distribution by the correction factor, an accurate representation of the energy distribution of neutrons from the spontaneous fission of ^{252}Cf is obtained. The average energy obtained from the corrected distribution is 2.13 MeV which corresponds to the measured value of the average energy of neutrons from the spontaneous fission of ^{252}Cf. An eight-point Gaussian quadrature integration scheme was used to integrate the spectrum from zero to an upper limit of E where E was varied from 0.00001 eV to 25 MeV. The integrated spectrum was then normalized to unity. The selection of the neutron energy is determined by setting a random number equal to the normalized integrated spectrum and then determining the energy that corresponds to this value of the normalized integrated spectrum. However, to save

computation time, a least-squares polynomial fit of the neutron energy as a function of the value of the normalized integrated spectrum was calculated. This resulted in an expression for the neutron energy as a function of the normalized integrated spectrum, that is, the neutron energy as a function of the random number.

3.2 Modified Gamma Ray Transport

The proper treatment of the prompt fission gamma rays is essential if the detector responses to gamma rays are to be calculated correctly. In MCNP, photon production from neutron events is determined by sampling a total "inelastic" photon production cross section. These cross sections contain data on the multiplicity and energy of gamma rays from neutron reactions that produce gamma rays. These reactions include neutron capture, inelastic neutron scattering, and fission. Although the cross sections are measured separately, these photon-producing reactions are lumped together in the evaluated nuclear data sets in ENDF. Consequently, these data cannot be easily separated without modifying the ENDF data files and may add an uncertainty to the calculation when analyzing individual reactions. This grouping does not allow the physics of gamma ray production process to be exact on an event-by-event basis but does give a correct average behavior.[27] This will lead to no error in the first moment of the populations but may introduce some error into the second moment on which noise-measured parameters depend, especially when inelastic neutron scatter and fission are equally probable. This may also remove some of the fluctuating phenomena associated with gamma ray production. The multiplicity and energy distribution of prompt gamma rays from the spontaneous fission of the ^{252}Cf source has been included in MCNP-DSP.

3.2.1 Prompt Gamma Ray Multiplicity for ^{252}Cf

The gamma ray multiplicity, like the neutron multiplicity, is a function of the fission fragment mass but has little dependence on the energy of the neutron inducing the fission. A sawtooth dependence of the gamma ray yield on fragment mass has been observed for the spontaneous fission of ^{252}Cf and for thermal neutron fission of ^{235}U.[19] Since the number of gamma rays emitted is mainly dependent on the fission fragment properties, a single distribution can be used to describe the gamma ray multiplicity for ^{252}Cf.

The gamma ray multiplicity was determined using Brunson's[28] measurements, which fitted the data to a double Poisson model. Brunson's model depends on the minimum energy of the gamma rays emitted. For a minimum energy of 85 keV, the resulting probability distribution is used to obtain the gamma ray multiplicity

$$\Pi(G) = 0.682\frac{7.20^{G}e^{-7.20}}{G!} + 0.381\frac{10.71^{G}e^{-10.72}}{G!}, \qquad (3.4)$$

where G is the gamma ray multiplicity. The gamma ray multiplicity ranges from 0 to 20 gamma rays per fission with an average value of 7.79 gamma rays per fission. This value does not differ greatly from that obtained by others.[28]

3.2.2 Prompt Gamma Ray Energy Distribution for ^{252}Cf

The gamma ray energy spectrum has been measured for the spontaneous fission of ^{252}Cf and the thermal-neutron-induced fission of ^{235}U. There appears to be little difference between the spectrum from ^{252}Cf and that from ^{235}U.[29] Because of the small difference between the two spectra and because the measurements of the ^{235}U gamma ray spectra are more precise, the gamma ray spectra from the thermal neutron fissioning of ^{235}U is used to obtain the gamma ray energy.

The energy spectrum of the prompt fission gamma rays is obtained from Maienschein's measurements.[30] Maienschein's experimental data were fitted with an exponential in two energy ranges.[31] From 0.3 to 1. MeV, the distribution is described as

$$N(E) = 26.8e^{-2.30E}. \qquad (3.5)$$

In the interval 1.0 to 8.0 MeV, the distribution is described as

$$N(E) = 8.0e^{-1.10E}. \qquad (3.6)$$

The upper energy limit of 8 MeV was selected because nuclear excitation above 8 MeV typically leads to neutron rather than gamma emission. Although Maienschein's experiment determined the gamma ray spectrum down to 0.25 MeV, there are several gamma ray energies that show preferential emission for low multiplicities below 0.3 MeV.[28] On the advice of Ray Nix,[25] the spectrum below 0.3 MeV is represented as

$$N(E) = 38.13(E-0.085)e^{1.648E}. \qquad (3.7)$$

The minimum gamma ray energy of 0.085 MeV coincides with Brunson's measurements. Below this energy, photon emission is due to K-shell X-rays from the fission fragments that occur later than the prompt gamma emission from fission. Using this functional representation of the prompt fission gamma ray energy spectrum, a value of 0.898 MeV is obtained for the average gamma ray energy per fission. This value agrees well with the accepted value of 0.88 MeV per fission.[28]

Some correlation exists between the total gamma ray energy release and the number of neutrons emitted from fission. Nifenecker[32] has observed that there is competition in the de-excitation mechanism of the fission fragments. This can be expected since it has been shown that the angular momentum of the fission fragments is transferred to the gamma rays and essentially no angular momentum is given to the neutrons as a

consequence of selection rules of quantum mechanics.[19] Nifenecker obtained the following linear relationship between the number of neutrons emitted from fission, ν, and the total gamma ray energy, E_t:

$$E_t = 0.75\nu + 4. \qquad (3.8)$$

This relationship can be used to put a limit on the total gamma ray energy from the spontaneous fission of ^{252}Cf source and also couples the gamma ray production with the neutron production.

3.3 The Detection Process

Although MCNP is capable of tracking electrons, the electron production and subsequent light production in the detectors were not treated rigorously in order to decrease the computation time. An intuitive approach was used to determine when particles contribute to the detector response. As will be seen in Chap. 4, this approximation faithfully reproduces the measured detector responses. Currently, three detector types can be employed in a calculation: capture, scatter, or fission detectors. The scattering detectors are the most commonly used detectors in the measurement and are sensitive to both neutrons and gamma rays. Fission detectors are included in the calculational model but are not used much in the measurements because of their low sensitivity.

3.3.1 Neutron Detection

In the MCNP-DSP calculation, neutron detection is characterized by a particular neutron event. The detector response of capture detectors is primarily due to the absorption of a neutron with the subsequent emission of secondary charged particles, which ionize the detection media and produce an electronic pulse proportional to the kinetic energy of the secondary charged particle. These detectors typically have a very

large absorption cross section and a very small scattering cross section. In MCNP-DSP, if a neutron is absorbed in a capture detector, a count is scored in the appropriate time bin, and the number of detections is incremented.

Scattering detectors are those in which the response is due primarily to neutron scattering in the detection media. To observe a count in a scattering detector, the neutron must transfer a certain preselected amount of energy to the detection material via the kinetic energy of the recoil nucleus, which excites electrons in the scintillation material which produce light that is converted into an electrical pulse by a photomultiplier tube. Although MCNP can handle this scintillation process directly, an intuitive approach was utilized to minimize computation time. This treatment assumes that the light production is proportional to the energy deposited by the neutron. An energy threshold is specified in the calculation for each detector. Since multiple neutron scatters can occur in the detector, special attention was given to modeling the multiple scattering in these detectors by specifying a time width, the pulse generation time, in which energy contributions from the events are summed together. If a neutron scatters in the detector and deposits an amount of energy greater than the neutron threshold, a count is registered and additional neutron scatters within the specified pulse generation time of the detector are ignored. However, if the amount of energy deposited in the detector is less than the neutron threshold, the energy of the subsequent neutron scatters in the detector are added together for those events that occur within the pulse generation time of the detector. In order to account for neutrons that may scatter between adjacent detectors several times, the time at which the neutron had its last scattering event in each detector is stored for each neutron track.

In fission detectors, the fission fragments travel through the detection media, ionizing the atoms in the detector. The large energy release per fission allows for easy discrimination of other events that may also produce ionized atoms in the detector. In the calculation, a count is registered each time a fission occurs in the detection media, and the fission neutrons are stored for tracking. The fission detectors may be used for other applications of interest such as time and frequency analysis studies.

3.3.2 Gamma Ray Detection

Various gamma ray events may lead to a detection in the capture and scattering detectors since the gamma ray events also produce secondary charged particles. If the gamma ray energy deposited is above a certain threshold, which is specified as input to the calculation, gamma ray absorption due to the photoelectric effect can lead to a detection. Likewise, if the gamma ray has an incoherent scatter in the detector and the recoil electron has an energy greater than the threshold, a detection will occur.

As with the neutrons, the multiple scattering of gamma rays in the detector media is modeled in great detail. A photon energy threshold is specified in the calculation for each detector to account for multiple photon scatters. If a photon scatters in the detector and deposits an amount of energy greater than the photon threshold, a count is registered, and additional photon scatters within the specified pulse generation time of the detector are ignored. However, if the amount of energy deposited in the detector is less than the photon threshold, the energy of the subsequent photon scatters in the detector are added together for those events that occur within the pulse generation time of the detector. In order to account for photons that may scatter between detectors several times, the time at which the photon had its last scattering event in each detector is stored for each photon track.

3.4 Detector Response Processing

In the measurement and in these calculations, the detector responses are divided into segments call data blocks of typically 256, 512, or 1024 points. A block of data is a sample of the detector response for a certain time period which is determined from the sampling rate of the data analyzers and the number of points. In the calculation, the number of ^{252}Cf fissions to occur within a data block is specified. The relationship between the actual ^{252}Cf source and the simulated source is described in Sec. 3.5.

As discussed in Chap. 2, there are two ways in which the blocks of detector signals may be processed. The first method involves taking the Fourier transform of the detector signals and computing the power spectral densities by complex multiplication of the Fourier transformed signals. The second method entails calculating the correlation functions for each data block and then Fourier transforming the average correlation functions to obtain the power spectral densities.

3.4.1 Direct Fourier Processing

In the measurements, the power spectral densities are obtained by Fourier transforming the processed detector signals and performing a complex multiplication. The detector signals are processed by passing the signal through a bandpass filter. To simulate the bandpass filter, two filter options can be employed in the calculation. A Rockland and a Precision filter are used in the measurements; hence, functions that represent these filters may be used in the calculations. The digitized waveforms for these filters were obtained from Paré[24] and are shown in Fig. 3.5. The filter functions have been normalized to one and are plotted as a function of the upper frequency cutoff, f_c. The upper frequency cutoff is set equal to 40% of the sampling rate as implemented in the measurement to prevent aliasing. These filter functions are only applicable for sampling

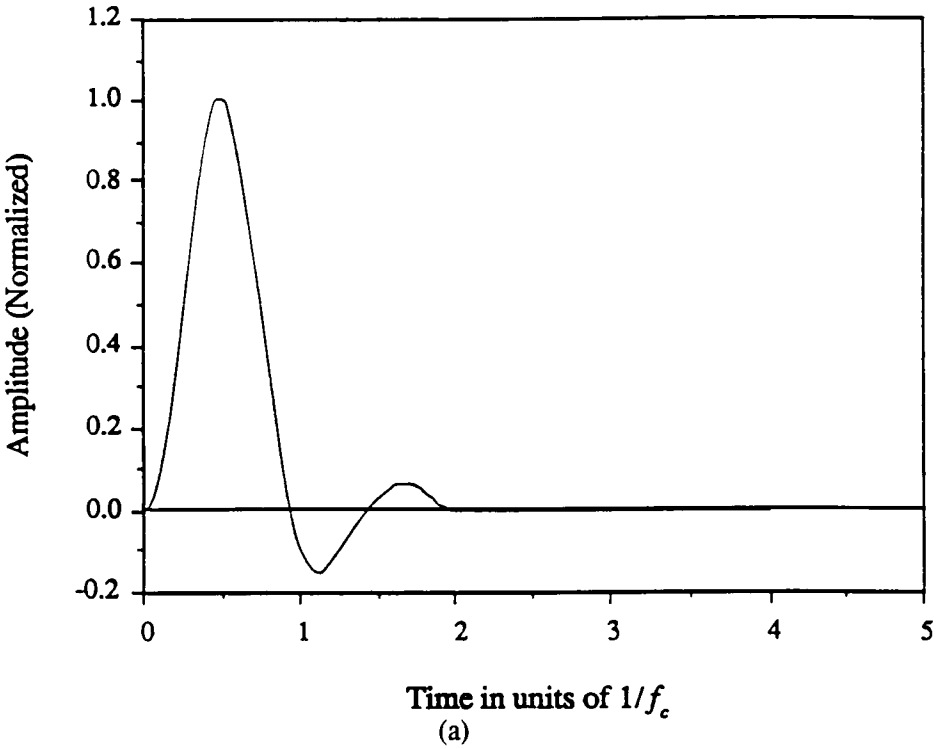

(a)

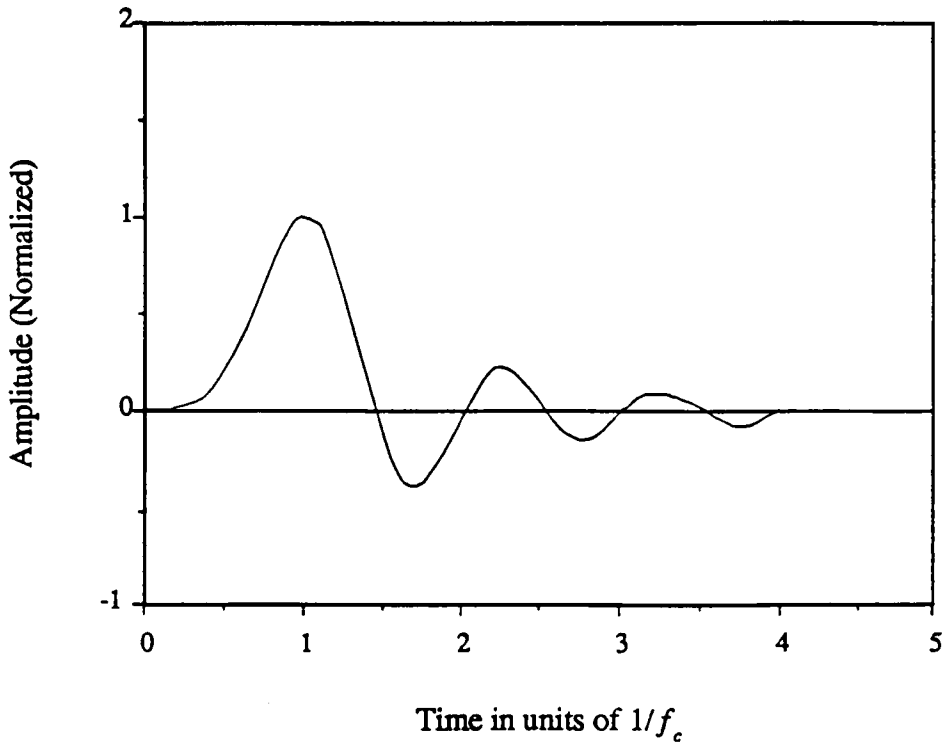

(b)

Figure 3.5 (a) Rockland and (b) Precision Filter Response Function

rates less than 100 kHz since the low pass filter has not been included in the model and its time response affects the detector response for sampling rates greater than 100 kHz. Other filter functions could easily be incorporated into the code if the waveforms are available. The time when a particle is detected is determined by adding the time of its birth to the time that the particle spent in the system before being detected. A count is registered in the appropriate time bin in the data block. The width of each time bin is determined from the inverse of the sampling rate. Therefore, the time length of the data block is equal to the number of time bins multiplied by the width of the time bins. If the filter functions are employed for each particle detection, the detector pulse is spread out over 10 time bins. This is accomplished by placing the digitized values of the normalized filter function which occur at the right boundary of the time bin in the time bins. If the particle detection occurs near the end of the data block, the digitized values in time bins beyond the length of the data block are ignored. A high-pass filter is used to eliminate low-frequency components of the detector signal. To simulate the implementation of a highpass filter, the average counts per bin are subtracted for each detector's time spectrum for each data block. The removal of the mean value is performed independently of the implementation of the low-pass filter. There are three commonly used windows that may be used in the calculation. These windows are the Bartlett, Hanning, and Hamming windows.[33] These windows are applied to the time spectra to correct for errors due to the finite length of the data block which coincides with a finite length Fourier transform. A Hanning window has been used in the measurements. A fast Fourier transform is applied to the data block. Using the Fourier transform of the detector responses (data blocks), the APSDs and CPSDs are calculated for each data block and averaged with the values from the previous data blocks. The coherences and the ratio of spectral densities can be

calculated using the average APSDs and CPSDs. The data blocks are continuously sampled until the desired convergence criteria are satisfied.

3.4.2 Correlation Function Analysis

In order to investigate an alternate processing concept to be used in an advanced processor, the calculation of the autocorrelation and cross-correlation functions were included in the code. The code calculates circular correlation functions from the detector time response since this is equivalent to performing the complex multiplication in the frequency domain.[33] The estimate of the circular autocorrelation function is given by

$$R_{xx}(r) = \sum_{k=0}^{N-1} x_k x_{(N-(r-k))}, \qquad (3.9)$$

where x is the detector signal, r is the lag index, and N is the number of points per data block. The detector signal is assumed to be periodic ($x_k = x_{(N+k)}$) since the circular correlation function is calculated. Likewise, the estimate of the circular cross-correlation function is given by

$$R_{xy}(r) = \sum_{k=0}^{N-1} x_k y_{(N-(r-k))}, \qquad (3.10)$$

where x and y are two different detector signals. Average values of the autocorrelation and cross-correlation functions are calculated as the data blocks are updated. The one-sided auto-power spectral density is defined as[34]

$$G_{xx}(\omega) = 4\int_0^{\infty} R_{xx}(\tau)\cos(\omega\tau)\,d\tau, \qquad (3.11)$$

for $0 < \omega \leq \infty$. This result is obtained because the autocorrelation function is symmetric. Since the code produces estimates of the correlation function at discrete lag times, the autocorrelation function can be expressed as a sequence of discrete samples

$$R_{xx}(\tau) = \sum_{k=0}^{N-1} R_{xx}^{k}\delta(\tau - k\Delta), \qquad (3.12)$$

where Δ is the sampling interval. Substitution of the sequence into Eq. 3.11 yields

$$G_{xx}(\omega) = 4\int_{0}^{N\Delta} \sum_{k=0}^{N-1} R_{xx}^{k}\delta(\tau - k\Delta)\cos(\omega\tau)\, d\tau, \qquad (3.13)$$

where the upper limit of the integral has been set equal to $N\Delta$ since this is the period of the data block. Interchanging the order of summation and integration and evaluation of the integral yields

$$G_{xx}(\omega) = 4\left[R_{xx}^{0} + \sum_{k=1}^{N-1} R_{xx}^{k}\cos(\omega k\Delta)\right], \qquad (3.14)$$

Since $\omega = 2\pi m/N\Delta$, the APSD becomes

$$G_{xx}(m) = 4\left[R_{xx}^{0} + \sum_{k=1}^{N-1} R_{xx}^{k}\cos(2\pi mk/N)\right], \qquad (3.15)$$

where $m = 0,1,\ldots,N/2$.

Because the cross-correlation function is not symmetric, the cross-power spectral density will be a complex quantity. The one-sided CPSD is defined as

$$G_{xy}(\omega) = 2\int_{-\infty}^{\infty} R_{xy}(\tau)\, e^{-j\omega\tau} d\tau, \qquad (3.16)$$

for $0 < \omega \leq \infty$.[34,35] The cross-power spectral density can be written as a real part and an imaginary part

$$G_{xy}(\omega) = C_{xy}(\omega) - jQ_{xy}(\omega), \qquad (3.17)$$

where C_{xy} is termed the co-spectra, and Q_{xy} is termed the quad-spectra.[33] The derivations of the expressions for the co-spectra and the quad-spectra are given by Uhrig[34] and are

presented here for completeness. First, the integral in Eq. 3.16 is separated into two integrals to yield

$$G_{xy}(\omega) = 2\int_{-\infty}^{0} R_{xy}(\tau)\, e^{-j\omega\tau} d\tau + 2\int_{0}^{\infty} R_{xy}(\tau)\, e^{-j\omega\tau} d\tau . \qquad (3.18)$$

A change of variable is performed in the first integral in Eq. 3.18 by setting $\tau = -\tau$ and using the asymmetry property of the cross-correlation function, $R_{xy}(-\tau) = R_{yx}(\tau)$ to obtain

$$G_{xy}(\omega) = 2\int_{0}^{\infty} R_{yx}(\tau)\, e^{j\omega\tau} d\tau + 2\int_{0}^{\infty} R_{xy}(\tau)\, e^{-j\omega\tau} d\tau . \qquad (3.19)$$

By substituting Euler's formula into Eq. 3.19 and grouping the real and imaginary parts, the following expressions are obtained for the co-spectra and the quad-spectra

$$C_{xy}(\omega) = 2\int_{0}^{\infty} [R_{xy}(\tau) + R_{yx}(\tau)] \cos(\omega\tau)\, d\tau \qquad (3.20)$$

and

$$Q_{xy}(\omega) = 2\int_{0}^{\infty} [R_{xy}(\tau) - R_{yx}(\tau)] \sin(\omega\tau)\, d\tau . \qquad (3.21)$$

The cross-correlation functions can be expressed as sequences of discrete samples

$$R_{xy}(\tau) = \sum_{k=0}^{N-1} R_{xy}^{k} \delta(\tau - k\Delta) \qquad (3.22)$$

and

$$R_{yx}(\tau) = \sum_{k=0}^{N-1} R_{yx}^{k} (\tau - k\Delta) . \qquad (3.23)$$

Substitution of Eqs. 3.22 and 3.23 into Eqs. 3.20 and 3.21 and rearranging and evaluating

the integrals yield the following expressions for the co-spectra and the quad-spectra:

$$C_{xy}(m) = 2\left[\sum_{k=0}^{N-1} R_{xy}^{k}\cos(2\pi mk/N) + \sum_{k=0}^{N-1} R_{yx}^{k}\cos(2\pi mk/N)\right] \qquad (3.24)$$

and

$$Q_{xy}(m) = 2\left[\sum_{k=1}^{N-1} R_{xy}^{k}\sin(2\pi mk/N) - \sum_{k=1}^{N-1} R_{yx}^{k}\sin(2\pi mk/N)\right], \qquad (3.25)$$

where the frequency variable has been discretized. These estimates of the APSDs and the CPSDs are then used to calculate the coherence functions and the ratio of spectral densities.

3.4.3 Time Domain Analysis

Since the code stores the time of particle detections, the time distribution of counts after ^{252}Cf fission can easily be obtained. The birth time of particles from the spontaneous fission of ^{252}Cf is set equal to zero to obtain the detector response after ^{252}Cf fission. The time response calculations are used to benchmark these calculational algorithms for simple measured configurations.

3.5 Modified MCNP Structure

The general structure of MCNP has been preserved as much as possible. However, some modifications had to be made in order to obtain the frequency data in a manner similar to the measurement. The general flow of MCNP4A is shown in Fig. 3.6. The program starts by reading the command line to determine which options the code uses. After determining the options, the program begins execution. The first step is to read the input file, which can be stated on the command line or the default input file name, INP. The arrays are initialized with a call to subroutine IMCN. If the frequency analysis calculation is to be performed, a separate data file containing options used in the

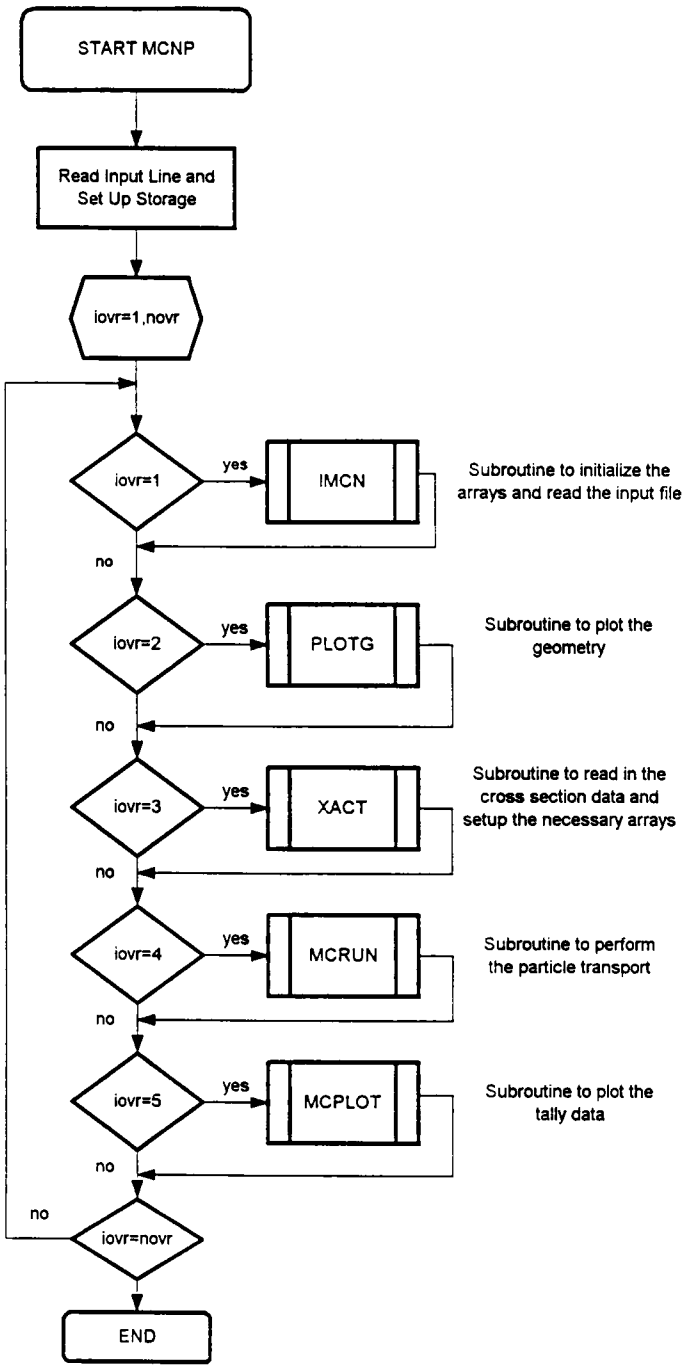

Figure 3.6 General MCNP4A Program Flow

noise calculation is read in IMCN. Appendix E contains an example of a typical input file and a description of the extra data file required to perform the noise calculation. After initializing the arrays, the interactive geometry plot subroutine PLOTG is called if the command line contains IP and the options to plot the geometry. Next, the cross section data are read into the appropriate arrays. Once the cross-section data have been placed in the arrays, the code begins the actual tracking of the particles by calling subroutine MCRUN. Subroutine MCRUN runs the particle histories by calling TRNSPT, which, in turn, calls HSTORY to follow the particle tracks throughout the system, and writes the detector information. Finally, the tallies are plotted with a call to MCPLOT after all the particles have been analyzed. This general structure has been maintained in the modified code. The major difference occurs in the actual transporting of the particles. The subroutine TRNSPT has been modified to call HSTORYCF if the noise calculation is to be performed.

The structure of the noise calculation is based on an outer and an inner loop. The outer loop controls the number of blocks of data (*bks*) to be calculated. The average number of source events per data block (*scd*) controls the inner loop. If the inherent spontaneous fission source option is invoked, there is a second inner loop that is controlled by the average number of inherent spontaneous fissions per block (*sfpd*). Because spontaneous fission is a Poisson process, the number of disintegrations per block (*ncdis*) is calculated from a Poisson distribution with mean *scd* for the source events per block and with mean *sfpd* for the inherent fission source fissions per block. The ratio of the ^{252}Cf source fission rate to the inherent source fission rate has to be known to specify *scd* and *sfpd*. Detected particles from induced fission caused by the inherent source neutrons contribute correlated information to G_{23} but also contribute uncorrelated

information to G_{12} and G_{13}. The average number of source events per data block is related to the actual source size by the following relation[10]

$$scd = \frac{m\, R_{sf}\, ntbn}{f_s}, \qquad (3.26)$$

where m is the mass of the source in micrograms, R_{sf} is the spontaneous fission rate of the source per microgram, *ntbn* is the number of points per block, and f_s is the sampling rate. Using this expression, the source specified in the calculation can be related to the actual source used in the measurements. For calculations employing the inherent fission source option, it has been shown that it is not necessary to use the actual R_{sf} but only maintain the ratio of *scd* and *sfpb*. The particle tracking begins with the first data block. First, the source particles and their progeny are tracked. Next, the particles from the inherent fission source and their progeny are tracked if this option is invoked. When the inner loops are finished, the block data are processed. This processing could be the direct calculation of the power spectral densities or the calculation of the correlation functions. After the block data have been processed, the outer loop variable is incremented and the inner loops are restarted. When all of the data blocks have been calculated, the outer loop is completed. The summary information is written to the output files, and if the data were processed in the correlation function mode, the power spectral densities are calculated and written to a file. This process is depicted in Fig. 3.7.

Since the inner loops control the actual particle transport, a detailed description of the particle tracking follows. The inner loop begins by obtaining information about the source particles. The position is specified in the extra data file for the source particles and is chosen randomly in a specified volume for the inherent fission source. The time of the spontaneous fission is chosen randomly in the data block. The number of particles from

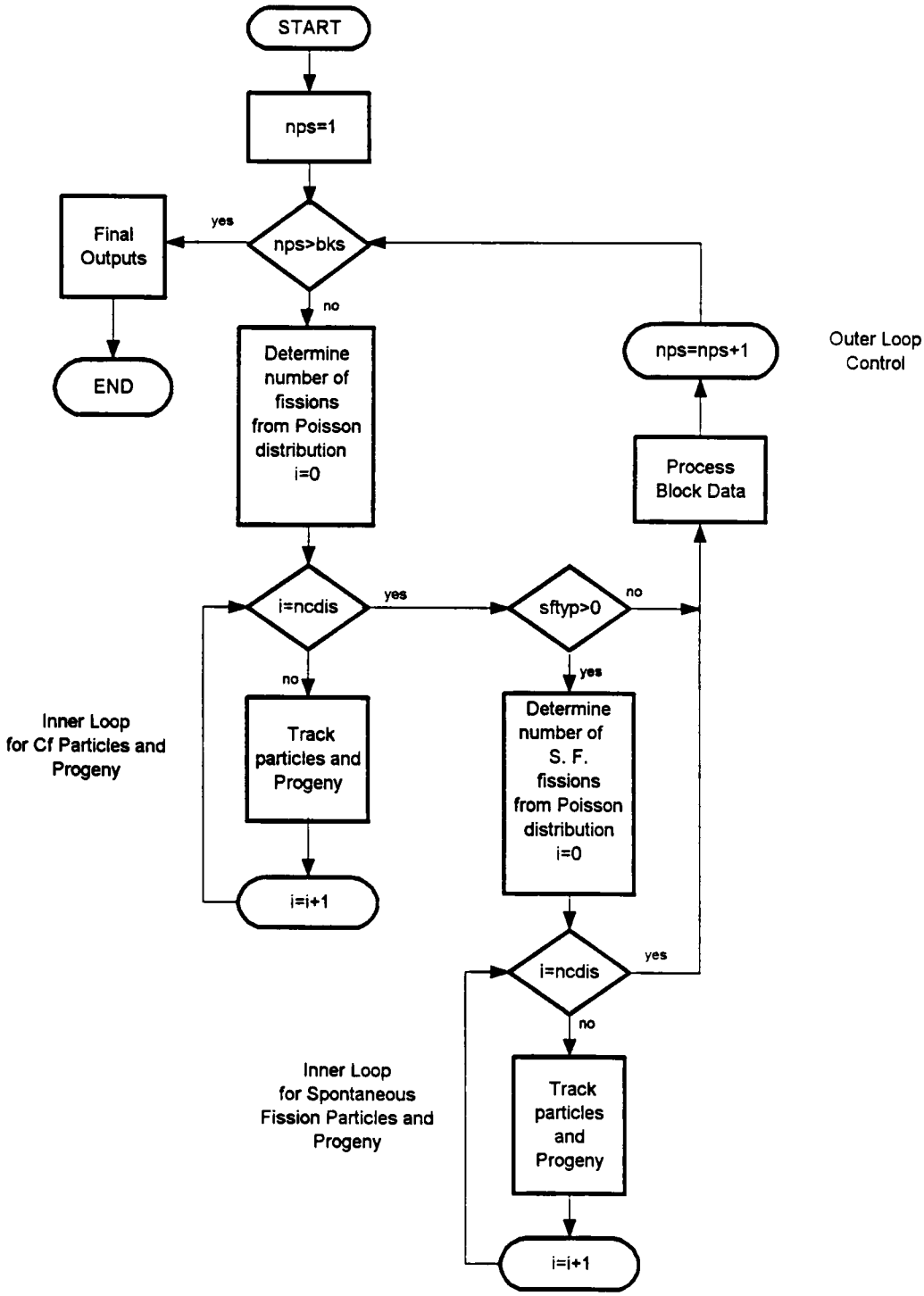

Figure 3.7 Structure of Inner and Outer Loops

the source is chosen randomly. Spencer's[22] distribution to is used to obtain the number of prompt neutrons from the ^{252}Cf source, and Brunson's[28] distribution is used to determine the number of prompt gamma rays from the ^{252}Cf source. Terrell's[20] formula is used to determine the number of prompt neutrons from the inherent spontaneous fission source. The energies of the ^{252}Cf neutrons are chosen from the corrected Maxwellian distribution, and the energies of the ^{252}Cf photons are chosen from Maienschein's spectrum. The energy spectra of the inherent fission source neutrons are chosen from the usual MCNP Watt fission spectrum. The direction of the source neutrons can be chosen isotropically or from the angular distribution data of Budtz-Jorgensen and Knitter. The particles are stored in the bank to be tracked. An overview of the particle tracking is shown schematically in Fig. 3.8. The distance to the cell boundary, d_b, is determined from the particle's starting location and the direction cosines. Next, the distance to the collision site, d_c, is calculated from

$$d_c = \frac{-\ln(R)}{\Sigma_t}, \qquad (3.27)$$

where R is a random number and Σ_t is the total macroscopic cross section. The minimum distance determines whether or not the particle has a collision. If d_b is less than d_c, the particle is transported through the cell boundary, where the distance to the next cell boundary and the distance to collision are calculated for the new cell. If the particle enters a region of zero importance (outside the system), the particle is said to have leaked, and the leakage tallies are updated. If the d_c is less than d_b, then the particle collides in the cell. When a particle collides, the collision nuclide is selected randomly from the materials present in the cell. If the particle is a neutron, the velocity of the collision nuclide is calculated, and the collision event is determined. The neutron is lost by analog

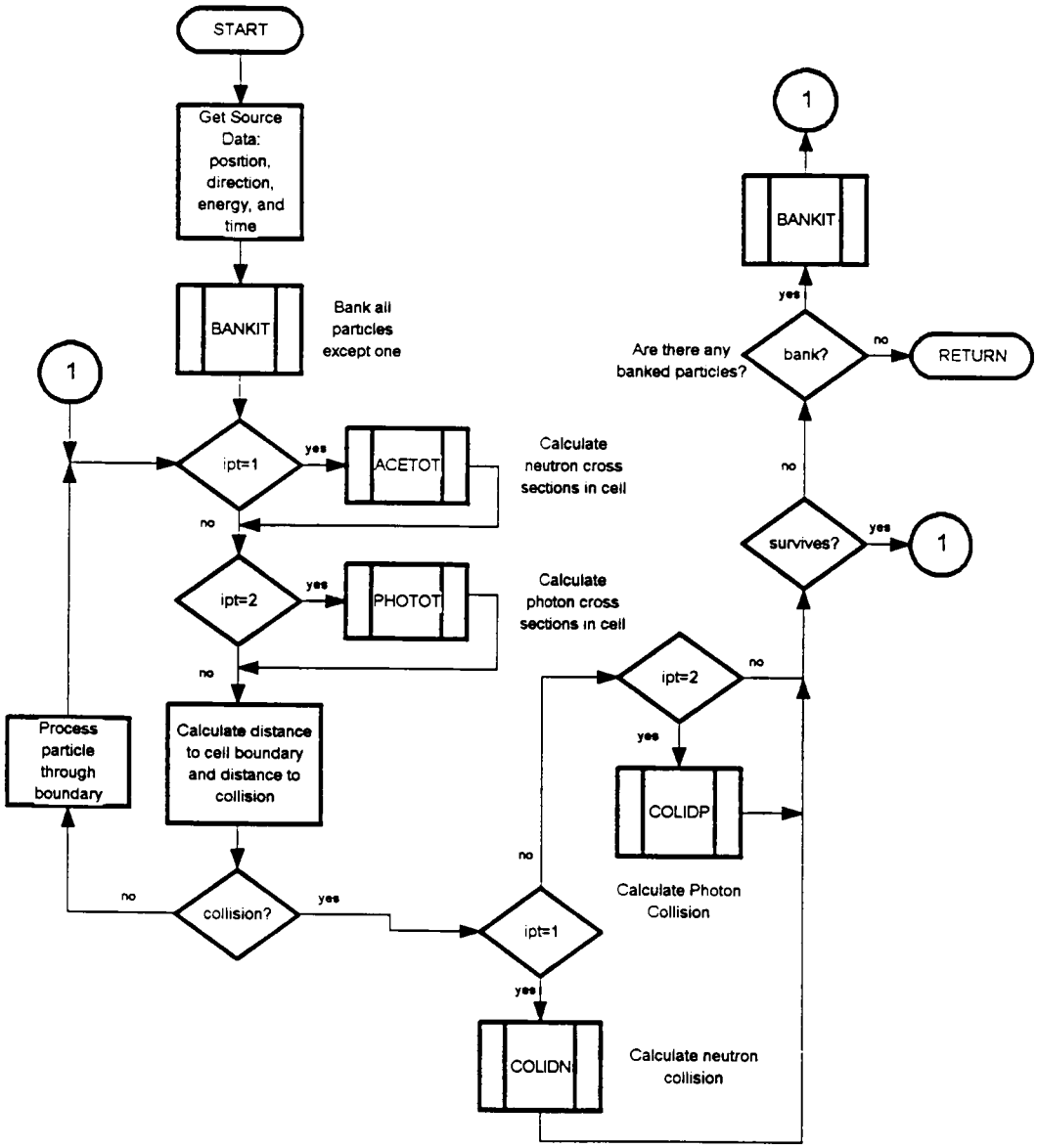

Figure 3.8 Particle Tracking Procedure

capture with probability σ_a/σ_t where σ_a is the microscopic absorption cross section and σ_t is the microscopic total cross section. If the problem is a dual neutron-photon calculation, photons are produced by the neutron interaction. If the particle is not lost by analog capture, the neutron will have either an elastic collision or an inelastic collision. The probability of having an elastic collision is given by $\sigma_{el}/(\sigma_{el}+\sigma_{in})$ where σ_{el} is the microscopic elastic scattering cross section and σ_{in} is the microscopic inelastic cross section. The type of inelastic event, n, is determined from

$$\sum_{i=1}^{n-1} \sigma_i < \xi \sum_{i=1}^{N} \sigma_i \leq \sum_{i=1}^{n} \sigma_i, \qquad (3.28)$$

where ξ is a random number on the interval $[0,1)$, N is the number of inelastic reactions, and the σ_i's are the inelastic reaction cross sections at the incident neutron energy.[12] If the inelastic event is fission, the number of neutrons produced from fission is determined from Zucker and Holden's data or from Terrell's formula, depending on the fissioning isotope. The energy of the emerging neutrons is sampled from the appropriate spectrum indicated in the cross-section data file. The direction cosines may be either isotropic or determined from the experimental angular distribution data. Any neutrons produced from fission are banked to be tracked later.

If the particle is a photon, the selection process of the collision nuclide is the same as that used for neutron collisions. However, the collision physics are different.[12] In the modified code the detailed physics treatment is used by default. The detailed physics treatment includes incoherent scattering, coherent scattering, the photoelectric effect with possible florescence, and pair production. Therefore, the total photon cross section, σ_t, is

$$\sigma_t = \sigma_{IC} + \sigma_{CO} + \sigma_{pe} + \sigma_{pp}, \qquad (3.29)$$

where σ_{IC} is the incoherent scattering cross section, σ_{CO} is the coherent scattering cross section, σ_{pe} is the photoelectric cross section, and σ_{pp} is the pair production cross section. The selection of the photon event is determined in a similar manner to the neutron events. If the event is the photoelectric effect, fluorescence photons are banked for later transport.

The tracking and collision process is repeated for each particle until the particle either leaves from the system or is absorbed by analog capture. Next, particles are retrieved from the bank, and the tracking process proceeds as before until all the source particles have been tracked for the given data block. Then, the particles for the inherent fission source are tracked if the spontaneous fission source option is invoked. The inner loops are now complete for one data block, and the detector responses are then processed. After processing the detector responses, the outer loop variable is incremented, and the inner loop procedure is repeated. After the desired number of blocks has been calculated, the program calculates the final estimates of the APSDs and CPSDs and writes the data to a file.

3.6 Analog Criticality Calculation

Since MCNP already contained an option to calculate the neutron multiplication factor of a fissile assembly, there were very few changes made to the code in order to perform an analog criticality calculation. The weighting and biasing options were disabled. The number of neutrons from fission is sampled using Terrell's formula, which employs the total $\overline{\nu}$ in order to include the effects of delayed neutrons on k_{eff}. This approximation modifies the neutron distributions to give the correct average value of $\overline{\nu}$, including delayed

neutrons. The angular distribution of neutrons from fission may also be used in the calculation of the neutron multiplication factor. A complete description of the flow of the criticality calculation can be found in the MCNP documentation[12] and is only summarized here.

The k_{eff} calculation entails generating a given number of source particles for the first k_{eff} cycle. These particles are transported through the MCNP geometry using the standard random walk procedure except that fission is treated as analog capture. The collision sites where fission is possible are used as the source starting points for the next cycle. After a specified number of cycles, k_{eff} is estimated using a collision estimator, an absorption estimator, a track length estimator, and various combinations of these estimators. A description of these estimators can be found in the MCNP documentation. After completion of all of the desired cycles, the final estimates of k_{eff} are obtained and written to the output file.

To compare the results of the analog criticality calculation with the standard MCNP criticality calculation, a uranyl nitrate solution system was analyzed. A detailed description of this system is included in Chap. 5. The results of these calculations are provided in Table 3.1. As can be seen, there are only statistical differences between the results obtained from the analog calculation and those obtained from the standard MCNP calculation.

Table 3.1 Calculated k_{eff} Values for the Uranyl Nitrate Solution System Using the ENDF/B-IV Cross Sections

Solution Height (mm)	Nominal Source Size	Number Skipped Cyles	Number Calculated Cyles	Standard k_{eff}	Analog k_{eff}
292	2000	10	1000	0.9544 ± 0.0008	0.9553 ± 0.008
258	2000	10	1000	0.9242 ± 0.0007	0.9254 ± 0.0007
203.2	2000	10	1000	0.8516 ± 0.0007	0.8520 ± 0.0007
153	2000	10	1000	0.7407 ± 0.0007	0.7405 ± 0.0007
101.2	2000	10	1000	0.5467 ± 0.0007	0.5471 ± 0.0007

CHAPTER 4

VALIDATING MCNP-DSP

4.0 Computer Code Validation

The principal means of validating a computer code is by direct calculation of measured observables or by calculating parameters that have a precise value known from accepted theoretical models. Several calculations were performed to validate the neutron and photon spectra of the spontaneous fission of ^{252}Cf, the detection process, the timing of the detection process, the time and frequency response calculations, and the alternate way of processing the detector responses. Calculations were also performed to validate certain properties of the ratio of spectral densities. The comparison of the calculated frequency analysis parameters to the measured frequency analysis parameters is presented in the next chapter to verify the code's ability to calculate the frequency analysis parameters of the ^{252}Cf-source-driven noise analysis method.

4.1 Energy Spectra and Detection Process Validation

The validation of the neutron and photon spectra and the validation of the detection process are obtained by performing a calculation with the source separated from a detector in air. The time distribution of counts in the detector after the spontaneous fission of ^{252}Cf is directly related to the neutron energy spectra. Experimentally, measurement of the time distribution of counts is used to verify that the detection equipment is functioning properly. In order to validate the neutron and photon energy spectra and the detection process, a measurement and a calculation were performed with the source placed 1105 mm away from the detector in air. The detector used in these

measurements and in these calculations is a proton recoil liquid organic scintillator that has a 114.3-mm OD and is 57.2 mm thick. In the calculation, the neutron threshold was set to 0.8 MeV, and the photon threshold was set to 0.1 MeV. Figure 4.1 is comparison of the measured and calculated neutron response as a function of time after ^{252}Cf fission. The calculated neutron response in counts per ^{252}Cf fission per Δt is in excellent agreement with the measured response expressed in the same units. This result indicates that the neutron energy spectra from fission used in this calculation is a good representation of the measured spectra and that the neutron detection process is adequately represented. The threshold is defined experimentally as the neutron energy at which the efficiency is half its maximum value. In the measurements, the detector efficiency curve rolls off to zero around 0.5 MeV. This allows for a small number of low-energy neutrons to be detected; therefore, there will be a slight difference between the measured and calculated response at the longer times. This is evident in Fig. 4.1 around 100 ns. The measured and calculated photon responses are shown in Fig. 4.2. Since the calculated photon response does not suffer from the lack of time resolution that occurs in these measurements, the photon peak obtained from the calculation is much more narrow than that obtained in the measurement, as is evident in the Fig. 4.2. The timing uncertainty in the measured response is due to the uncertainties in the measurement of the time of ^{252}Cf fission and the time of detection. Nonetheless, the area under the curves should be equivalent. The areas under the measured and calculated curves are the same, thus validating the photon energy spectra and the photon detection process. The photon energy spectra is considered validated because the photon threshold used in the calculation is the same as the threshold of the detectors used in the measurement and the areas of the photon responses are the same. Because all photons travel at the speed of light, the

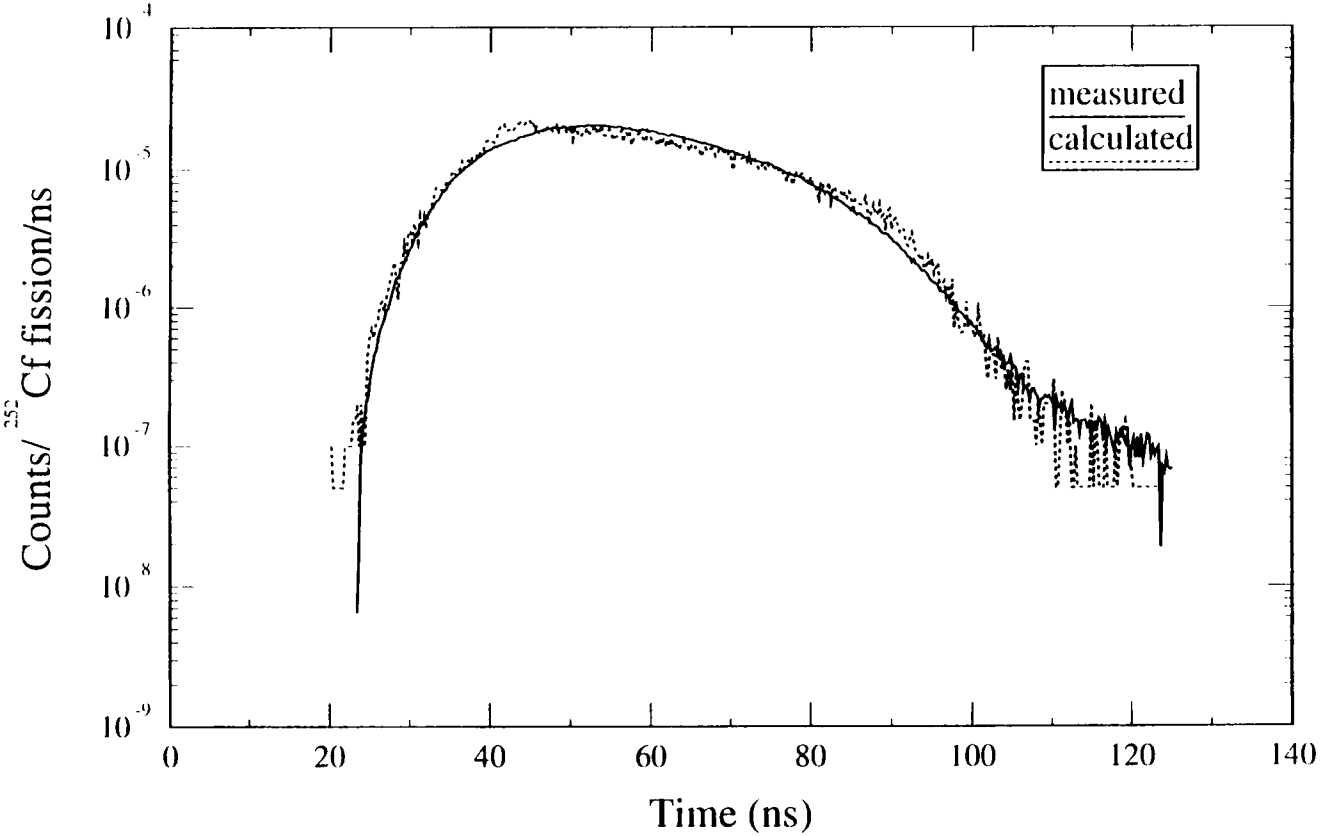

Figure 4.1 Calculated and Measured Neutron Response for Source and Detector in Air

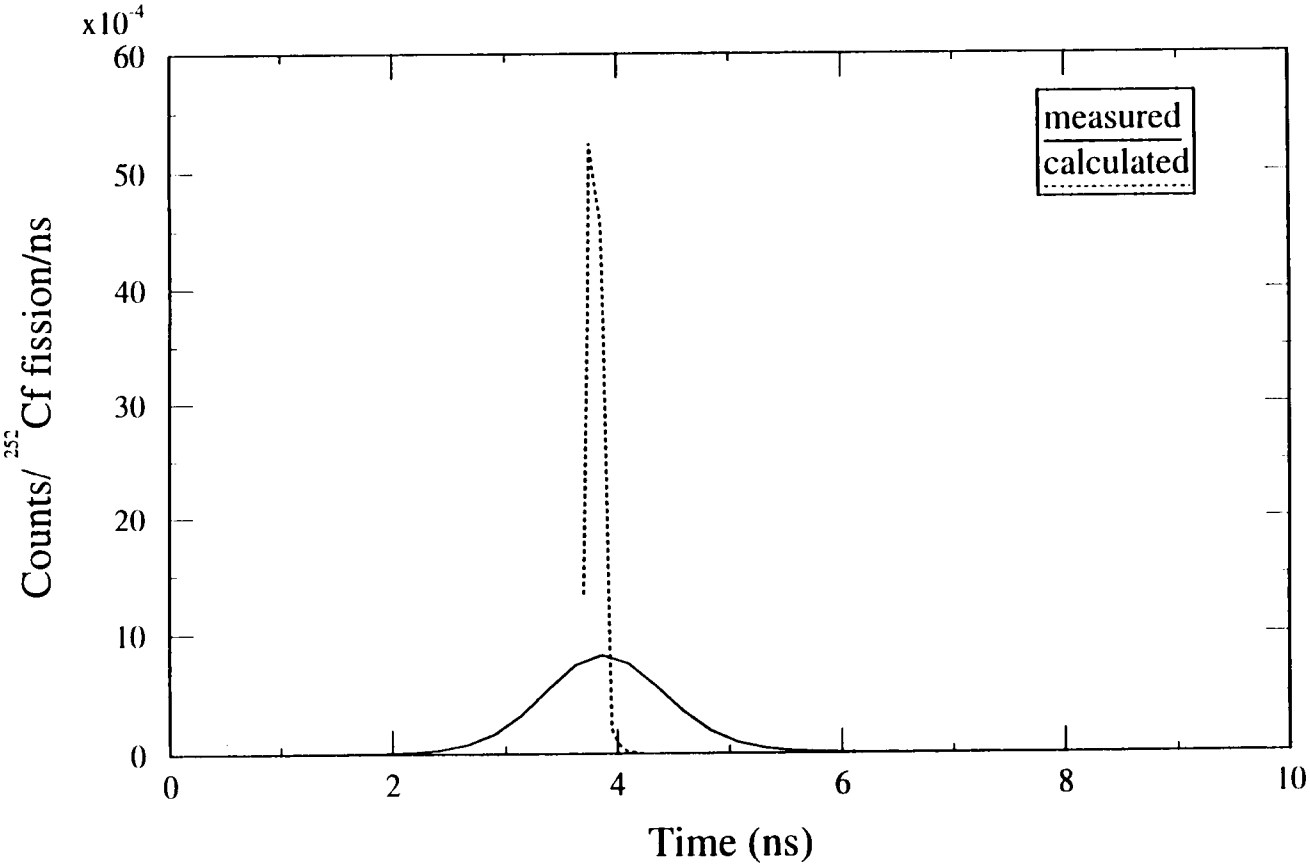

Figure 4.2 Calculated and Measured Photon Response for Source and Detector in Air

time of arrival of the photons at the detector is known precisely. For the given source-detector configuration, the time of arrival of the photons is 3.72 ns; consequently, this time corresponds to the photon peak in the calculation. From this test, it is evident that the neutron and gamma ray spectra are very good representations of the actual spectra and that the particle detection process for this type of detector is adequately represented, thus confirming the simplifying assumptions made for this type of detector.

4.2 Time Response Validation with Attenuating Media

To obtain an accurate representation of the detector responses from particles traveling through an attenuating medium, the time of detection needs to be calculated precisely and the cross-section data need to be adequate. In order to test the detector time response when material is placed between the source and the detector, a calculation was performed with a 36.3-mm-thick piece of beryllium metal placed between the source and the liquid scintillator, as shown in Fig. 4.3. Beryllium metal was chosen because the total cross section of beryllium is well known and has a well-characterized resonance at 2.78 MeV. The total cross section has been measured using the given source and detector configuration.[36] The detector response in counts per ^{252}Cf fission per Δt is shown in Fig. 4.4. The depression in the detector response near 44 ns corresponds to the resonance in the total cross section at 2.78 MeV. This is verified by calculating the energy of the neutrons, which travel 1010 mm in 44 ns.

A second calculation was performed to analyze the attenuating properties of concrete. The experimental configuration of the concrete block is shown in Fig. 4.5. The concrete block is 142.9 mm wide, 298.5 mm long, and 203.2 mm high. The concrete as mixed has a density of 2.4 g/cm^3 and is composed of 20 wt% cement, 8 wt% water, and 72 wt% limestone. A carbon steel plate was placed on each end of the block. These

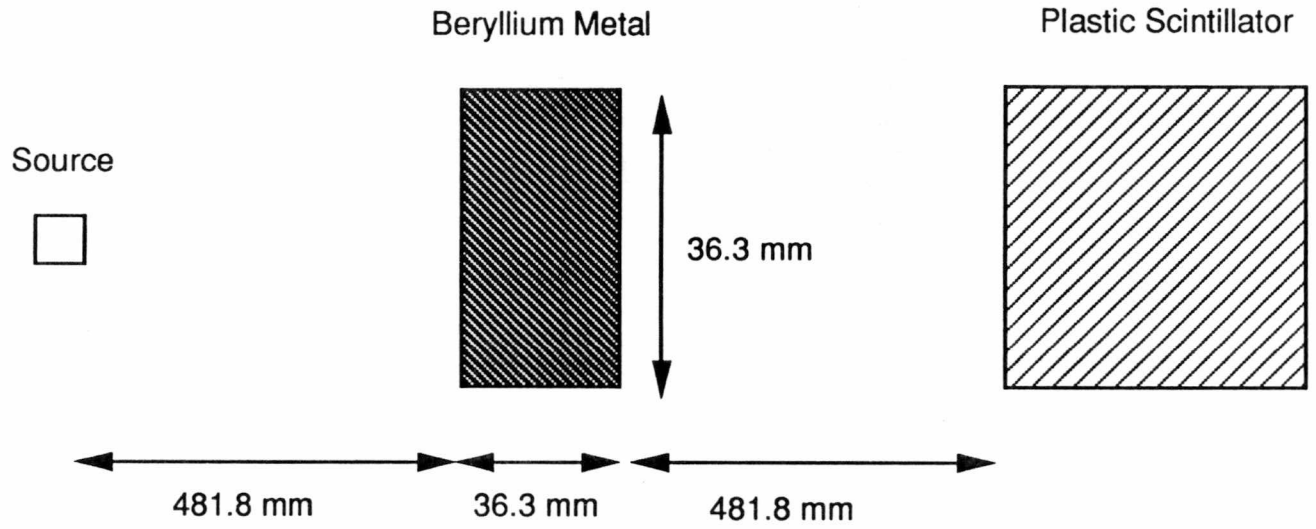

Figure 4.3 Sketch of Model for Beryllium Attenuation Calculation

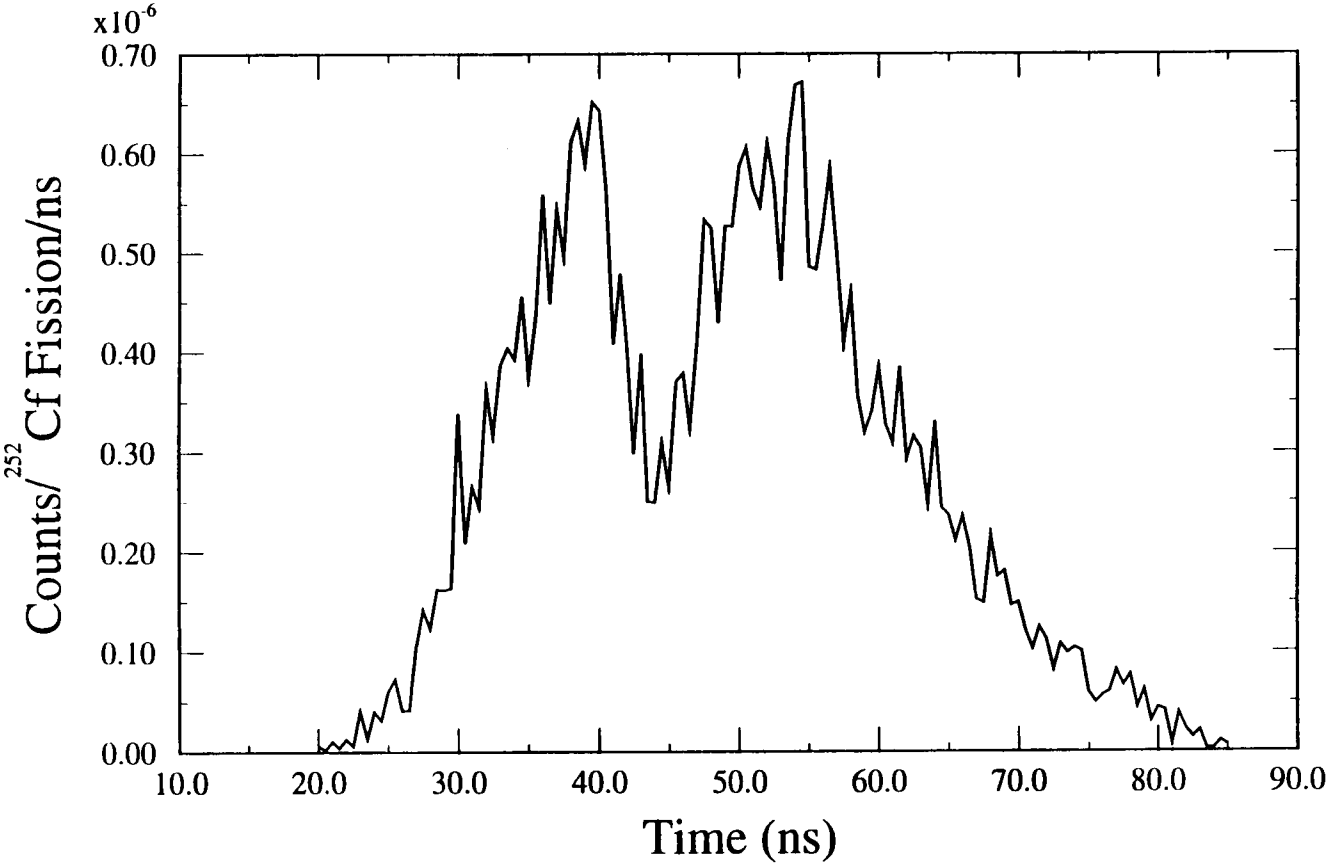

Figure 4.4 Calculated Neutron Attenuation for Beryllium Metal Cylinder

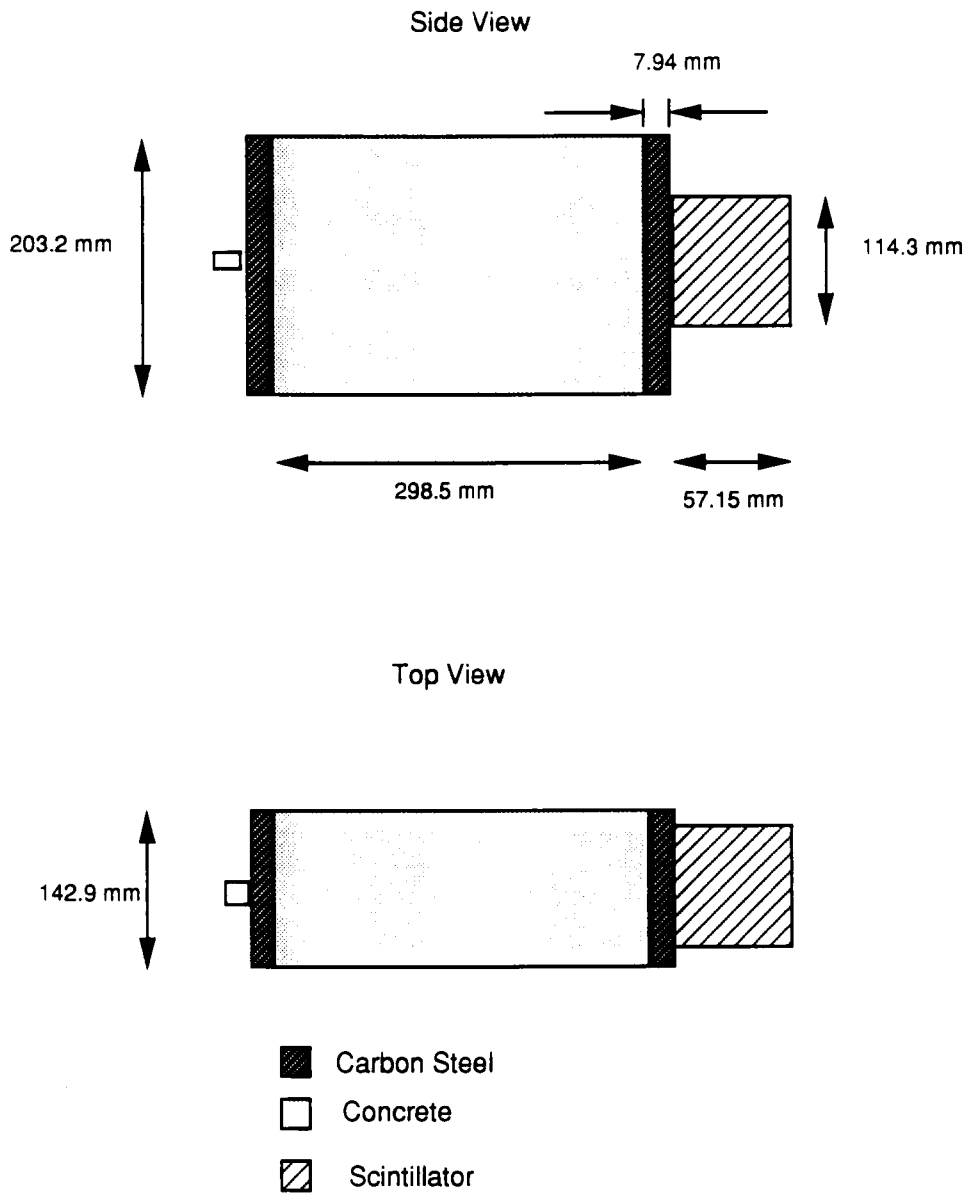

Figure 4.5 Sketch of Model for Concrete Block Attenuation Calculation

plates were 7.94 mm thick, 142.9 mm wide, and 203.2 mm high. These plates produced a unique gamma ray response in the measurement because of gamma rays produced from the inelastic neutron scattering in iron. The detector used in the measurement and in the calculation is a liquid scintillator. The detector has a 114.3 mm diameter and is 57.15 mm long. In the calculation, the neutron threshold was set to 0.8 MeV, and the photon threshold was set to 0.1 MeV. The selection of the neutron threshold is determined from the detector efficiency as a function of energy, while the photon threshold is determined using a ^{137}Cs source with a known gamma ray energy of 0.662 MeV. The measured and calculated detector responses are provided in Figs. 4.6 and 4.7. The time distribution of counts for the neutrons is in excellent agreement with the measured response. The small difference near 50 ns may again be due to the sharp threshold used in the calculations. The depression in the neutron response around 13 ns is due to resonances in ^{16}O around 2.5 MeV. The results for the photon calculation are not as good as those for the neutron calculation. The differences between the measured and calculated gamma ray response have not been resolved.

4.3 Frequency Response Test

In order validate the computation of the frequency spectra, the Fourier processing routines had to be validated. A simple procedure to test the processing routines is to perform a noise calculation with the ^{252}Cf source placed between the detectors. This test is frequently used to ensure that the measurement system is working properly. The ratio of spectral densities, $R(\omega)$, has a well defined value for this particular source-detector configuration. The measured ratio of spectral densities is theoretically equal to the inverse of the Diven factor for the ^{252}Cf source. If all of the ^{252}Cf neutrons were detected, the measured ratio would be precisely equal to the inverse of the Diven factor.[16] The Diven

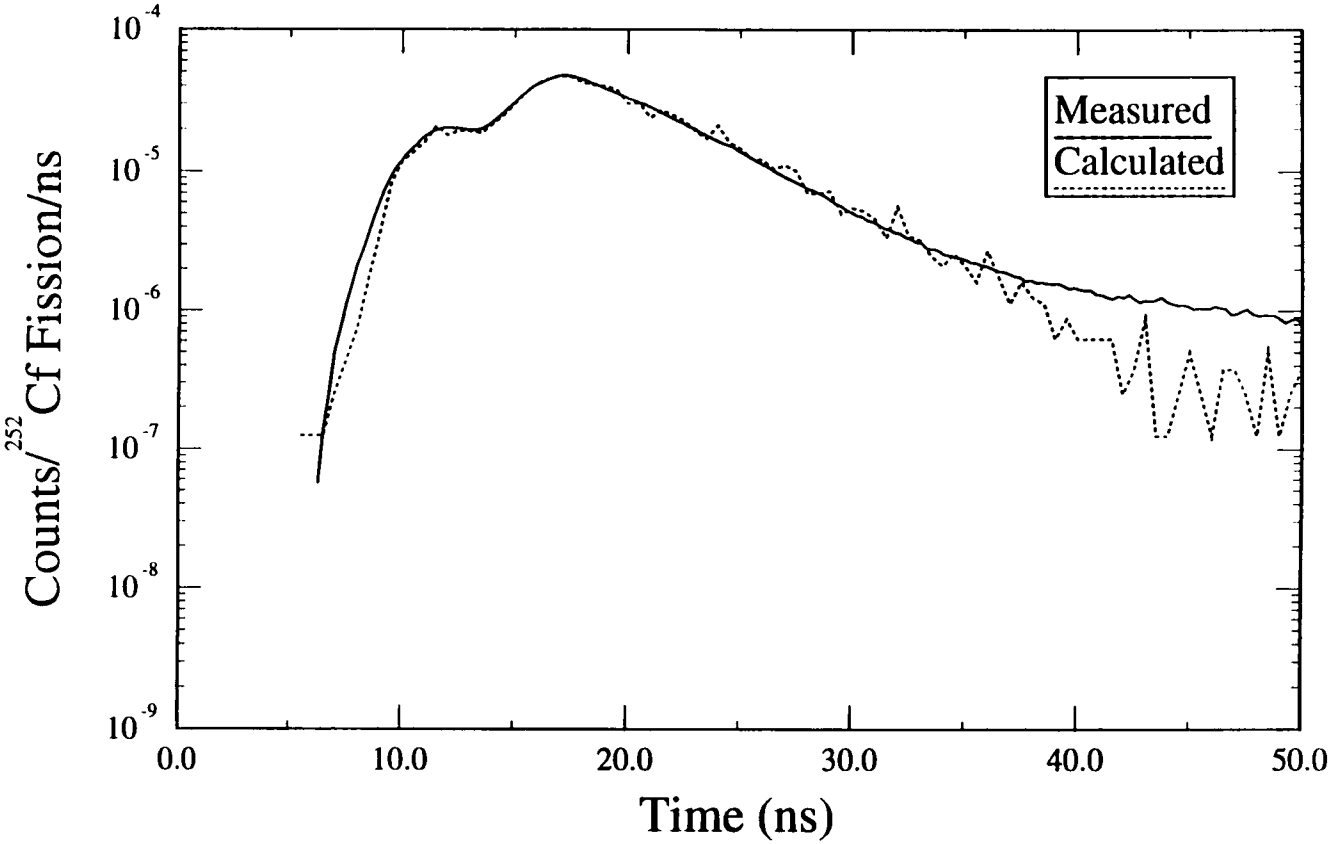

Figure 4.6 Calculated and Measured Neutron Attenuation for Source and Concrete Block Geometry

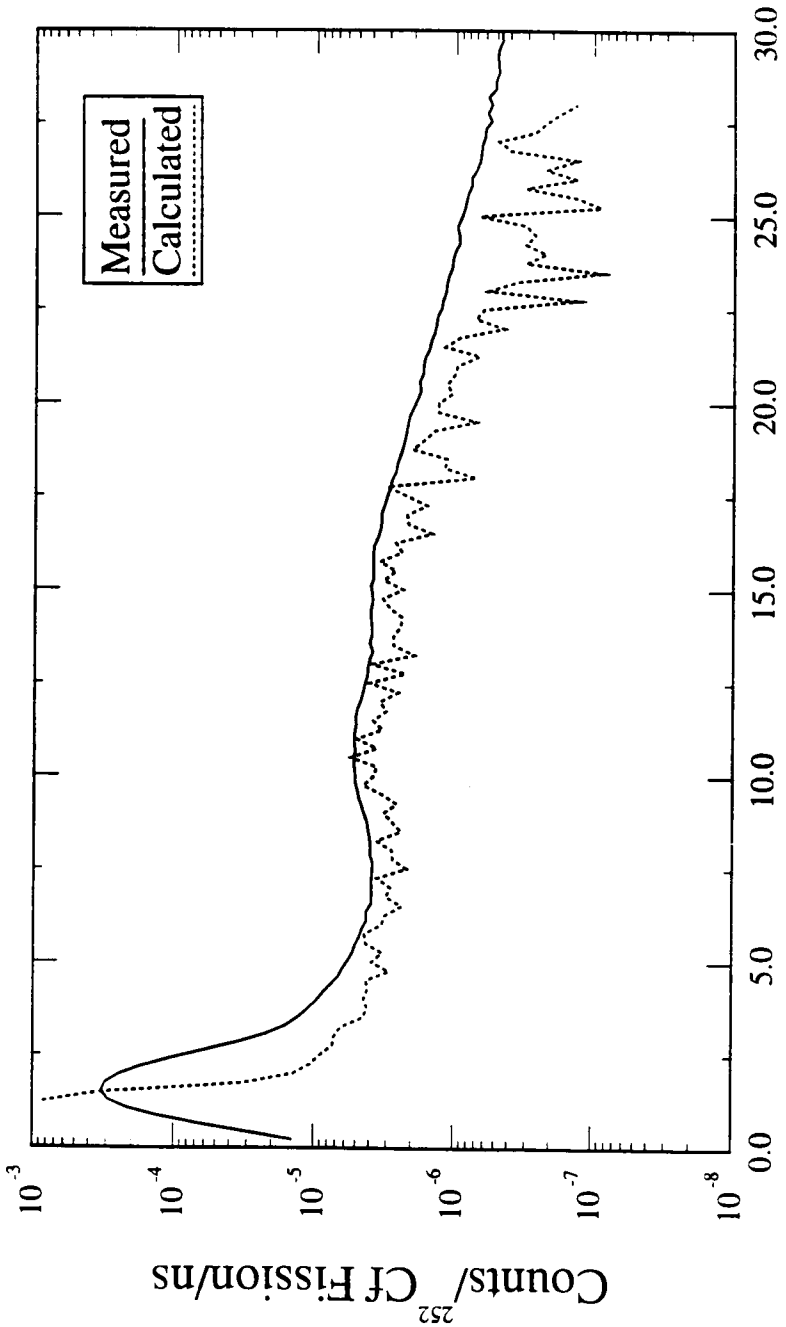

Figure 4.7 Calculated and Measured Photon Attenuation for Source and Concrete Block Geometry

factor for the ^{252}Cf source from Spencer's data is equal to 0.846. This results in the ratio of spectral densities being approximately 1.18. The detectors used for this calculation were ^{3}He detectors in which the gas pressure was 3000 atm in order to detect all neutrons from the source. For this particular source-detector configuration, the calculated value of the ratio of spectral densities is 1.181 ± 0.001 using highly absorbing neutron detectors. If neutron scattering detectors were used in the analysis, the ratio would be less than 1.18 because of those neutrons that would scatter from one detector to another, thus increasing the coherence between detectors and reducing the ratio of spectral densities. This effect occurs experimentally using proton recoil scintillators. A similar calculation was performed for the gamma rays. The theoretical value of the ratio of spectral densities for the gamma rays is 0.966, obtained from the Diven-like factor obtained from Brunson's data for gamma ray emission from ^{252}Cf. A calculation was performed placing the source between two large pieces of lead which were treated as the detectors. The calculated value of the ratio of spectral densities is 0.956 ± 0.002. The 1% difference between the theoretical and the calculated value is attributed to gamma rays that scatter between detectors thus increasing the coherence between detectors and reducing the ratio of spectral densities. These tests indicate that the Fourier processing routines, which obtain the spectra by directly Fourier transforming the detector time responses, are correct.

4.4 Direct or Indirect Frequency Analysis Calculations

Because there are two ways to process the detector signals, both methods for processing the detector time responses should produce essentially the same results. To perform this analysis, a 108.17-mm-high uranium metal cylinder with a 177.71-mm diameter was analyzed with detectors of varying size. The uranium metal had a density of 18.76 g/cm^3 and consisted of 93.15 wt% ^{235}U, 5.64 wt% ^{238}U, 0.97 wt% ^{236}U, and 0.24 wt%

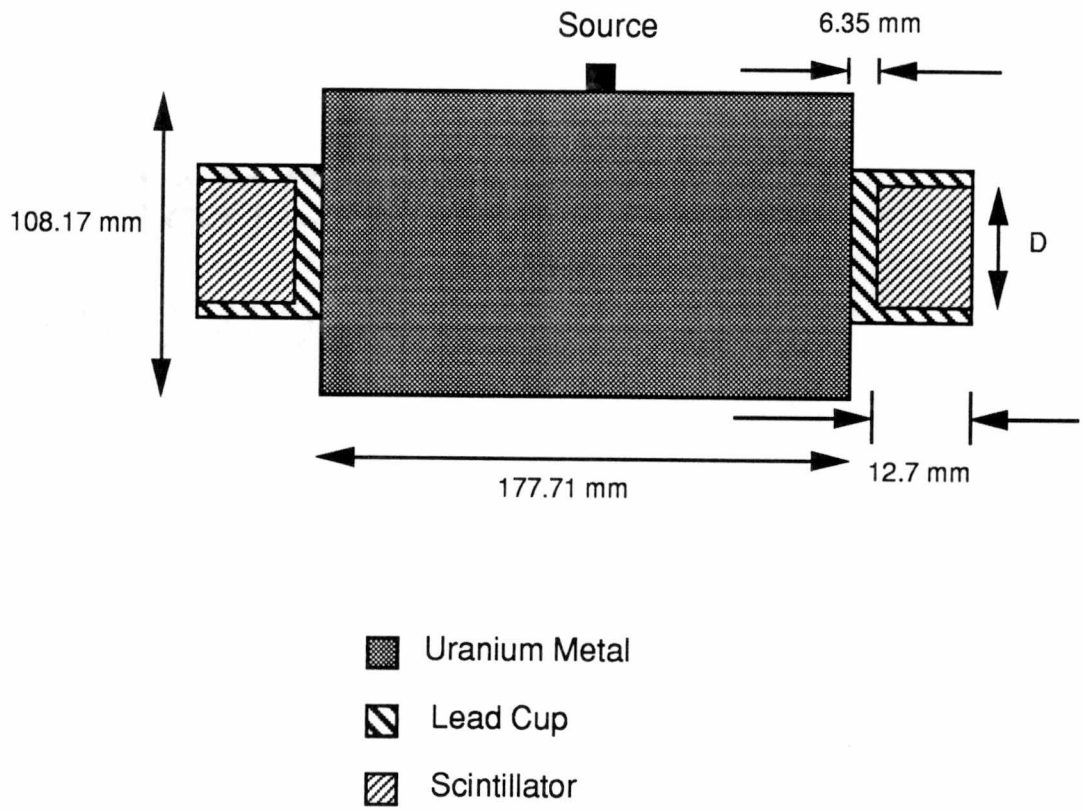

Figure 4.8 Sketch of 108.17-mm-High Uranium Metal Cylinder

^{234}U. The detectors used in the calculation are plastic scintillators surrounded by a 6.35-mm-thick lead cup. The detectors were symmetrically positioned adjacent to the radial surface at the midplane, while the source was located on top of the cylinder on the centerline. This configuration is shown in Fig. 4.8. By varying the detector diameter, the coherences between the detectors will change. A comparison of the low frequency values of the coherences and the ratio of spectral densities obtained from both methods are presented in Tables 4.1 and 4.2. As can be seen from these results, the low frequency values of the coherences are independent of the way in which the data were processed; therefore, the ratio of spectral densities does not depend on the way in which the data were processed. Figure 4.9 contains a comparison of the coherence between the source and detectors obtained by directly Fourier transforming the detector signals and that obtained by Fourier transforming the cross-correlation function. Figure 4.10 is a comparison of the coherence between detectors for the two processing methods. As can be seen in Figs. 4.9 and 4.10, there is no statistically significant difference between the two methods of processing the data. Additional comparisons of the two processing methods are presented in Appendix F. The major difference in the two methods is the time required to obtain a given number of data blocks. As presently implemented, it takes twice the amount of time to calculate the correlation functions than it takes to calculate the direct fast Fourier transforms; therefore, the rest of the calculations in this work are performed using the direct Fourier processing method unless otherwise stated.

In measurements, which Fourier transform the data blocks, estimates of the spectra are obtained by complex multiplication of the data blocks that are then averaged with the previous data blocks. In this process, the detector signals are AC coupled, thus removing the DC part of the signal. In the calculation the background is subtracted block by block

Table 4.1 Low Frequency Values of Calculated Coherences Obtained by Direct Fourier Processing of Detector Responses			
Detector Diameter (mm)	Number of Data Blocks	γ_{12}^2	γ_{23}^2
50.8	5000	0.0174 ± 0.0007	0.137 ± 0.002
25.4	25000	0.00641 ± 0.00016	0.0130 ± 0.0021
10.37	200000	0.00110 ± 0.00002	0.00039 ± 0.000011
4.234	200000	0.000189 ± 0.000007	0.0000114 ± 0.0000006

Table 4.2 Low Frequency Values of Calculated Coherences Obtained by Calculating the Fourier Transform of the Correlation Functions			
Detector Diameter (mm)	Number of Data Blocks	γ_{12}^2	γ_{23}^2
50.8	5000	0.0174 ± 0.0007	0.137 ± 0.002
25.4	25000	0.00649 ± 0.00016	0.0131 ± 0.0021
10.37	200000	0.00110 ± 0.00002	0.00039 ± 0.000009
4.234	200000	0.000190 ± 0.000010	0.0000114 ± 0.0000006

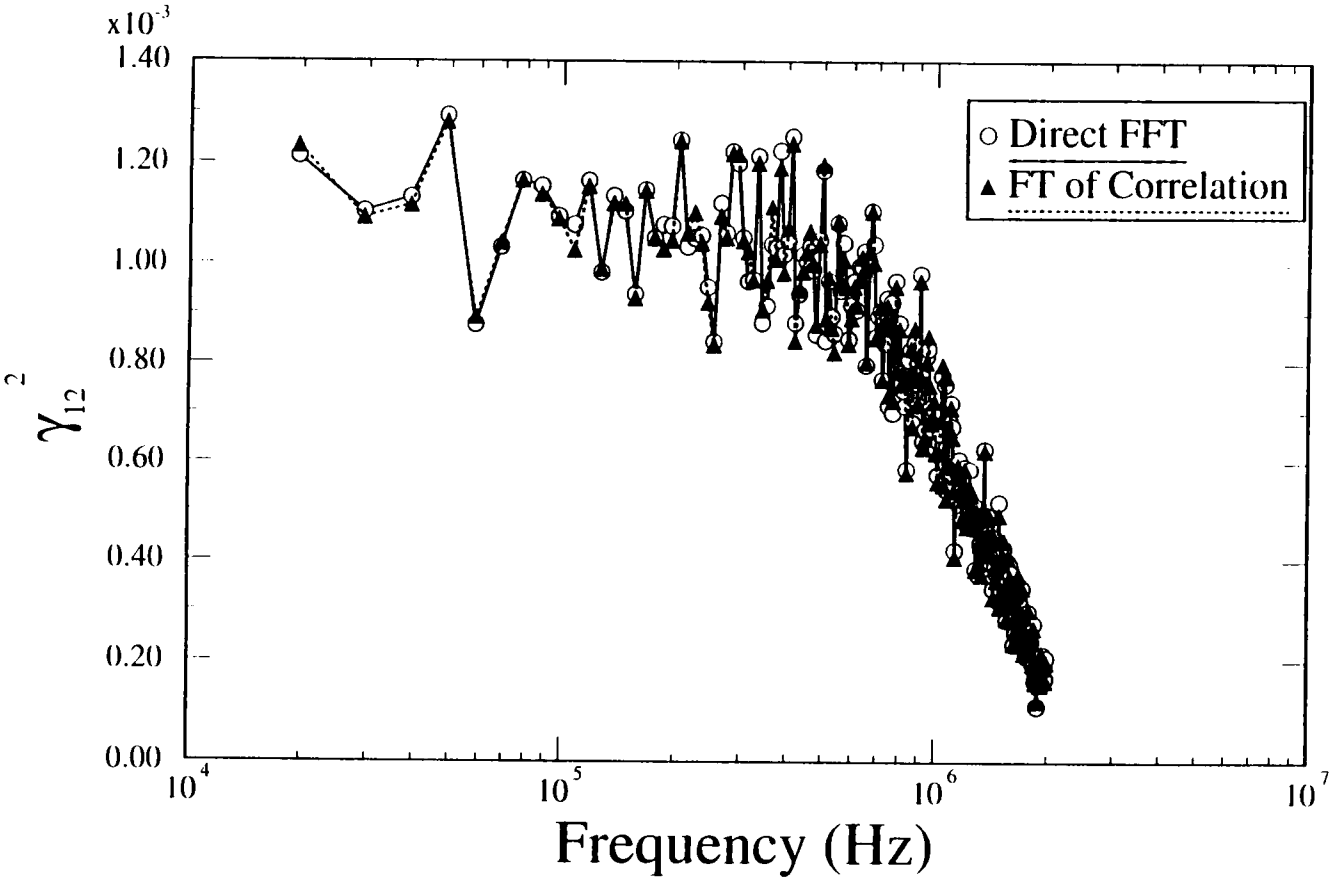

Figure 4.9 Comparison of γ_{12}^2 Between the Direct FFT of the Detector Response and the Fourier Transform of the Correlation Function

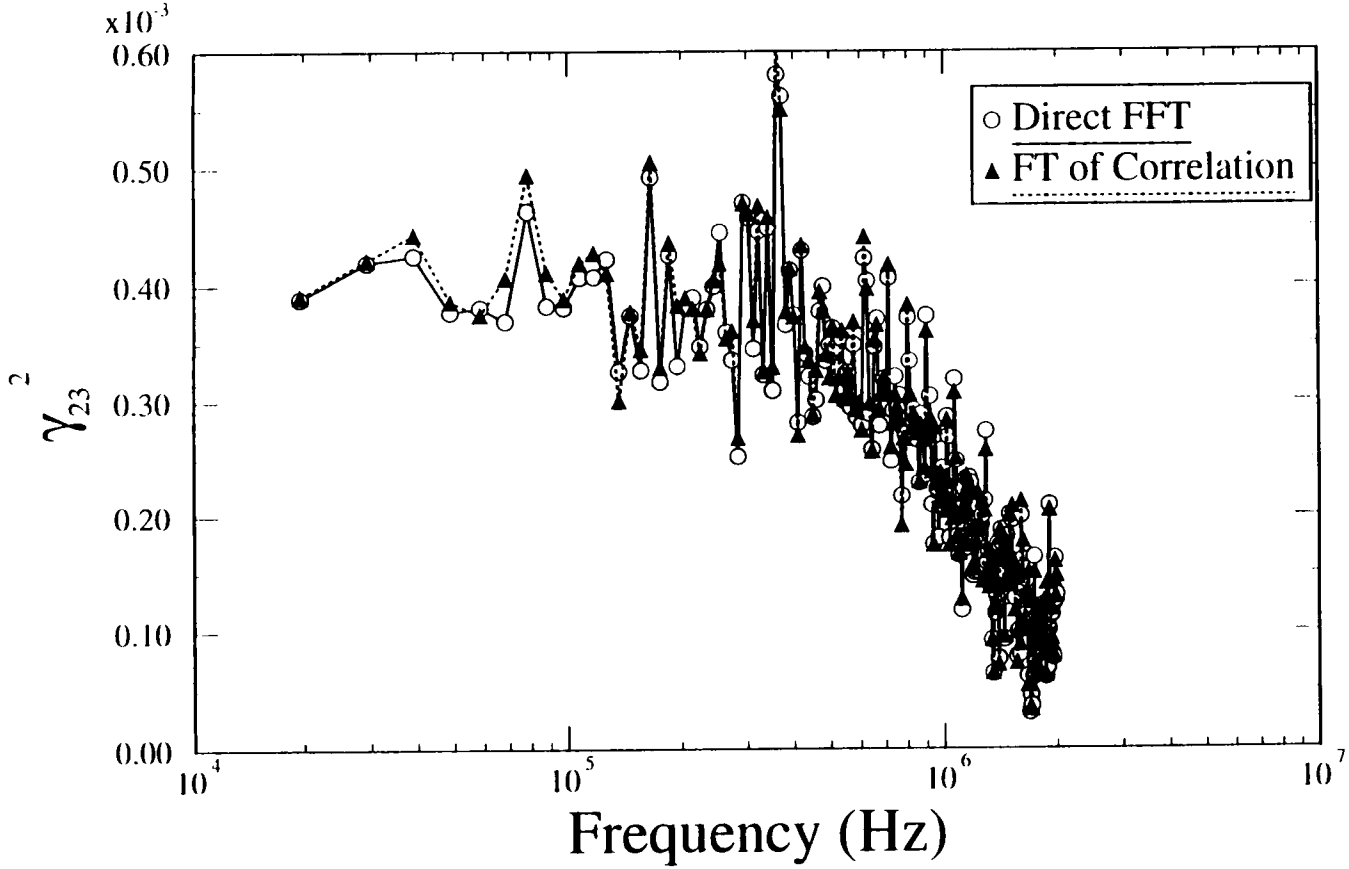

Figure 4.10 Comparison of γ_{23}^2 Between the Direct FFT of the Detector Response and the Fourier Transform of the Correlation Function

and is the equivalent of *AC* coupling. In indirect Fourier processing where the autocorrelation and cross-correlation functions are obtained, these functions contain a background or *DC* component that after Fourier transforming, appears only as zero frequency components of the CPSDs. In this way, the CPSD has no background for $\omega > 0$, as is the case for the direct Fourier transform method. A question arises as to any differences in the error of the coherence functions with the same number of data blocks for the two methods. The errors for both methods are the same for the same number of data blocks. This means that processors using the indirect method will produce data as accurately as direct Fourier processing.

4.5 Analysis of the Ratio of Spectral Densities

There are certain known properties of the ratio of spectral densities confirmed by measurements that allow for the validation of the calculational procedure. The low-frequency value of the ratio of spectral densities has been shown to be dependent on the placement of the detectors.[16] However, the low-frequency value of the ratio of spectral densities is independent of the detector efficiency and of the ^{252}Cf source strength for systems with no inherent fission source.

To show that the ratio of spectral densities is affected by the location of the detectors, a calculation was performed with detectors spaced 200 mm from the source at 90° angles to each other in a vacuum. This spacing was chosen to have a small solid angle and to ensure that no particles scattered from one detector into another. Table 4.3 contains a comparison of the ratio of spectral densities for detectors positioned at 90° and 180° from each other. The results show that the ratio of spectral densities is affected by the position of the detectors due to the angular distribution of neutrons from the spontaneous fission of ^{252}Cf. For the detector 180° apart, the probability of a count in the

Table 4.3 Angular Distribution Effects on Ratio of Spectral Densities for Source and Detectors in a Vaccuum				
Angle (Degrees)	Number of Data Blocks	γ_{12}^2 ($*10^{-3}$)	γ_{23}^2 ($*10^{-4}$)	R(ω)
90	1200000	8.98 ± 0.02	0.213 ± 0.009	2.07 ± 0.05
180	1200000	8.98 ± 0.03	5.12 ± 0.04	0.398 ± 0.002

second detector after a count in the first detector is enhanced because of the angular distribution data since the angular distribution data have a strong back-forward asymmetry.

To test the insensitivity of the ratio of spectral densities to the source strength and the detector efficiency, several calculations were performed for the 292-mm-high uranyl nitrate solution in a 251-mm-ID cylindrical tank. A detailed description of this geometry can be found in Chap. 5. This system was selected because the detection efficiency could be changed without changing the physical size of the detectors and because the measured value of $R(\omega)$ is available for comparison purposes. The analyses were done for neutrons since the ratio of spectral densities from the photon response is calculated with the same routines that are used to calculate the ratio of spectral densities with the neutron response.

To demonstrate that the ratio of spectral densities is independent of the source size, the number of source disintegrations per data block was altered. This corresponds to altering the mass of the ^{252}Cf source. The results of these calculations are given in Table 4.4. As is evident from these results, the ratio of spectral densities indeed is not dependent on the source strength as has been verified by measurements with uranium systems. To demonstrate that the ratio of spectral densities is independent of the detector efficiency, several calculations were performed by varying the neutron threshold of the detector. By increasing the neutron threshold, the number of neutrons that contribute to the detector response is reduced. Table 4.4 also contains a comparison of the results obtained from these calculations. From these analyses, it is obvious that the calculated ratio of spectral densities behaves in the same manner as the ratio of spectral densities obtained from the measurements.

Table 4.4 Calculation of Known Characteristics of the Ratio of Spectral Densities for 292-mm-High Uranyl Nitrate Solution System

Number of Data Blocks	^{252}Cf Source Strength (fissions/block)	Neutron Threshold	R(ω)
5000	32	0.8 MeV	0.0446 ± 0.0006
10000	32	1.5 MeV	0.0451 ± 0.0006
25000	16	0.8 MeV	0.0451 ± 0.0003

4.6 Summary

The ability of MCNP-DSP to accurately calculate the time distribution of counts after ^{252}Cf fission was demonstrated for a source and detector in air. The calculated neutron response as a function of time after ^{252}Cf fission agreed well with the measured response for this configuration. The calculated photon response was shown to be much more narrow than the measured response because the calculation does not suffer from the time resolution of the measurement. The integral of the calculated photon time distribution agreed with the integral of the measured photon time distribution. The ability to calculate the neutron and photon attenuation through concrete was demonstrated, and the results were in agreement with the measured responses. The Fourier processing algorithms were validated by obtaining excellent agreement with known theoretical values of the ratio of spectral densities for neutrons and photons for a source placed between two adjacent detectors. Several calculations were performed to demonstrate that the frequency spectra obtained by direct Fourier transformation of the detector response is the same as the frequency spectra obtained by Fourier transforming the correlation functions. Finally, the calculated low-frequency value of $R(\omega)$ was shown to have the same characteristics as the measured low-frequency value of $R(\omega)$, that is, to be independent of the source size for a uranium system and of the detection efficiency.

CHAPTER 5

COMPARISON OF MEASURED AND CALCULATED FREQUENCY ANALYSIS PARAMETERS

5.0 Introduction

This chapter presents the results of several calculations for systems that have been measured using the ^{252}Cf-source-driven noise analysis method. Three different types of subcritical fissile systems were chosen for which there were measurements with detectors sensitive to gamma rays. First, an unmoderated and unreflected uranium metal system[37,38] was analyzed to determine the ability of the code to calculate fast systems where there is no material present to slow down the neutrons. The next system was a tightly coupled system consisting of two uranium metal cylinders separated by a thin, borated plaster disk. The third system consisted of a uranyl nitrate solution.[13] The uranyl nitrate solution is unique in that the detector response is significantly affected by the slowing down and diffusion of neutrons in the system since the fissile and moderator atoms are intermingled.

5.1 Uranium Metal Cylinders

The experimental configuration for these measurements consisted of several 177.71-mm-diam. right-circular cylinders. The cylinders were supported by a 0.25-mm-thick stainless steel diaphragm held in position by a aluminum clamping ring. This structure supported the cylinder 2.7 m above the floor and was positioned 3 m away from the nearest wall. A sketch of the experimental setup is provided in Fig. 5.1. The uranium metal cylinders have a density of 18.76 g/cm^3. The uranium metal weight isotopic percentages are 93.15 wt% ^{235}U, 5.64 wt% ^{238}U, 0.97 wt% ^{236}U, and 0.24 wt% ^{234}U. In the

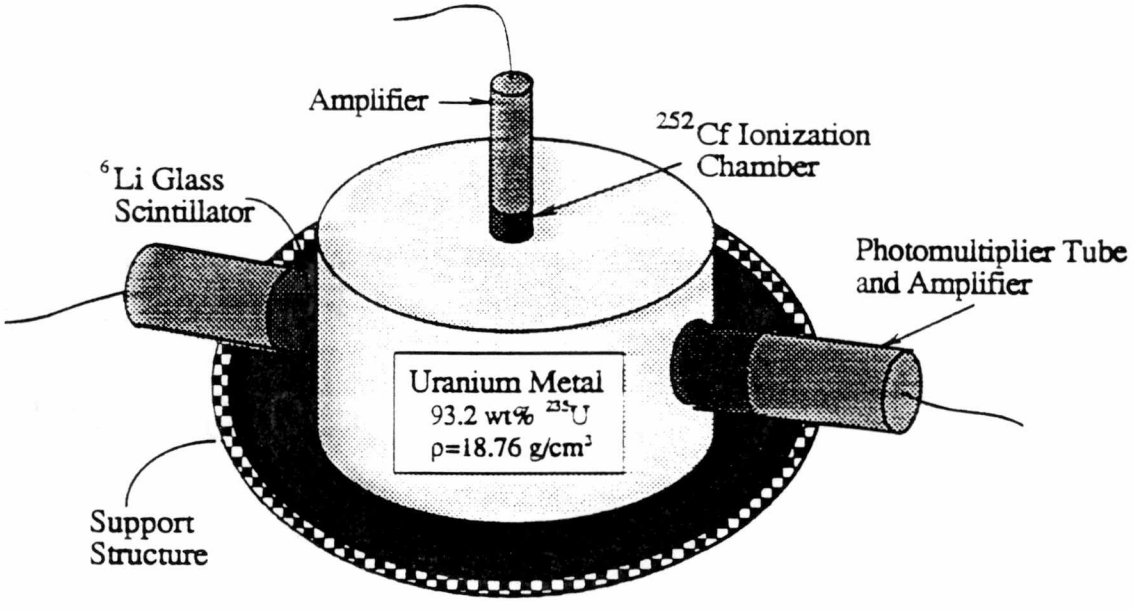

Figure 5.1 Experimental Configuration of Uranium Metal Cylinder

measurements, the ^{252}Cf source was located at the center on the top surface of the cylinders. The ^{6}Li glass scintillators were positioned at the midplane of the cylinders, placed 180° apart, and adjacent to the radial surface. These detectors had a diameter of 38.1 mm and were 25.4 mm long. ^{6}Li glass scintillators are sensitive to both neutrons and to gamma rays. Since the energy distribution of neutrons in these cylinders is a slightly degraded fission emission spectrum, much of the detector response is from gamma rays. Most of the neutron response is in the energy range of 300 keV, where ^{6}Li has a large neutron resonance cross section.

The calculation model for this system consisted of the uranium metal cylinder with the detectors and the source. The effects of the support structure are negligible. The model used in the calculations is shown in Fig. 5.2. Measurements with these uranium metal cylinders were first performed in 1975 and were repeated in 1984 with different detectors and different sources. The ratio of spectral densities from both sets of measurements were in good agreement and demonstrated that the measurements are reproducible. Calculations were performed for four different cylinder heights using the ENDF/B-IV[39] cross sections to compare with results obtained from KENO-NR calculations. Table 5.1 is a comparison of the low frequency values of $R(\omega)$ obtained from the measurement, the KENO-NR calculations,[10] and the MCNP-DSP calculations. The low-frequency values of $R(\omega)$ from the MCNP-DSP calculations are for the combined neutron and gamma ray response, while the low-frequency values of $R(\omega)$ from the KENO-NR calculations are only from neutrons since KENO-NR is a neutron-only Monte Carlo code. For these four cylinder heights, there is excellent agreement between both the calculations and the measurements. This demonstrates that the MCNP-DSP calculation is able to reproduce KENO-NR results and sufficiently reproduce the measured

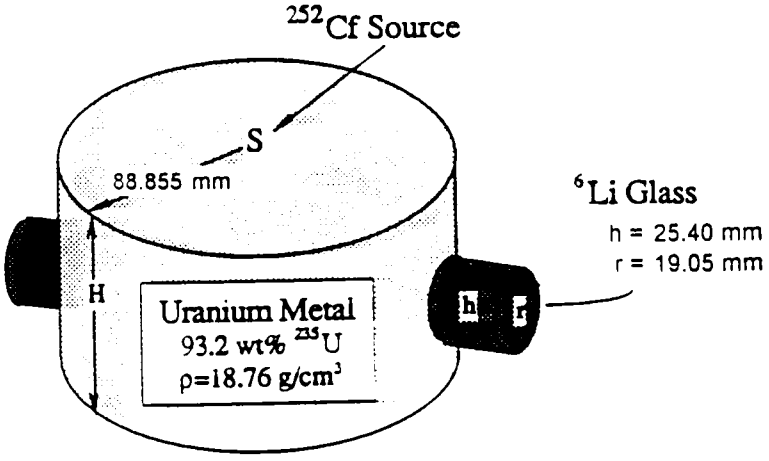

Figure 5.2 Calculational Model of Uranium Metal Cylinder

Table 5.1 Comparison of ENDF/B-IV Calculations of Uranium Metal Cylinders with Measurements

Cylinder Height (mm)	KENO-NR[10]	MCNP-DSP	Measurements
101.6	0.0697 ± 0.0041	0.0695 ± 0.0003	0.0694 ± 0.0008
91.4	0.101 ± 0.009	0.108 ± 0.001	0.0995 ± 0.0013
81.3	0.160 ± 0.012	0.156 ± 0.001	0.150 ± 0.003
71.1	0.215 ± 0.015	0.214 ± 0.002	0.215 ± 0.006

values for the unmoderated, unreflected uranium metal cylinders. A comparison of the frequency dependence of $R(\omega)$ is not possible because of the limited frequency response of the measurement system.

MCNP-DSP calculates the detector responses to neutrons and gamma rays. The neutron and photon responses can also be combined to form the total detector response. Table 5.2 is a comparison of the low-frequency values of $R(\omega)$ obtained from the neutron, photon, and combined neutron and photon responses using the ENDF/B-IV cross-section data sets. There is good agreement for the average values of $R(\omega)$ between the neutron, photon, and combined neutron and photon responses. This is to be expected since the photons are mainly produced from fission. The frequency dependence of the various spectral densities is also in good agreement. Various APSDs, CPSDs, and coherences are plotted as a function of frequency in Figs. 5.3 to 5.8 for the 91.4-mm-high uranium metal cylinder. The spectra are normalized to their low frequency values. Figure 5.3 is a plot of the normalized G_{22} as a function of frequency for the neutron and photon responses. These APSDs have essentially the same frequency dependence. The differences at the high frequencies are less than a percent and are not considered important. Figures 5.4 and 5.5 show the frequency dependence of the normalized CPSDs, G_{12} and G_{23}. The frequency dependence of the CPSDs are also in good agreement. The normalized coherences are plotted in Figs. 5.6 and 5.7. The coherences are in good agreement. Finally, Fig. 5.8 is a plot of the normalized value of $R(\omega)$. These frequency spectra demonstrate that the detector responses in this case are independent of the particle that causes the detection since gamma rays from fission can also be used to obtain correlated information about the fission chain multiplication process.

Table 5.2 ENDF/B-IV Calculated Values of $R(\omega)$ as a Function of Height for the Uranium Metal Cylinders with the Source at the Top and with the ^{6}Li-Glass Detectors

Cylinder Height (mm)	R(ω) (neutron)	R(ω) (photon)	R(ω) (neutron & photon)	k_{eff}
101.6	0.0712 ± 0.0008	0.0704 ± 0.0005	0.0695 ± 0.0003	0.9268 ± 0.0004
91.4	0.109 ± 0.001	0.105 ± 0.001	0.108 ± 0.001	0.8879 ± 0.0005
81.3	0.165 ± 0.003	0.151 ± 0.001	0.156 ± 0.001	0.8424 ± 0.0004
71.1	0.216 ± 0.004	0.210 ± 0.003	0.214 ± 0.002	0.7903 ± 0.0004

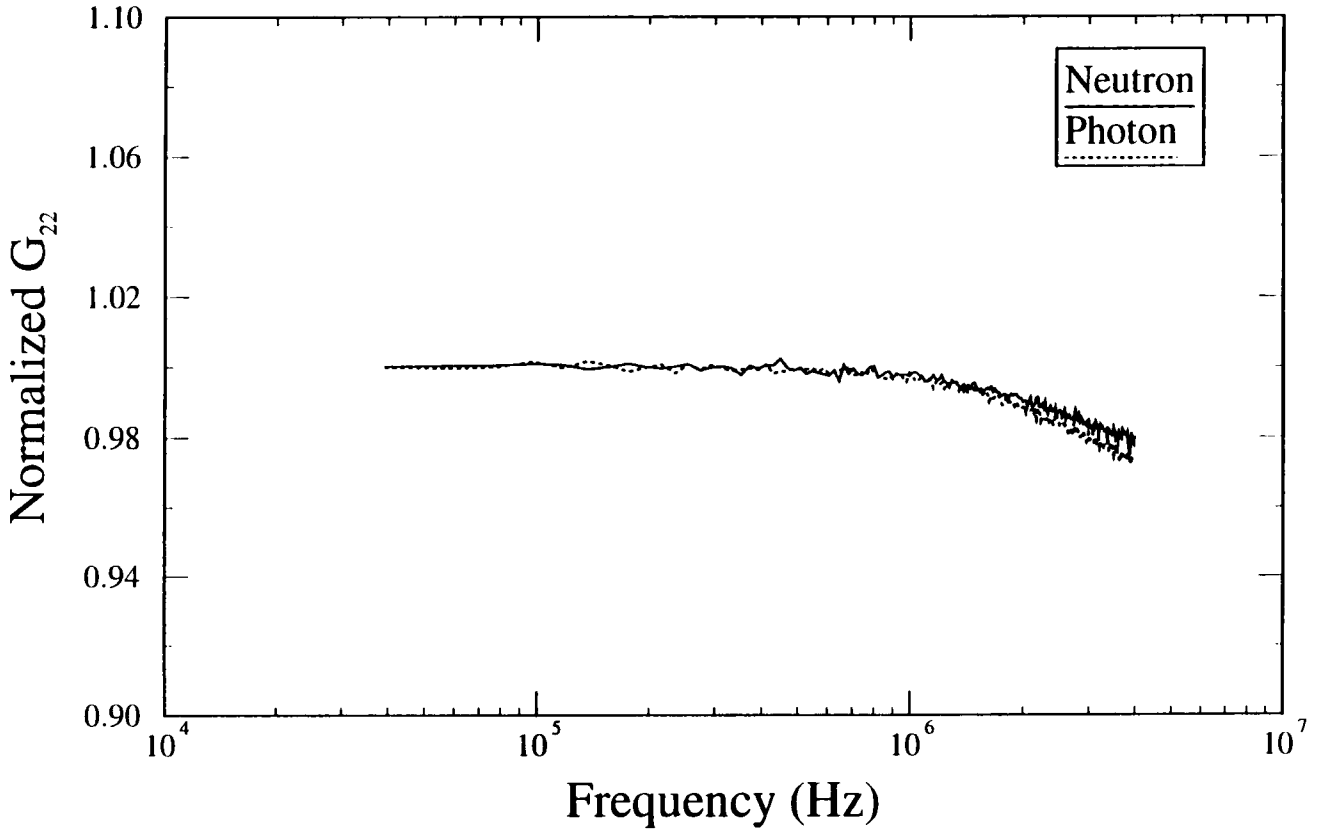

Figure 5.3 Comparison of the Calculated Normalized G_{22} from the Neutron and Photon Response for the 91.4-mm-High Uranium Metal Cylinder

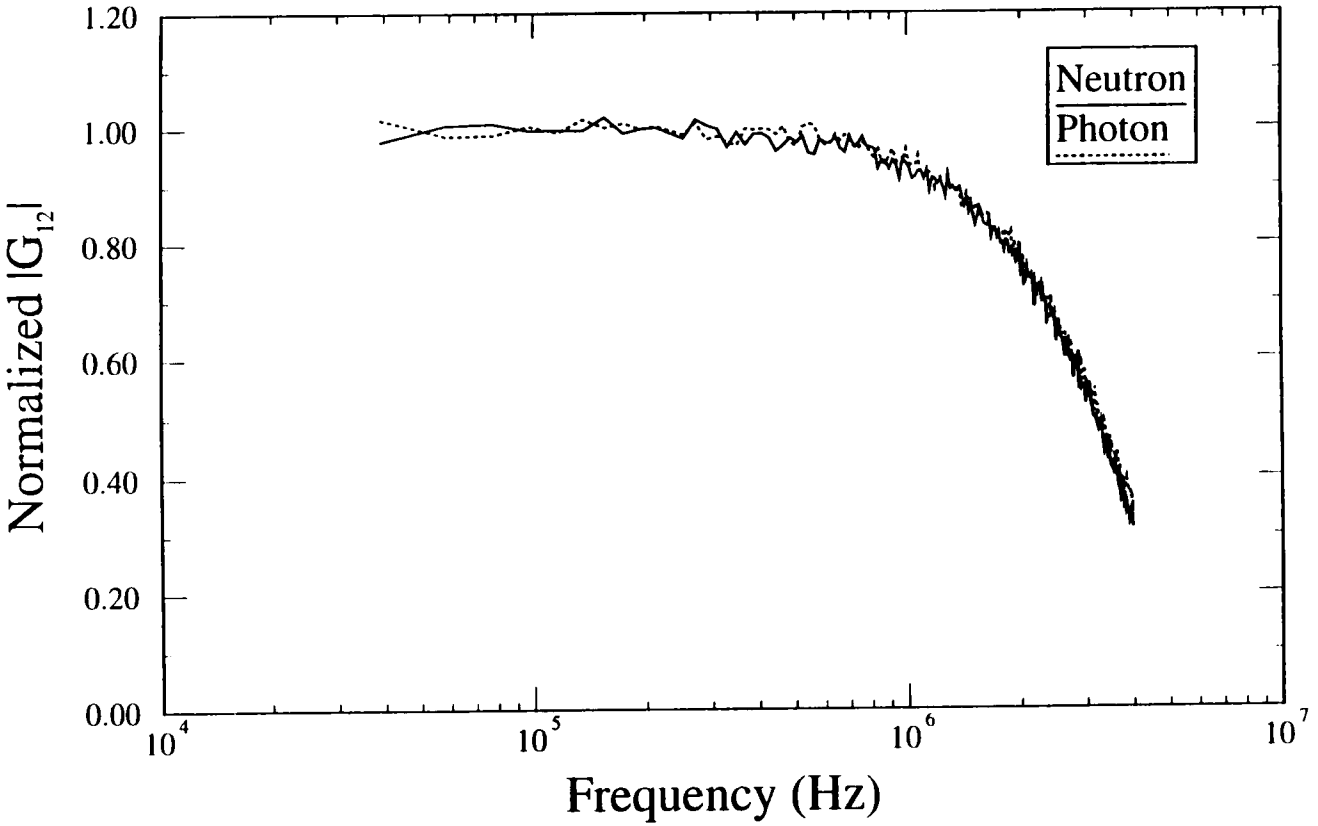

Figure 5.4 Comparison of the Calculated Normalized G_{12} from the Neutron and Photon Response for the 91.4-mm-High Uranium Metal Cylinder

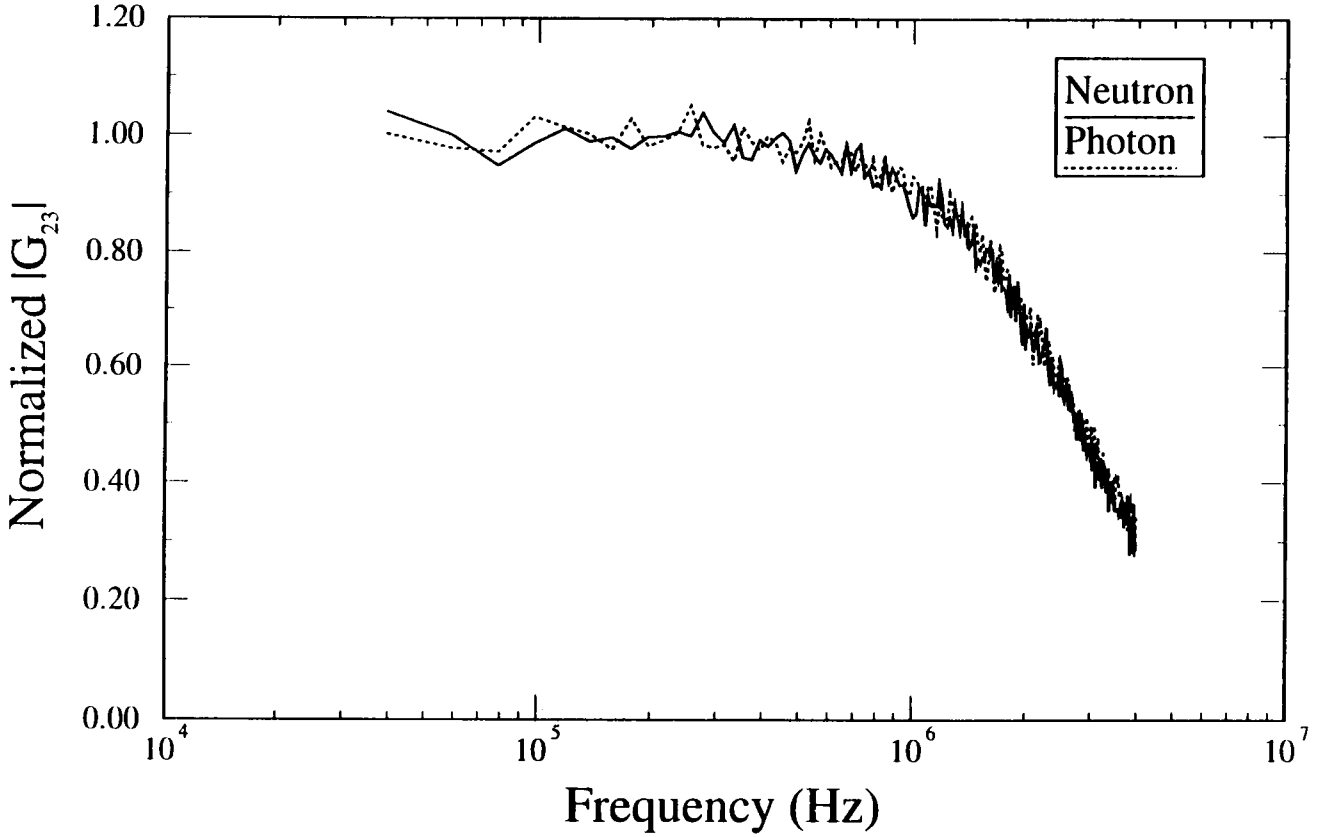

Figure 5.5 Comparison of the Calculated Normalized G_{23} from the Neutron and Photon Response for the 91.4-mm-High Uranium Metal Cylinder

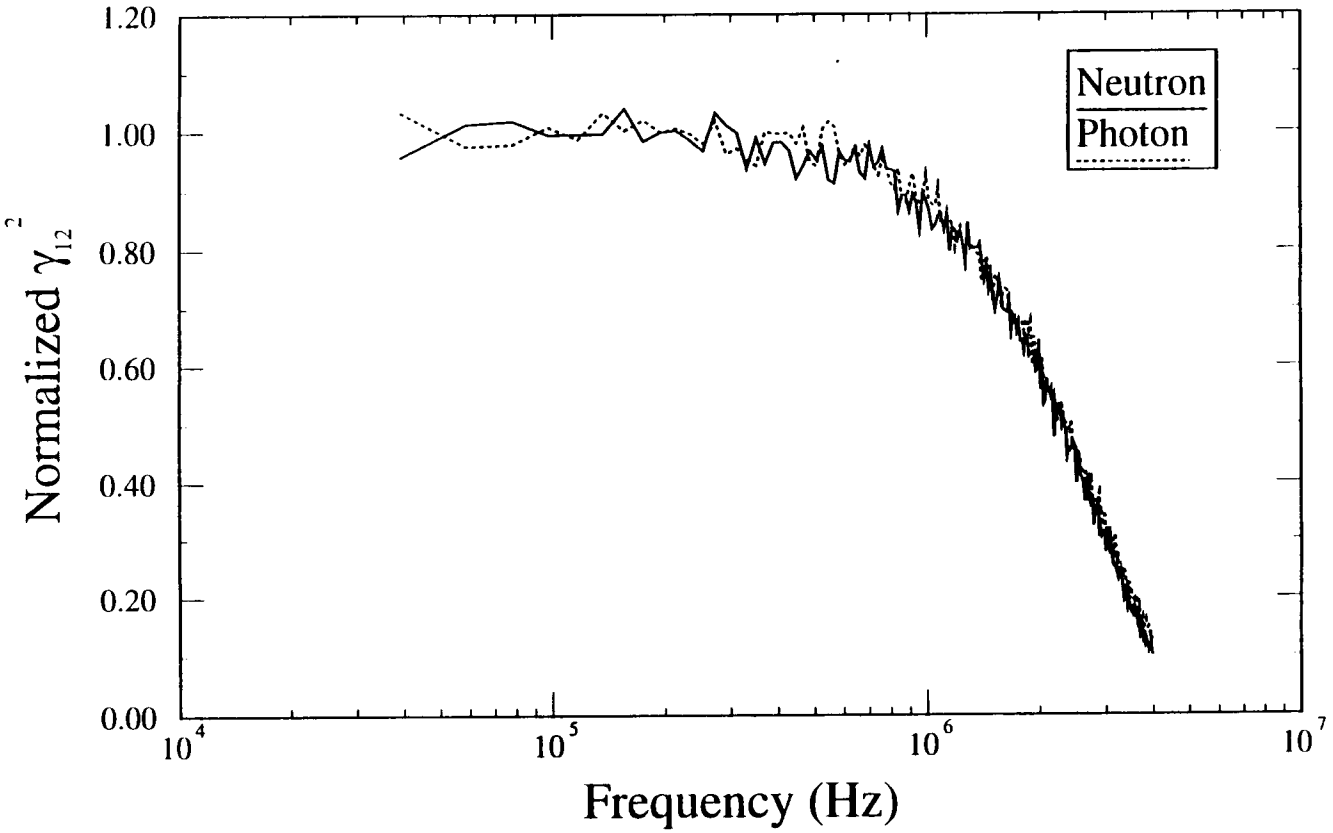

Figure 5.6 Comparison of the Calculated Normalized γ_{12}^2 from the Neutron and Photon Response for the 91.4-mm-High Uranium Metal Cylinder

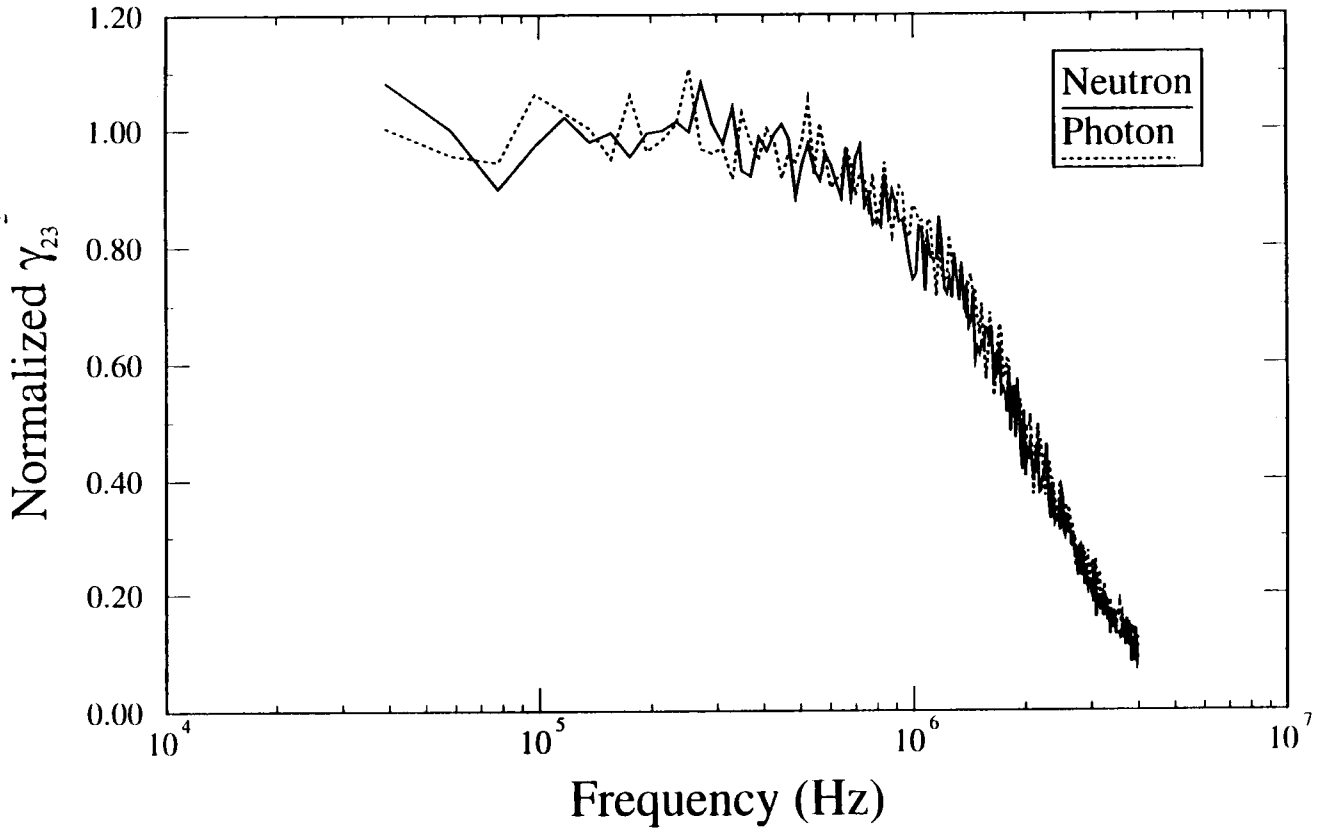

Figure 5.7 Comparison of the Calculated Normalized γ_{23}^2 from the Neutron and Photon Response for the 91.4-mm-High Uranium Metal Cylinder

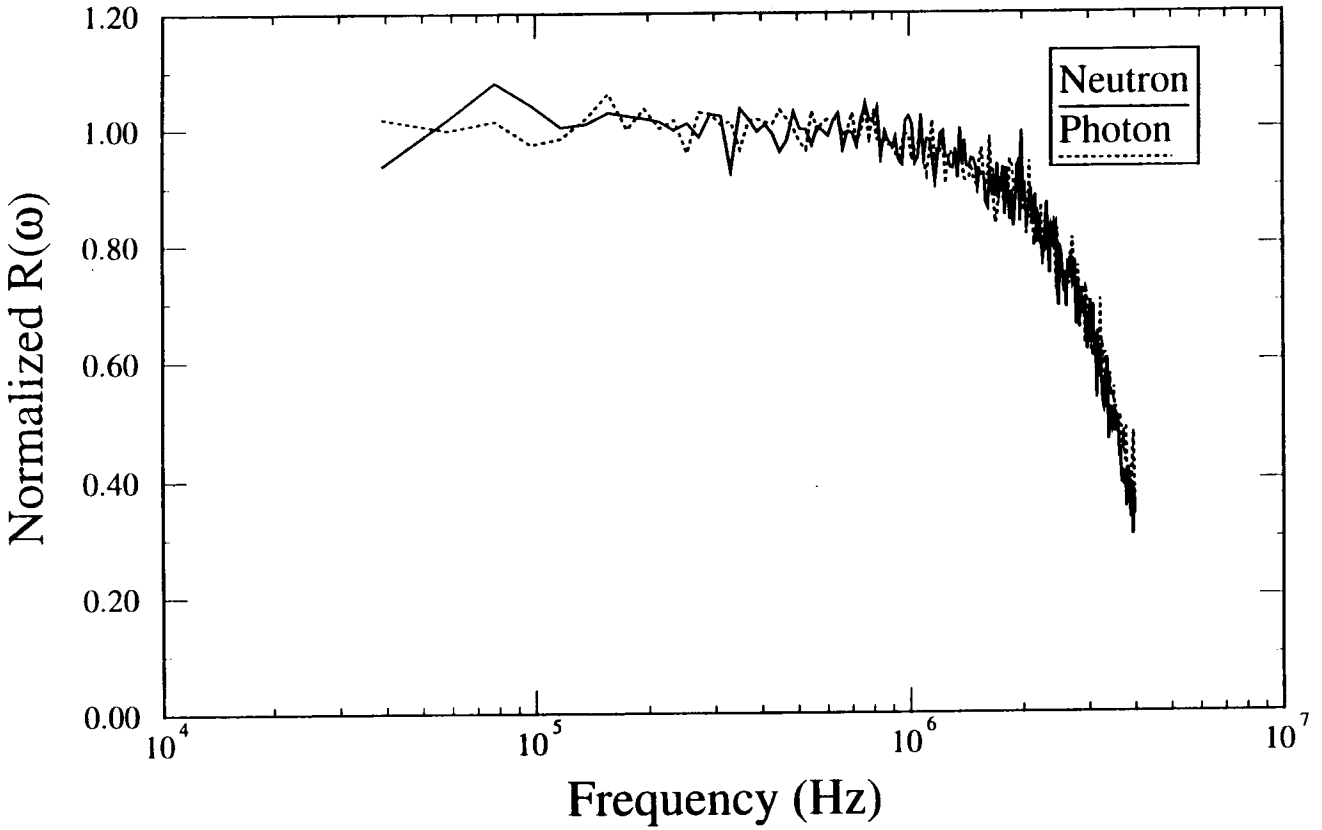

Figure 5.8 Comparison of the Calculated Normalized $R(\omega)$ from the Neutron and Photon Response for the 91.4-mm-High Uranium Metal Cylinder

The results of calculations for different cylinder heights employing the ENDF/B-V cross sections are presented in Table 5.3. The low frequency values of $R(\omega)$ and the values of k_{eff} from the measurement are presented in Table 5.4. The difference between the calculated and measured values of $R(\omega)$ varies from 2% to 15%. However, the calculated values of k_{eff} are consistently lower than the measured values of k_{eff} as can be seen from the results presented in Tables 5.3 and 5.4. Since the calculated values of k_{eff} are lower than the measured values of k_{eff}, the calculated low frequency value of $R(\omega)$ should be greater than the measured value of $R(\omega)$. This behavior of $R(\omega)$ is evident in Table 5.3. Since the ratio of spectral densities is a function of reactivity, a small difference in the k_{eff} values results in a larger difference in the values of $R(\omega)$ which is also evident from the results presented in Table 5.3. It is difficult to determine the exact cause of these discrepancies between the calculations and the measurements. In these unmoderated, unreflected uranium metal cylinders, small discrepancies in the cross sections or in the prompt neutron energy spectrum could result in errors in the calculated value of $R(\omega)$ and k_{eff}.

The ratio of spectral densities obtained from the photon response agrees well with that obtained from the neutron response. This is expected since the majority of the photons produced in the calculation are due to fission. The difference between the measured low-frequency value of $R(\omega)$ and the calculated low-frequency value of $R(\omega)$ from the photon response varies from 2% to 9%. These differences may also be attributed to small errors in the cross sections. The most significant result from these calculations is that the low frequency value of $R(\omega)$ from the photon response agrees well with that obtained from the neutron response.

Table 5.3 ENDF/B-V Calculated Values of $R(\omega)$ as a Function of Height for the Uranium Metal Cylinders with the Source at the Top and with the ^{6}Li-Glass Detectors

Cylinder Height (mm)	R(ω) (neutron)	R(ω) (photon)	R(ω) (neutron & photon)	k_{eff}
101.6	0.0725 ± 0.0007	0.0710 ± 0.0010	0.0736 ± 0.0007	0.9201 ± 0.0004
91.4	0.1112 ± 0.0013	0.1041 ± 0.0011	0.1079 ± 0.0007	0.8808 ± 0.0005
81.3	0.1737 ± 0.0015	0.1633 ± 0.0012	0.1635 ± 0.0008	0.8356 ± 0.0004
71.1	0.2371 ± 0.0051	0.2251 ± 0.0023	0.2228 ± 0.0021	0.7834 ± 0.0004
61.0	0.3184 ± 0.0077	0.2839 ± 0.0088	0.2815 ± 0.0052	0.7227 ± 0.0004

Table 5.4 Measured Values of $R(\omega)$ and k_{eff} as a Function of Height for the Uranium Metal Cylinders with the Source at the Top and with ^{6}Li-Glass Detectors

Cylinder Height (mm)	$R(\omega)$	k_{eff}
101.6	0.0694 ± 0.0008	0.929 ± 0.001
91.4	0.0995 ± 0.0013	0.904 ± 0.001
81.3	0.150 ± 0.003	0.859 ± 0.003
71.1	0.215 ± 0.006	0.799 ± 0.007
61.0	0.298 ± 0.018	0.717 ± 0.020

A calculation was also performed for the 101.6-mm-high uranium metal cylinder using ENDF/B-VI cross sections. A comparison of the results of the calculations for the 101.6-mm-high uranium metal cylinder using the ENDF/B-IV, ENDF/B-V, and ENDF/B-VI[41] cross sections are presented in Table 5.5. As can be seen from the results presented in Table 5.5, the best agreement is obtained with the ENDF/B-IV cross-section data set. The results of the ENDF/B-VI calculation show a large disagreement with the measured values of $R(\omega)$. The calculated value of k_{eff} using the ENDF/B-VI is 1.0 percent lower than the measured value of k_{eff}. This reduction in k_{eff} results in the ratio of spectral densities being over-predicted by 11.0 percent. It is beyond the scope of this work to define what inadequacy in the cross-section data produced these differences.

5.2 Tightly Coupled Uranium Metal Cylinders

To further demonstrate the ability to obtain the ratio of spectral densities from the photon response only, a uranium metal system with borated plaster using NaI detectors, which are sensitive only to gamma rays, was analyzed.[16] The uranium metal cylinders are the same materials as those just described in Sec. 5.1. The uranium metal cylinders were 50.8 mm high with 177.71 mm ID. These coupled cylinders were separated by a 10.2-mm-high, 177.71-mm-ID borated plaster disk. The NaI detectors were positioned 180° apart spaced 6.35 mm away from the radial surface of the second cylinder and were contained in a 12.9-mm-thick lead cup to shield the detectors from the natural emission of gamma rays of uranium. A sketch of this configuration is shown in Fig. 5.9.

Only one measurement was calculated with this configuration. The measured low-frequency value of $R(\omega)$ is 0.102 ± 0.003 for 11000 blocks of data. The same low-frequency value of $R(\omega)$ was obtained from a measurement performed with neutron detectors.[38] Since only the low-frequency value of $R(\omega)$ was available experimentally, a

Table 5.5 Effects of Cross Section Data on Calculated Values of $R(\omega)$ and k_{eff} for the 101.6-mm-High Uranium Metal Cylinder[1]

Cross Data Set	Number of Data Blocks	R(ω) (neutron)	R(ω) (photon)	R(ω) (neutron & photon)	k_{eff}
ENDF/B-IV	71000	0.0712 ± 0.0008	0.0704 ± 0.0005	0.0695 ± 0.0003	0.9268 ± 0.0004
ENDF/B-V	64000	0.0725 ± 0.0007	0.0710 ± 0.0010	0.0736 ± 0.0007	0.9201 ± 0.0004
ENDF/B-VI	44000	0.0771 ± 0.0011	0.0747 ± 0.0009	0.0758 ± 0.0007	0.9178 ± 0.0004

1 Measured: $R(\omega)=0.0694 \pm 0.0008, k_{eff}=0.929 \pm 0.001$
KENO-NR with ENDF/B-IV cross sections: $R(\omega)=0.0697 \pm 0.0004, k_{eff}=0.927 \pm 0.002$

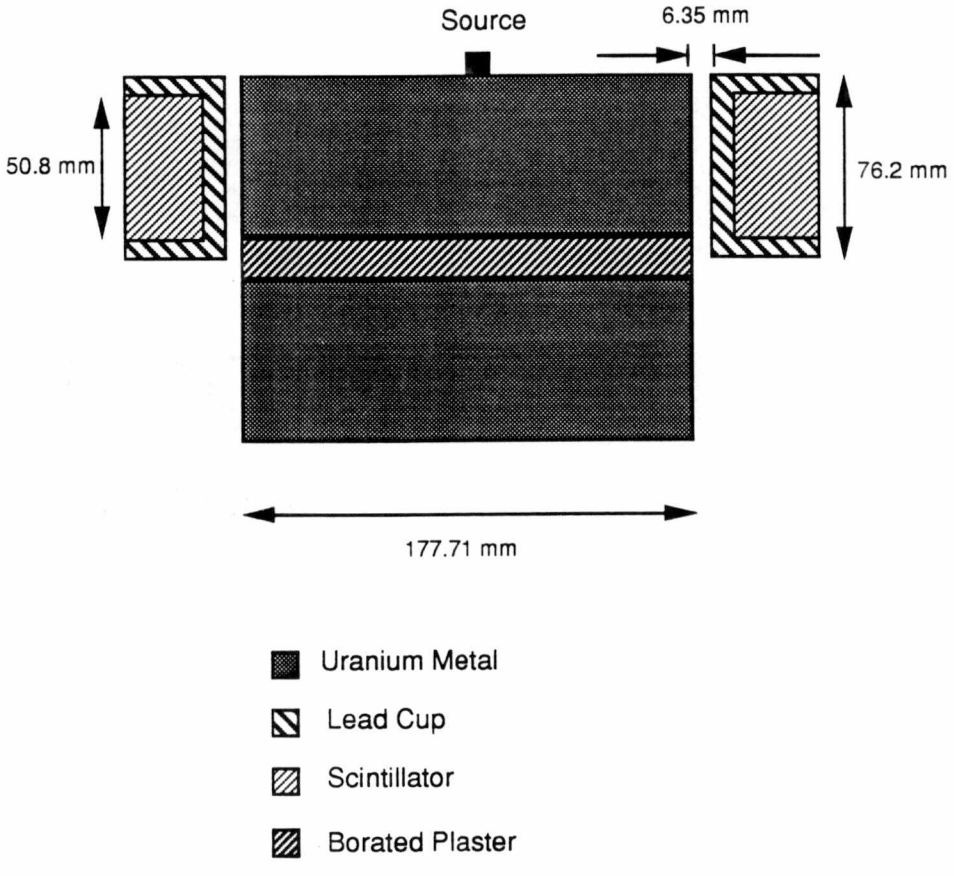

Figure 5.9 Coupled Uranium Metal Cylinder Configuration

comparison of the frequency dependence of $R(\omega)$ could not be made. The measured value of k_{eff} obtained from the low-frequency value of $R(\omega)$ is 0.900 ± 0.003. The calculations were performed with the ENDF/B-V cross sections since improved gamma production data are available in the ENDF/B-V data. The calculated low frequency value of $R(\omega)$ is 0.109 ± 0.003 for 160000 blocks of data. The calculated value of k_{eff} is 0.886 ± 0.001. The difference between the measured and the calculated low frequency value of $R(\omega)$ is consistent with the results previously presented for uranium metal cylinders and is consistent with the lower calculated value of the k_{eff}. These results further indicate that the ratio of spectral densities can be calculated using either the neutron or the photon response.

5.3 Uranyl Nitrate Solution System

The experimental configuration for this measurement was a 251-mm-ID right-circular acrylic cylindrical tank that was 533 mm high and had a wall thickness of 9.5 mm. The base of the cylinder was a 6.3-mm-thick type 304 stainless steel plate. The tank was filled with a uranyl nitrate solution to various heights. An ultrasonic transmitter was located above the tank to measure the height of the solution. The transmitter was mounted to a 6.3-mm-thick acrylic plate attached to the tank and supported by a steel flange that was attached to four steel tie rods. The experimental configuration is shown in Fig. 5.10. A 19-mm-OD, 12.7-mm-ID Lexan tube was placed in the center of the tank to allow the ^{252}Cf source to be located at different axial positions in the tank. The vessel was mounted on a 1270-mm-square aluminum table, which was positioned over 4 m above the concrete floor and 4 m and 3 m from the walls of the experiment room.

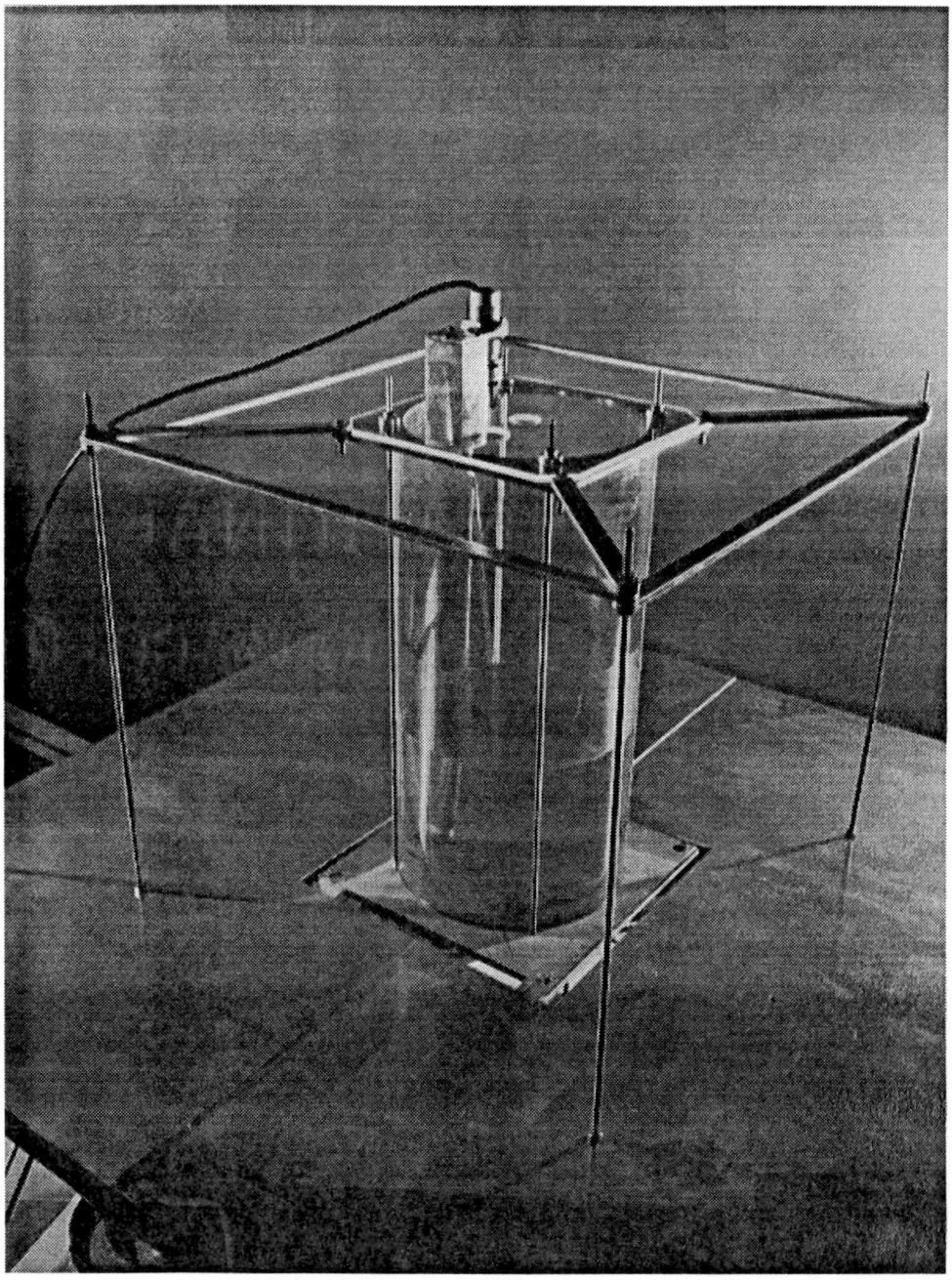

Figure 5.10 Experimental Configuration of the Uranyl Nitrate Solution System

The uranyl nitrate solution contained 482 g of uranium per liter of solution and had a density of 1.643 g/cm^3. The highly enriched uranyl nitrate solution contained 93.15 wt% ^{235}U, 5.37 wt% ^{238}U, 1.02 wt% ^{234}U, and 0.41 wt% ^{236}U. Trace elements in the solution are negligible. The hydrogen-to-^{235}U ratio is 49. Composite ^{6}Li-glass-plastic scintillators were used in some of the measurements. These detectors were sensitive to both fast and thermal neutrons and gamma rays. Figure 5.11 is a sketch of the experimental configuration with the ^{6}Li-glass-plastic scintillators. Each scintillation detector consisted of a 152-mm-wide, 152-mm-high, and 5-mm-thick ^{6}Li-glass scintillator, which is sensitive to thermal neutrons, that was optically coupled to a 152-mm-wide, 152-mm-high, and 102-mm-thick plastic scintillator that is sensitive to both fast neutrons and gamma rays. Each detection channel consisted of two adjacent scintillators whose detector responses were summed together to form the signal for the detection channel. There were two detection channels, one on each side of the vessel separated 25.4 mm from the outside of the acrylic tank.

The calculational model of this system consisted of the acrylic tank, the stainless steel plate, the Lexan tube for the source, and the composite scintillators. Figure 5.11 is a sketch of the model of the system used in the calculation. The effect of the aluminum table and the other support structure on the measured ratio of spectral densities was assumed to be negligible. Continuous energy cross sections were used in the calculations. The calculations were performed with the source positioned in the bottom of the vessel for the different solution heights. The ^{6}Li-glass scintillators were treated as capture detectors, and the plastic scintillators were treated as scattering detectors. The responses for the capture and scatter detectors were summed together to obtain the total detector response, as was done in the measurement.

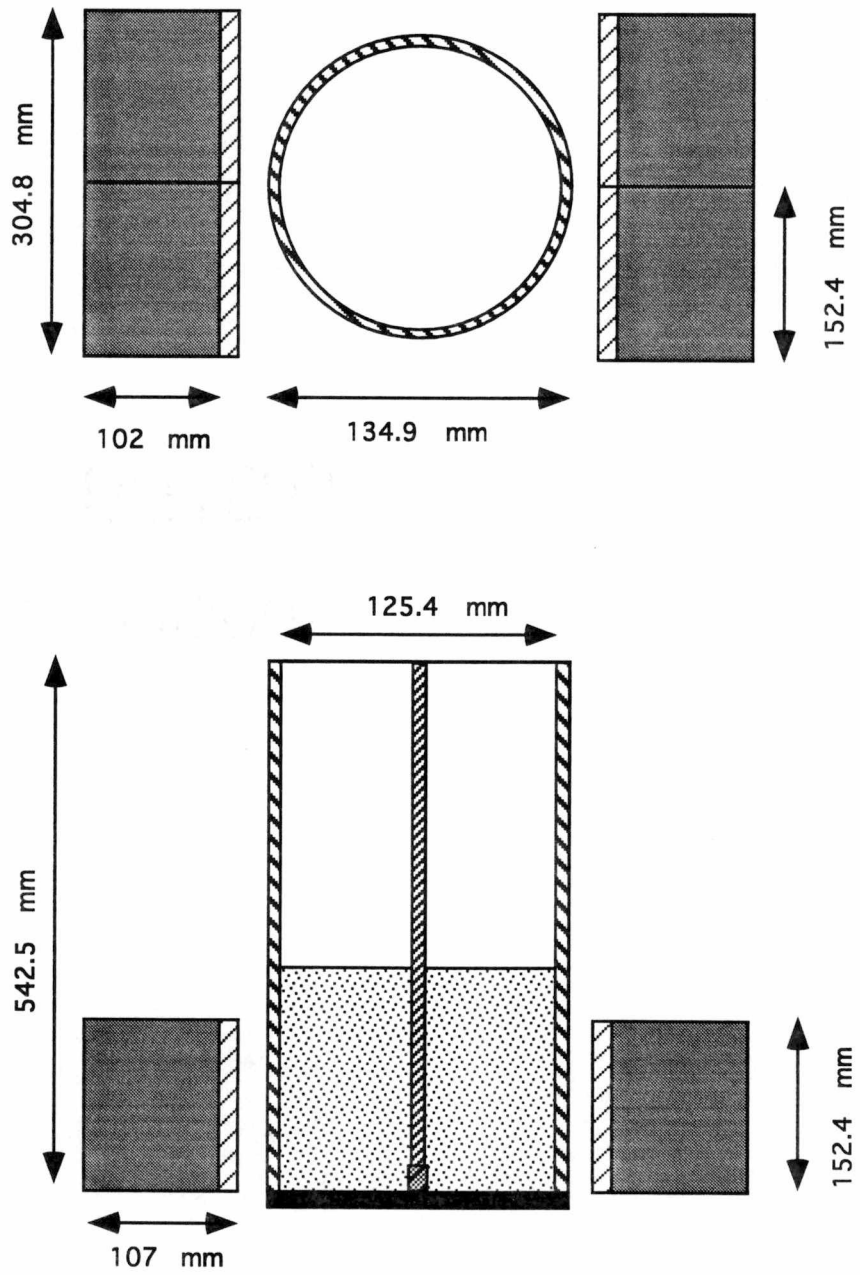

Figure 5.11 Calculational Model for the Uranyl Nitrate Solution System

In order to do a comparison of the previously calculated results obtained with KENO-NR,[10] the ENDF/B-IV[37] cross-section data sets were used as the basis for these MCNP-DSP calculations. Calculations were also performed for the 292-mm-high uranyl nitrate solution system using the ENDF/B-V[38] and ENDF/B-VI[40] cross-section data sets to investigate the effects of varying the cross-section data on the noise measured parameters. For these calculations all absorptions by ^{6}Li produced a detection, and the threshold for the neutron and gamma ray detections were 0.8 MeV and 0.3 MeV, respectively, for the plastic scintillator. A comparison of the results obtained from the different cross-section data sets for the one height (292 mm) is presented in Table 5.6. The measured value of the ratio of spectral densities is 0.0436 ± 0.0005, and the measured value of k_{eff} is 0.954 ± 0.001 for the 292-mm-high solution height. As can be seen in Table 5.6, the calculated value of the ratio of spectral densities (0.0446 ± 0.006), that was obtained using the ENDF/B-IV cross sections, agrees well with the measured value of the ratio of spectral densities; however, the calculations performed using the ENDF/B-V and ENDF/B-VI cross sections differed significantly from the measured value of $R(\omega)$ although the calculated values of k_{eff} were within less than 0.5% of the measured value of k_{eff}. A comparison of the coherence between the source and the detector (γ_{12}^2) and the coherence between the two detectors (γ_{23}^2) for the neutron response for the different cross-section data sets is shown in Fig. 5.12. The break frequency of γ_{23}^2 for the ENDF/B-IV calculation is lower than the break frequencies for the ENDF/B-V and ENDF/B-VI cross sections which is to be expected since the calculated value of k_{eff} using the ENDF/B-IV cross sections is slightly higher than that obtained using the ENDF/B-V or the ENDF/B-IV. From these analyses, it is difficult to determine the major factor contributing

Table 5.6 Effects of Cross Section Data on Calculated Values of $R(\omega)$ and k_{eff} for the 292-mm-High Uranyl Nitrate Solution[1]

Cross Data Set	Number of Data Blocks	R(ω) (neutron)	R(ω) (photon)	R(ω) (neutron & photon)	k_{eff}
ENDF/B-IV	5000	0.0446 ± 0.0006	0.0498 ± 0.0008	0.0466 ± 0.0006	0.9553 ± 0.0008
ENDF/B-V	7500	0.0538 ± 0.0004	0.0587 ± 0.0006	0.0560 ± 0.0004	0.9527 ± 0.0007
ENDF/B-VI	7500	0.0579 ± 0.0006	0.0643 ± 0.0006	0.0605 ± 0.0006	0.9508 ± 0.0007

1 Measured: $R(\omega)=0.0436 \pm 0.0005, k_{eff}=0.954 \pm 0.001$
KENO-NR with ENDF/B-IV cross sections: $R(\omega)=0.0440 \pm 0.0005, k_{eff}=0.954 \pm 0.001$

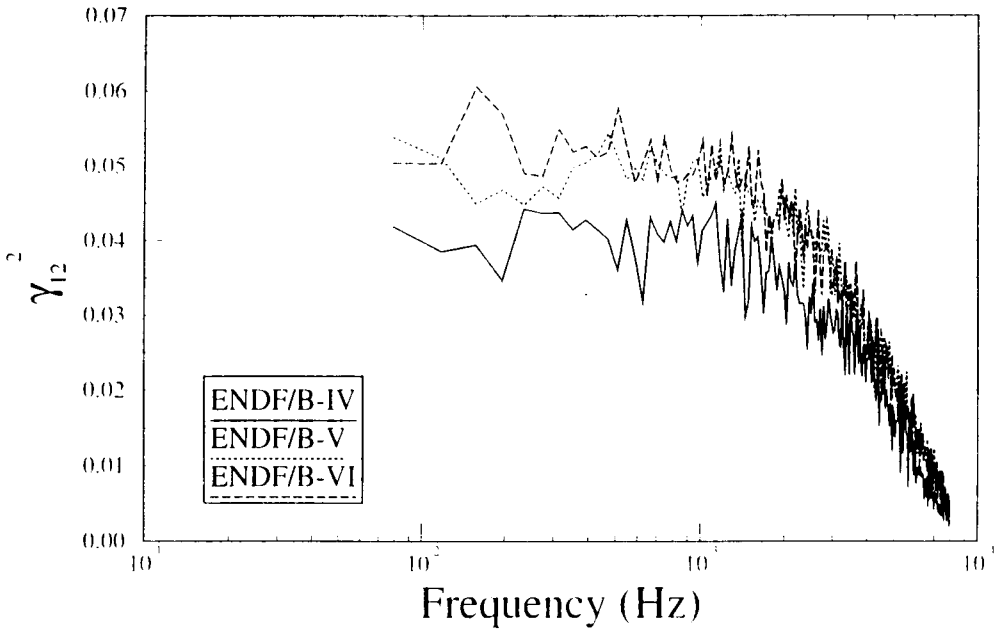

(a)

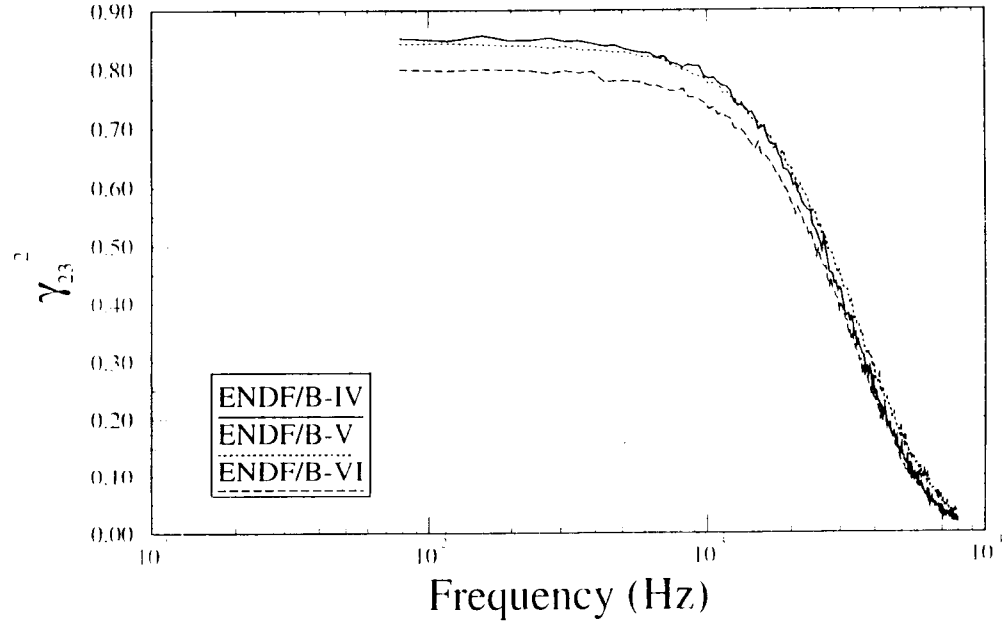

(b)

Figure 5.12 Calculated (a) γ_{12}^2 and (b) γ_{23}^2 for 292-mm-High Uranyl Nitrate Solution System

to the differences between the various cross-section sets since the noise measurement is an integral measurement. It is well known that the Watt spectrum, which is used in the ENDF/B-IV and ENDF/B-V cross sections to represent the spectrum of neutrons from induced fissions, differs slightly from the measured neutron spectra. In the ENDF/B-VI cross section data set, a more detailed model is used to represent the neutron spectrum using the tabulated values of the Madland and Nix[42] spectrum for ^{235}U, ^{237}Np, and ^{239}Pu. The average energy of the neutron spectrum obtained from the model, which uses an energy dependent compound nucleus cross section, is closer to the measured value for the average energy of the neutron spectrum than the value obtained using a Watt spectrum.[43] However, the largest difference between the calculated and measured value of $R(\omega)$ occurs with the ENDF/B-VI cross sections. Therefore, these differences are attributed to discrepancies in the cross section data and not in the neutron energy spectra. Although the calculated value of $R(\omega)$ from the photon response differs significantly from the measured value of $R(\omega)$ for all three cross section libraries, the photon response exhibits the same behavior as the neutron response when comparing the different cross-section data sets. The calculations with the ENDF/B-IV cross sections agree closer with the measured response than the calculations with the ENDF/B-VI cross sections. These results demonstrate the sensitivity of the calculation of the measured parameters to the data contained in the cross-section data sets.

The results of the calculations for different solution heights using the ENDF/B-IV cross-section data sets are presented in Table 5.7. Table 5.8 contains the results from the measurements. There is excellent agreement between the measured value of $R(\omega)$ and the calculated value of $R(\omega)$ for the neutron response for heights more than 200 mm. The calculated value of $R(\omega)$ for the 153-mm-high and the 101-mm-high solutions differ

Table 5.7 ENDF/B-IV Calculated Values of $R(\omega)$ as a Function of Solution Height for the Uranyl Nitrate Solution System with the Source at the Bottom of the Tank and with the Composite ^{6}Li-Glass Plastic Scintillator Detectors

Solution Height (mm)	R(ω) (neutron)	R(ω) (photon)	R(ω) (neutron & photon)	k_{eff}
292	0.0446 ± 0.0006 (0.0435 ± 0.0004)[a]	0.0498 ± 0.0008	0.0466 ± 0.0006	0.9553 ± 0.0008
258	0.0794 ± 0.0007 (0.0790 ± 0.0024)	0.0907 ± 0.0009	0.0839 ± 0.0008	0.9254 ± 0.0008
203.2	0.1693 ± 0.0009 (0.170 ± 0.003)	0.2044 ± 0.0015	0.1828 ± 0.0015	0.8520 ± 0.0008
153	0.3133 ± 0.0016 (0.307 ± 0.006)	0.3899 ± 0.0021	0.3443 ± 0.0021	0.7405 ± 0.0007
101.2	0.5716 ± 0.0032 (0.575 ± 0.010)	0.6784 ± 0.0044	0.6257 ± 0.0021	0.5471 ± 0.0007

a These are results of KENO-NR calculations taken from ref. 10.

Table 5.8 Measured Values of $R(\omega)$ and k_{eff} as a Function of Solution Height for the Uranyl Nitrate Solution System with the Source at the Bottom of the Tank and with the Composite ^{6}Li-Glass Plastic Scintillator Detectors

Solution Height (mm)	$R(\omega)$	k_{eff}
292	0.0436 ± 0.0005	0.954 ± 0.001
258	0.0774 ± 0.0020	0.923 ± 0.003
203.2	0.1616 ± 0.0010	0.850 ± 0.005
153	0.2843 ± 0.0010	0.738 ± 0.010
101.2	0.4477 ± 0.0060	0.540 ± 0.027

significantly from the measured value. Consequently, results from KENO-NR calculations using the ENDF/B-IV cross sections show the same behavior as a function of solution height, and the values of the ratio of spectral densities obtained from the KENO-NR calculations agree well with those obtained from the neutron responses from the MCNP-DSP calculations. This indicates that the results seem more dependent on the cross-section data used to perform the calculations than the code used to perform the calculations. At solution heights of 153 mm and 101 mm, errors in the cross-section data sets or errors in the neutron spectrum may have a greater impact on the calculated value of the ratio of spectral densities.

The ratio of spectral densities obtained from the calculated photon response does not agree with the measured value of $R(\omega)$ for all of the solution heights. The exact cause of these differences has not been determined and requires further investigation. The calculated neutron and photon responses were combined. The calculated value of $R(\omega)$ using the combined neutron and photon responses falls between the value of $R(\omega)$ from the neutron response and the value of $R(\omega)$ from the photon response since an almost equal number of neutrons and photons are detected. After obtaining the ratio of spectral densities, the k_{eff} values were calculated with the detectors present because these detector have a minor effect on the reactivity of the solution heights. The calculated values of k_{eff} are presented in Table 5.7, and the measured values of k_{eff} are shown in Table 5.8. There is good agreement between the calculated and measured values of k_{eff} for solution heights above 200 mm. For the lower solution heights, there is too much uncertainty in the measured value of k_{eff} to adequately determine how well the calculated and measured values of k_{eff} agree. Since there is good agreement between the measured and calculated values of the ratio of spectral densities for the solution heights greater than 200 mm, the

calculated value of k_{eff} obtained using these models and the ENDF/B-IV cross sections should be within a few percent of the measured k_{eff}. However, for solution heights of 153 mm and 101 mm, there are significant differences between the measured and calculated values of the ratio of spectral densities. Hence, the k_{eff} obtained for these solution heights from the analog Monte Carlo calculation have a greater uncertainty. The uncertainty could be determined by varying parameters in the calculation model until obtaining agreement between the measured and calculated value of the ratio of spectral densities. After obtaining agreement between the measured and calculated values of the ratio of spectral densities, k_{eff} can then be calculated with the modified model and the uncertainty in k_{eff} can be obtained from the difference in the k_{eff} value obtained with the modified model and the original model.

To further ensure that the differences between the measured value of $R(\omega)$ and the calculated value of $R(\omega)$ from the neutron response is due to a cross-section inadequacy, calculations were performed with the source in the center of the solution using ^{3}He neutron absorbing detectors. Only thermal neutrons are detected by the ^{3}He detectors. In the measurements, one 381-mm-long, 254-mm-ID ^{3}He detector was positioned 180° apart on each side of the vessel. However, in order to decrease the computation time, two 381-mm-long, 254-mm-ID ^{3}He detectors were placed symmetrically on each side of the vessel in the calculations.

The results of these calculations are presented in Table 5.9. There is good agreement between the measured and calculated values of $R(\omega)$ for solution heights greater than 200 mm. However, at the lower solution heights, there are significant differences between the measured and calculated values of $R(\omega)$. These differences are consistent with the results obtained using the ^{6}Li-glass plastic scintillators. Therefore, the

Table 5.9 Comparision of Measured and ENDF/B-IV Calculated Values of $R(\omega)$ as a Function of Solution Height for the Uranyl Nitrate Solution System with the Source at the Center of the Tank and with the ^{3}He Detectors

Solution Height (mm)	Calculated R(ω)	Measured R(ω)
304.8	0.104 ± 0.002	0.100 ± 0.001
254	0.196 ± 0.003	0.190 ± 0.001
203.2	0.316 ± 0.006	0.304 ± 0.003
152.4	0.518 ± 0.012	0.465 ± 0.003
101.6	0.786 ± 0.029	0.635 ± 0.020

differences between calculated and measured values of $R(\omega)$ are attributed to deficiencies in the cross-section data and are not due to the detection process.

5.4 Summary

The ability to calculate the low-frequency value of $R(\omega)$ with MCNP-DSP for the unmoderated, unreflected uranium metal cylinders from the neutron, photon, and the combined neutron and photon response using the ENDF/B-IV cross sections has been demonstrated. The results of the calculations for the uranium metal cylinders showed that the low-frequency value of $R(\omega)$ can be obtained from the neutron or photon response and that the spectra obtained from the neutron and photon responses have the same frequency dependence. This was to be expected since the gamma rays from fission can be correlated in the same manner in which neutrons from fission are correlated. MCNP-DSP was also able to adequately calculate $R(\omega)$ for the tightly coupled uranium metal cylinder system separated by borated plaster in which detectors sensitive only to gamma rays were used in the measurement. The results of the calculations for the uranyl nitrate solution system indicated that MCNP-DSP could accurately calculate the low-frequency value of $R(\omega)$ using the neutron response for solution heights greater than 200 mm independent of the detector used in the calculations. For the lower solution heights, the results of the calculation differed significantly from the measurements, which is attributed to inadequacies in the cross-section data. Furthermore, the calculated results were shown not to depend on the kind of detector. The results of the calculations for the uranyl nitrate solution system obtained from the photon response differed significantly from the measured value of $R(\omega)$, and the cause of these differences has not been resolved. The results of the calculations for the uranium metal cylinders and for the uranyl nitrate solution system were shown to be strongly dependent on the cross-section data used in the

calculations. The calculated noise-measured parameters changed significantly when using different cross sections even though k_{eff} may not have changed. This demonstrated the increased sensitivity in calculating the noise-measured parameters rather than calculating k_{eff} when validating computational methods and cross-section data.

CHAPTER 6

CONCLUSIONS AND RECOMMENDATIONS FOR FUTURE WORK

6.0 Summary

The CSDNA method is a measurement technique that is used to characterize the subcriticality of a fissile configuration. The CSDNA method employs a ^{252}Cf source and two or more particle detectors that provide measured quantities that can be directly calculated for the verification of calculational models and cross-section data sets. A certain ratio of spectral densities from the measured detector response is independent of detection efficiency and in some cases source intensity. This ratio of spectral densities is defined as

$$R(\omega)=\frac{G_{12}^{*}(\omega)G_{13}(\omega)}{G_{11}(\omega)G_{23}(\omega)}, \tag{6.1}$$

where G_{12}^{*} is the complex conjugate of the CPSD between the source detector #1 and the particle detector #2, G_{13} is the CPSD between the source detector #1 and particle detector #3, G_{11} is the APSD of the source detector, and G_{23} is the CPSD between detector #2 and detector #3.

MCNP-DSP was developed in order to calculate $R(\omega)$, other frequency analysis parameters, time analysis quantities such as autocorrelation and cross-correlation functions, and the time distribution of counts after ^{252}Cf fission using the Monte Carlo technique. MCNP-DSP provides a more general model for interpretation of subcriticality and other measurements and does not suffer from the inadequacies of the point kinetics model. The only limitations of the Monte Carlo method are the accuracies of the cross-section data

used to represent the physical processes. In order to calculate the ratio of spectral densities in a similar manner in which they are experimentally obtained, several modifications were made to the MCNP code. The structure of the code had to be modified in order to obtain the calculated parameters in the form of data blocks, as is done in the measurement. The weighting and biasing in MCNP were disabled in order to have a strictly analog Monte Carlo calculation. A dual particle source was developed which produces both neutrons and gamma rays from the spontaneous fission of ^{252}Cf. An option for including an inherent fission source was also added to the code. Evaluated measured data were also incorporated into the code for certain neutron and photon interactions. Several detector options were incorporated in MCNP-DSP to simulate the various detectors used in the measurements. Detector processing algorithms were incorporated into the code to process the data blocks of the detector responses. The frequency spectra can be obtained by direct Fourier processing of the blocks of data to obtain the APSDs and CPSDs. The APSDs and CPSDs can also be obtained by Fourier transforming the autocorrelation and cross-correlation functions. The time distribution of detector counts after ^{252}Cf fission is also obtained.

A series of calculations was performed to validate the MCNP-DSP code. To validate the ^{252}Cf neutron and gamma ray energy spectra and the detection process, a calculation was performed with the source and detector in air. The calculated neutron response as a function of the time after ^{252}Cf fission agreed well with the measured neutron response for this source and detector configuration. The calculated photon response differed from the measured photon response because the measured photon response suffers from a lack of time resolution causing the gamma peak to be spread out over several time bins. However, the integrals of the peaks are in good agreement, and

thus the calculated photon time distribution is considered to be in good agreement with the measured. To show that the code put the data into the proper time bins, a calculation was performed with a piece of beryllium placed between the source and detector. The depression in the neutron response occurred at a time which is directly related to a known resonance in the beryllium cross section. A third calculation was performed with an attenuating media between the source and the detector. The calculated responses were in good agreement with the measured responses. There was better agreement for the neutron response than with the gamma response. The differences between the measured and calculated photon response have not been resolved. In order to validate the Fourier processing algorithms, two calculations were performed with the source placed between two adjacent detectors. Excellent agreement between the calculated value of $R(\omega)$ and the theoretically exact value of $R(\omega)$, which is obtained from the emission probability distribution, was obtained for both the neutron and gamma ray response. Next, a series of calculations was performed to demonstrate that the frequency spectra are not dependent on the manner in which the spectra are calculated. There was excellent agreement between the frequency spectra obtained by direct Fourier transforming the detector responses and by Fourier transforming the correlation functions. In addition, it was demonstrated that the convergence of the calculations is the same. The value of $R(\omega)$ obtained from the calculations has been shown to be independent of the source strength and the detection efficiency as had been established in the measurements.

Several calculations were performed for systems that have been measured using the CSDNA technique. There were three systems analyzed. The first was an unmoderated, unreflected uranium metal cylinder, the second was a coupled system consisting of uranium metal cylinders separated with a borated plaster disk, and the third was a uranyl nitrate

solution system. Several calculations were performed to demonstrate the sensitivity of the calculated value of $R(\omega)$ to the cross-section data set used. Calculations were performed with the ENDF/B-IV, ENDF/B-V, and ENDF/B-VI cross-section data sets.

The initial calculations of the unmoderated, unreflected uranium metal cylinders were performed with the ENDF/B-IV, ENDF/B-V, and ENDF/B-VI cross-section data sets to demonstrate the sensitivity of the calculation of the noise parameters to cross-section data sets used. Detailed calculations were performed with the ENDF/B-IV cross sections and the ENDF/B-V cross sections. Using the ENDF/B-IV cross sections, good agreement was obtained between the calculated and measured values of $R(\omega)$. These results also showed that in this case the spectra obtained from the neutron and photon responses have the same frequency dependence. This was expected since the gamma rays from fission can be correlated in a similar manner in which neutrons from fission are correlated. For the ENDF/B-V calculations, the calculated low-frequency value of $R(\omega)$ was consistently greater than the measured low-frequency value of $R(\omega)$ since the calculated value of k_{eff} was consistently lower than the measured value of k_{eff}. The significant result from these calculations are that the calculated low-frequency value of $R(\omega)$ obtained from the photon response agrees well with that obtained from the neutron response and that the neutron and photon spectra have the same frequency dependence. This shows that the calculated ratio of spectral densities can be obtained from either the neutron or the photon response for systems in which the majority of the photons come from fission events. The sensitivity of the calculation to different cross-section data sets was also demonstrated.

The second system analyzed was the coupled uranium metal cylinders with a borated plaster divider. The low-frequency value of $R(\omega)$ from this calculation, which used detectors sensitive only to gamma rays, was in good agreement with the measured value.

This calculation further verified that the ratio of spectral densities could be calculated from the photon response for systems in which the majority of the photons are produced from fission events.

The initial calculations for the uranyl nitrate solution system were performed with the various cross-section sets. Good agreement was obtained between the calculated low frequency value of $R(\omega)$ from the neutron response and measured low-frequency value of $R(\omega)$ for solution heights greater 200 mm using the ENDF/B-IV cross sections. For lower solution heights there was more disagreement between the calculated values and the measured values of $R(\omega)$. This difference may be attributed to inadequacies in the cross-section data. The calculated results were shown to be independent of the detectors used to perform the calculation. The calculated low-frequency value of $R(\omega)$ obtained from the photon response differs significantly from the measured value of $R(\omega)$ at all solution heights. The cause of these differences has not been resolved and requires further investigation. Since there is good agreement between the calculated low-frequency value of $R(\omega)$ obtained from the neutron response and the measured low-frequency value of $R(\omega)$ for solution heights greater than 200 mm, the calculated value of k_{eff} using the ENDF/B-IV cross sections should be within a percent of the measured values. Since the calculated values of $R(\omega)$ are greater than the measured values for the lower solution heights, the k_{eff} obtained from the analog Monte Carlo calculations have a greater uncertainty.

From these analyses, the following conclusions can be drawn. First, the ability to calculate the time response of proton recoil scintillators for both neutron and photons from the spontaneous fission of ^{252}Cf has been demonstrated. Secondly, the calculational procedure of the code has been validated by obtaining good agreement between calculated

and measured detector responses for simple systems. The calculated frequency spectra are not dependent on the processing method, that is, there are no significant differences between the spectra or the convergence obtained from direct Fourier processing or from Fourier processing the correlation functions for $\omega > 0$. Next, the calculated low-frequency value of $R(\omega)$, like the measured value, is independent of detection efficiency and source intensity for low inherent-source systems. The sensitivity of the calculated frequency spectra to cross sections has been demonstrated and may explain why some calculations differ from measurements. For some systems, the calculated low-frequency value of $R(\omega)$ obtained from the neutron response agrees well with the measured value of $R(\omega)$ and for these systems the calculated value of k_{eff} should be within a percent of the measured value of k_{eff}. For those systems in which the calculated results differ from the measured results, the differences may be attributed to the inadequacy of the cross-section data. The calculated low-frequency value of $R(\omega)$ obtained from the photon response agrees well with the calculated value obtained from the neutron response for systems in which the majority of the gamma rays are produced from fission.

Thus, MCNP-DSP provides a more general continuous energy Monte Carlo model for calculation of measured observables which includes not only neutrons but also gamma rays. This code can be used to calculate frequency analysis parameters for relevant in-plant configurations of fissile material. Agreement with the measured data for a particular application will verify the calculated value of k_{eff} for the particular application. This code can also be used to produce calculated blocks of detector response, which can be analyzed within MCNP-DSP in two ways to obtain the frequency spectrum: (1) by obtaining autocorrelation and cross-correlation functions from blocks of data and then Fourier transforming to obtain frequency spectra and (2) by obtaining the fast Fourier transform

of the blocks of data which are complex multiplied to obtain the frequency spectra. The calculated blocks of data can be used as input to measurement systems to verify this operation (special provision has been made to allow computed blocks of data to be input to the processors for verification). Finally, MCNP-DSP provides a more general tool for planning experiments for criticality safety, safeguards, nondestructive assay, and arms control verification.

6.1 Recommendations for Future Work

Several other tasks could be performed to investigate the ability of the modified MCNP code to calculate the measured frequency spectra. A more extensive analysis of the effects of cross sections on the calculated spectra could be performed for a wider variety of fissile systems. By varying different parameters in the cross-section data, some insight into systems that cannot be accurately calculated may be obtained. However, since there are so many parameters that could be modified, good judgment will be required to determine which parameters are the most significant for a given system. If the gamma ray production cross-section data are separated into the contributions from capture, inelastic scatter, fission, etc., in the ENDF files, the code could be modified to account for this change in the gamma ray production cross-section data. Other theoretical neutron spectra may be substituted for the ^{252}Cf spectrum to analyze the effect of the ^{252}Cf neutron spectrum on the calculated results. Improved models of the prompt gamma rays from fission may also be included in the code.

Other possible tasks would be to include the natural background radiation from fissile material in the calculation since uncorrelated detector background such as from the natural long lived decay of fissile isotopes has not been included in these modifications. This affects the APSDs and coherences but does not affect the CPSDs and $R(\omega)$. Also

in these calculations, it has been assumed that all of the ^{252}Cf fissions are detected. In the measurements, a small percentage of the ^{252}Cf fissions are not detected. This effect is well known, and the measured values of G_{11}, G_{12}, G_{13}, and $R(\omega)$ are usually corrected to account for this. The gamma rays from the inherent fission source need to be added in the code in order to accurately calculate the detector response to gamma rays for systems with inherent fission sources. The Madland and Nix spectra[42] may be substituted for the Watt spectrum for the inherent fission source to analyze the sensitivity of the calculated results to the neutron spectrum of the inherent fission source. There are numerous systems that have been measured with the CSDNA technique that could be analyzed with MCNP-DSP.

LIST OF REFERENCES

LIST OF REFERENCES

1. Sastre, C. A.,"The Measurement of Reactivity," *Nucl. Sci. Eng.*, 8, 443 (1960).

2. Mueller, R. E., Nicholson, R. B., and Zweifel, P. F.,"Localized Source Multiplication and Reactor Startup," *Trans. Am. Nucl. Soc.*, 5, 67 (1962).

3. Ricker, C. W., Fry, D. N., Mann, E. R., and Hanauer, S. H.,"Investigation of Negative Reactivity Measurement by Neutron Fluctuation Analysis," *Proc. of the Symposium on Noise Analysis in Nuclear Systems*, University of Florida, Gainesville, 1963.

4. Jankowski, F. J., Klein, D., and Miller, T. M.,"Calibration of Control Rods," *Nucl. Sci. Eng.*, 2, 288 (1957).

5. Simmons, B. E., and King, J. S.,"APulsed Neutron Technique for Reactivity Determination," *Nucl. Sci. Eng.*, 3, 595 (1958).

6. Pare, V. K., and Mihalczo, J. T.,"Reactivity from Power Spectral Density Measurements with Californium-252," *Nucl. Sci. Eng.*, 56, 213 (1975).

7. Mihalczo, J. T., and Valentine, T. E.,"Calculational Verification and Process Control Applications Utilizing the High Sensitivity of Noise Measurement Parameters to Fissile System Configuration," Submitted to *Nucl. Sci. Eng.* (1994).

8. Orndoff, J. D.,"Prompt Neutron Periods of Metal Critical Assemblies," *Nucl. Sci. Eng.*, 2, 450 (1957).

9. Sjostrand, N. G.,"The Pulsed Neutron Method for Diffusion, Slowing Down, and Reactivity Measurements," Workshop on Subcritical Reactivity Measurements, Albuquerque, New Mexico, August 1985, CONF-8508105.

10. Ficaro, E. P., "KENO-NR: A Monte Carlo Code Simulating the ^{252}Cf-Source-Driven Noise Analysis Experimental Method for Determining Subcriticality," Ph.D Dissertation, Univ. of Michigan, 1991.

11. Petrie, L. M., and Landers, N. F.,"KENO V.a: An Improved Monte Carlo Criticality Program with Supergrouping," ORNL/NUREG/CSD-2, Oak Ridge National Laboratory, 1984.

12. Briesmeister, J. F., Ed.,"MCNP4A-A General Monte Carlo N-Particle Transport Code,"La-12625-M, Los Alamos National Laboratory, 1993.

13. Mihalczo, J. T., Blakeman, E. D., Reagan, G. E., Johnson, E. B., and Hachiya, Y.,"Dynamic Subcriticality Measurements Using the ^{252}Cf-Source-Driven Noise Analysis Method," *Nucl. Sci. Eng.*, 104, 314 (1990).

14. Valentine, T. E. and Mihalczo, J. T.,"Sensitivity of Calculations of ^{252}Cf-Source-Driven Noise Analysis Measurements to Cross Sections for Aqueous Fissile Solutions," *Proc. 1993 Topical Meeting on Physics and Methods in Criticality Safety*, Nashville, 1993.

15. Valentine, T. E., Mihalczo, J. T., and Potter, J. W.,"Sensitivity of Calculations of ^{252}Cf-Source-Driven Noise Analysis Measurements to Cross Sections for Aqueous Fissile Plutonium Solutions," *Proc. 1994 Topical Meeting on Advances in Reactor Physics*, Knoxville, 1994.

16. Mihalczo, J. T., personal communication (1994).

17. King, W. T.,"Feasibility of Neutron Noise Measurements in Water Moderated Reactors," Ph.D Dissertation, Univ. of Tennessee, 1980.

18. Stevens, P. N., unpublished class notes (1993).

19. Vandenbosch, R. and Huizenga, J. R., Nuclear Fission, Academic Press, New York, 1973.

20. Keepin, G. R., Physics of Nuclear Kinetics, Addison-Wesley Publishing Company, Inc., Reading, Massachusetts, 1965.

21. Zucker, M. S. and Holden, N. E.,"Energy Dependence of the Neutron Multiplicity P_ν in Fast-Neutron-Induced Fission for ^{235,238}U and ^{239}Pu," *Trans. Am. Nucl. Soc.*, 52, 630 (1986).

22. Spencer, R. R., Gwin, R., and Ingle, R.,"A Measurement of the Average Number of Prompt Neutrons from Spontaneous Fission of Californium-252," *Nucl. Sci. Eng.*, 80, 603 (1982).

23. Budtz-Jorgensen, C. and Knitter, H. H.,"Simultaneous Investigation of Fission Fragments and Neutrons in ^{252}Cf (SF)," *Nucl. Phys.*, A490, 307 (1988).

24. Paré, V. K., personal communication (1994).

25. Nix, J. R., personal communication (1994).

26. Mannhart, W.,"Evaluation of the Cf-252 Fission Neutron Spectrum Between 0 MeV and 20 MeV," *Proc. Advisory Group Mtg. Neutron Sources*, Leningrad, USSR, 1986 (IAEA-TECDOC-410, Vienna, 1987.

27. Seamon, R., personal communication (1994).

28. Brunson, G. S. Jr.,"Multiplicity and Correlated Energy of Gamma Rays Emitted in the Spontaneous Fission of Californium-252," Ph.D Thesis, Univ. of Utah, 1982.

29. Wagemans, C., The Nuclear Fission Process, CRC Press, Inc., Boca Raton, Florida, 1991.

30. Maienschein, F. C., Peelle, R. W., and Love, T. A., *Neutron Phys. Ann. Prog. Rep. Sept. 1*, 1958, ORNL-2609, Oak Ridge National Laboratory.

31. Goldstein, H., Fundamental Aspects of Reactor Shielding, Addison-Wesley Publishing Company, Inc., Reading, Massachusetts, 1959.

32. Nifenecker, H., Signarbieux, C., Ribrag, M., Poitou, J., and Matuszek, J., "Gamma-Neutron Competition in the De-excitation Mechanism of the Fission Fragments of ^{252}Cf," *Nucl. Phys.*, A189, 209 (1972).

33. Oppenheim, A. V. and Schafer, R. W., Discrete-Time Signal Processing, Prentice-Hall Inc., Englewood Cliffs, New Jersey, 1989.

34. Uhrig, R. E., Random Noise Techniques in Nuclear Reactor Systems, The Ronald Press Company, New York, 1970.

35. Bendat, J. S. and Piersol, A. G., Random Data: Analysis and Measurement Procedures, John Wiley & Sons, Inc., New York, 1971.

36. Mihalczo, J. T. and Hill, N. W.,"Simple Time-of-Flight Transmission Measurement for Incorporation in Nuclear Engineering Curricula," *Trans. Am. Nucl. Soc.*, 14, 60 (1971).

37. Mihalczo, J. T.,"Prompt-Neutron Lifetime in Critical Enriched-Uranium Metal Cylinders and Annuli," *Nucl. Sci. Eng.*, 20, 60 (1964).

38. Mihalczo, J. T., King, W. T., and Blakeman, E. D.,"Subcriticality Measurements for Coupled Uranium Metal Cylinders Using the ^{252}Cf-Source-Driven Neutron Noise Analysis Method," *Nucl. Sci. Eng.*, 95, 1 (1987).

39. Garber, D.,"ENDF-201, ENDF/B Summary Documentation,"BNL-17541, Brookhaven National Laboratory (1975).

40. Garber, D.,"ENDF/B-V,"BNL-17541 (ENDF-201),Brookhaven National Laboratory (1975).

41. Rose, P. F.,"ENDF-201, ENDF/B-VI Summary Documentation,"BNL-17541, Brookhaven National Laboratory (1991).

42. Madland, D. G. and Nix,J. R.,"NewCalculation of Prompt Fission Neutron Spectra and Average Prompt Neutron Multiplicities," *Nucl. Sci. Eng.*, 81, 213 (1982).

43. Madland, D. G., Personal Communication (1994).

44. Lewis, E. E. and Miller, W. F., Jr.,Computational Methods of Neutron Transport, American Nuclear Society, Inc., La Grange Park, Illinois, 1993.

45. Munoz-Cobo, J., Perez, R. B., Verdu, G.,"Stochastic Neutron Transport Theory: Neutron Counting Statistics in Nuclear Assemblies,"*Nucl. Sci. Eng.*, 95, 83 (1987).

APPENDICES

APPENDIX A

INTEGRAL TRANSPORT THEORY

The fundamental equation used to describe the average behavior of neutral particles in any system is the Boltzmann transport equation. The Boltzmann transport equation can be written as

$$\frac{1}{v}\frac{\partial}{\partial t}\phi(\vec{r},E,\vec{\Omega},t)+\vec{\Omega}\cdot\nabla\phi(\vec{r},E,\vec{\Omega},t)+\Sigma_t(\vec{r},E)\phi(\vec{r},E,\vec{\Omega},t)$$
$$=S(\vec{r},E,\vec{\Omega},t)+\int\int dE'd\vec{\Omega}'\Sigma_s(\vec{r},E'\rightarrow E,\vec{\Omega}'\rightarrow\vec{\Omega})\phi(\vec{r},E',\vec{\Omega}',t), \quad \text{(A.1)}$$

where $\phi(\vec{r},E,\vec{\Omega},t)$ is the time-dependent angular particle flux, v is the particle's speed, $\Sigma_t(\vec{r},E)$ is the total macroscopic cross section, $\Sigma_s(\vec{r},E'\rightarrow E,\vec{\Omega}'\rightarrow\vec{\Omega})$ is the differential scattering cross section, and $S(\vec{r},E,\vec{\Omega},t)$ is the particle source. The assumptions made in deriving the transport equation are as follows: the wave behavior of the particles is ignored, the particles travel in straight lines from one collision point to another, particle-particle interactions are ignored, collisions occur instantaneously with the one exception of including delayed particles from fission, there are a sufficient number of particles present such that the particle variations from the mean are relatively small, and macroscopic variables will suffice in the characterization of the radiation field.[44]

To convert the integro-differential equation into an integral equation, the convection and storage terms are combined. The convection and storage terms are expressed in terms of the spatial variable R that relates a fixed point in space, r, to an arbitrary point in space, r'. R is the distance along the line of neutron travel, as shown in Fig. A.1. The point r' is

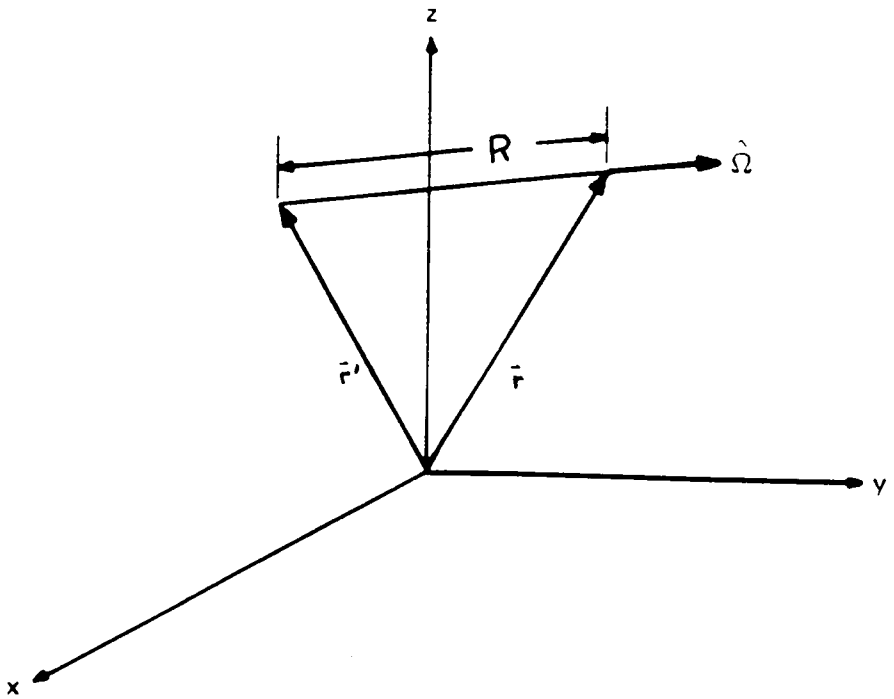

Figure A.1 Flight Path for Particle Travel

related to the point r by $r'=r-R\vec{\Omega}$, and the time t' is related to time t by $t'=t-R/v'$. The total derivative of the angular flux with respect to R is given by the total (substantial) derivative

$$\frac{d}{dR}\phi(\vec{r}',E,\vec{\Omega},t')=\frac{\partial x}{\partial R}\frac{\partial\phi}{\partial x}+\frac{\partial y}{\partial R}\frac{\partial\phi}{\partial y}+\frac{\partial z}{\partial R}\frac{\partial\phi}{\partial z}+\frac{\partial t}{\partial R}\frac{\partial\phi}{\partial t}. \qquad (A.2)$$

The partial derivatives with respect to R can be expressed as

$$\frac{d}{dR}\phi(\vec{r}',E,\vec{\Omega},t')=-\vec{\Omega}_x\frac{\partial}{\partial x}\phi-\vec{\Omega}_y\frac{\partial}{\partial y}\phi-\vec{\Omega}_z\frac{\partial}{\partial z}\phi-\frac{1}{v}\frac{\partial}{\partial t}\phi, \qquad (A.3)$$

or

$$\frac{d}{dR}\phi(\vec{r}',E,\vec{\Omega},t')=-\vec{\Omega}\cdot\nabla\phi(\vec{r}',E,\vec{\Omega},t')-\frac{1}{v}\frac{\partial}{\partial t}\phi(\vec{r}',E,\vec{\Omega},t'). \qquad (A.4)$$

This total derivative is substituted into the transport equation to obtain

$$\begin{aligned}&-\frac{d}{dR}\phi(\vec{r}',E,\vec{\Omega},t')+\Sigma_t(\vec{r}',E)\,\phi(\vec{r}',E,\vec{\Omega},t')\\&=S(\vec{r}',E,\vec{\Omega},t')+\int\int dE'd\vec{\Omega}'\Sigma_s(\vec{r}',E'\to E,\vec{\Omega}'\to\vec{\Omega})\,\phi(\vec{r}',E',\vec{\Omega}',t').\end{aligned} \qquad (A.5)$$

Equation A.5 can be changed in form by introducing an integrating factor as follows:

$$\begin{aligned}&\frac{d}{dR}\left[\phi(\vec{r}',E,\vec{\Omega},t')\,e^{-\int_0^R\Sigma_t(r-R'\vec{\Omega},E)\,dR'}\right]=-e^{-\int_0^R\Sigma_t(r-R'\vec{\Omega},E)\,dR'}\\&\left[-\frac{d}{dR}\phi(\vec{r}',E,\vec{\Omega},t')+\Sigma_t(\vec{r}',E)\,\phi(\vec{r}',E,\vec{\Omega},t')\right].\end{aligned} \qquad (A.6)$$

Substitution of Eq. A.6 into Eq. A.5 yields

$$-\frac{d}{dR}\left[\phi(\vec{r}',E,\vec{\Omega},t')\,e^{-\int_0^R \Sigma_t(r-R'\vec{\Omega},E)\,dR'}\right] = e^{-\int_0^R \Sigma_t(r-R'\vec{\Omega},E)\,dR'} \tag{A.7}$$

$$\left[S(\vec{r}',E,\vec{\Omega},t)+\int\int dE'd\vec{\Omega}'\Sigma_s(\vec{r}',E'\to E,\vec{\Omega}'\to\vec{\Omega})\,\phi(\vec{r}',E',\vec{\Omega}',t')\right].$$

Multiplying Eq. A.7 by dR and integrating over the interval $(0,\infty)$ leads to

$$\phi(\vec{r},E,\vec{\Omega},t)-\phi(\infty,E,\vec{\Omega},t_\infty)\,e^{-\int_0^\infty \Sigma_t(r-R'\vec{\Omega},E)\,dR'} = \int_0^\infty dR\, e^{-\int_0^R \Sigma_t(r-R'\vec{\Omega},E)\,dR'} \tag{A.8}$$

$$\left[S(r-R\vec{\Omega},E,\vec{\Omega},t-\frac{R}{v})+\int\int dE'd\vec{\Omega}'\Sigma_s(r-R\vec{\Omega},\vec{\Omega}'\to\vec{\Omega})\,\phi(r-R\vec{\Omega},E',\vec{\Omega}',t-\frac{R}{v})\right].$$

By considering problems with no sources at infinity and/or requiring the contribution from particle fluxes at infinity to be zero, Eq. A.8 is simplified to

$$\phi(\vec{r},E,\vec{\Omega},t)=\int_0^R dR e^{-\beta(\vec{r},E,R,\vec{\Omega})}\left[S(r-R\vec{\Omega},E,\vec{\Omega},t-\frac{R}{v})+\right. \tag{A.9}$$

$$\left.\int\int dE'd\vec{\Omega}'\Sigma_s(r-R\vec{\Omega},E'\to E,\vec{\Omega}'\to\vec{\Omega})\,\phi(r-R\vec{\Omega},E',\vec{\Omega}',t-\frac{R}{v})\right],$$

where $\beta(r,E,R,\vec{\Omega})$ is the optical thickness.

Equation A.9 is used to formulate the emergent particle density equation. The emergent particle density, $\chi(r,E,\vec{\Omega},t)$, is defined as the density of particles leaving a source or emerging from a real collision:

$$\chi(r,E,\vec{\Omega},t)=S(r,E,\vec{\Omega},t)+ \tag{A.10}$$

$$\int\int dE'd\vec{\Omega}'\Sigma_s(r,E'\to E,\vec{\Omega}'\to\vec{\Omega})\,\phi(r,E',\vec{\Omega}',t).$$

Then, Eq. A.9 can be written as

$$\phi(r, E, \vec{\Omega}, t) = \int_0^R dR\ e^{-\beta(r, E, R, \vec{\Omega})} \chi(\vec{r}', E, \vec{\Omega}, t') \,. \qquad \text{(A.11)}$$

Substitution of Eq. A.11 into Eq. A.10 yields the integral emergent particle density equation

$$\chi(r, E, \vec{\Omega}, t) = S(r, E, \vec{\Omega}, t) + \iint dE' d\vec{\Omega}' \Sigma_s(r, E' \to E, \vec{\Omega}' \to \vec{\Omega}) \int_0^\infty dR\ e^{-\beta(r, E, R, \vec{\Omega})} \chi(\vec{r}', E', \vec{\Omega}', t') \,. \qquad \text{(A.12)}$$

The integral emergent particle density equation is another form of the Boltzmann transport equation that can provide a basis for the Monte Carlo random walk.

The Boltzmann transport equation has been shown by Munoz-Cobo et. al.[45] to be the first moment of the more general stochastic neutron transport equation which is defined by generating an equation for the probability generating function that relates neutron loss and production as a probability balance. Higher moments of the particle flux can also be obtained from the probability balance equation. Since the Monte Carlo technique is defined on the basis of interaction probabilities, the Monte Carlo calculation may be considered as the phenomological realization of the master probability balance equation. Therefore, the Monte Carlo calculation may be used to obtain information about the higher moments of the particle flux. The higher moments are the basis of the noise analysis methods.

APPENDIX B

NEUTRON DISTRIBUTION DATA FOR ^{252}Cf

The P(ν) for ^{252}Cf was obtained from the measured data of Spencer. These probabilities are listed in Table B.1. The average number of neutrons from the spontaneous fission of ^{252}Cf is 3.773.

Table B.1 P(ν) Probabilities for ^{252}Cf

ν	P(ν)
0	0.00211
1	0.02467
2	0.12290
3	0.27144
4	0.30763
5	0.18770
6	0.06770
7	0.01406
8	0.00167
9	0.00010

APPENDIX C

NEUTRON ANGULAR DISTRIBUTION FROM FISSION

The angular distribution of neutrons relative to the light fission fragment in the laboratory system has been measured by Budtz-Jorgensen and Knitter.[22] This data has been included in the modified MCNP code. The probability distribution (Fig. 3.4) is sampled as a function of the neutron's outgoing energy to obtain the neutron's direction relative to the direction of the light fission fragment. The light fission fragment's direction relative to the laboratory reference frame is randomly sampled from an isotropic distribution. The coordinate axes for the fission fragment and laboratory frames is shown in Fig. C.1. The fission fragments direction vector is given by

$$\bar{r}=\sin\theta\cos\phi\hat{e}_x+\sin\theta\sin\phi\hat{e}_y+\cos\theta\hat{e}_z, \tag{3.1}$$

where θ is the light fission fragment's polar angle, ϕ is the light fission fragment's azimuthal angle, and $\hat{e}_i$ is the unit direction vector of the ith axis. The neutron's direction relative to the light fission fragment is given by

$$\bar{r}'=\sin\psi\cos\eta\hat{e}_{x'}+\sin\psi\sin\eta\hat{e}_{y'}+\cos\psi\hat{e}_{z'}, \tag{C.2}$$

where ψ is the neutron's polar angle relative to the light fission fragment, η is the neutron's azimuthal angle relative to the light fission fragment, and $\hat{e}_{i'}$ is the unit direction vector of the primed axis. To transform the neutron's coordinates from the reference frame of the light fission fragment to the laboratory system, $\hat{e}_{z'}$ is made colinear to the fission fragment direction vector, resulting in the following expression

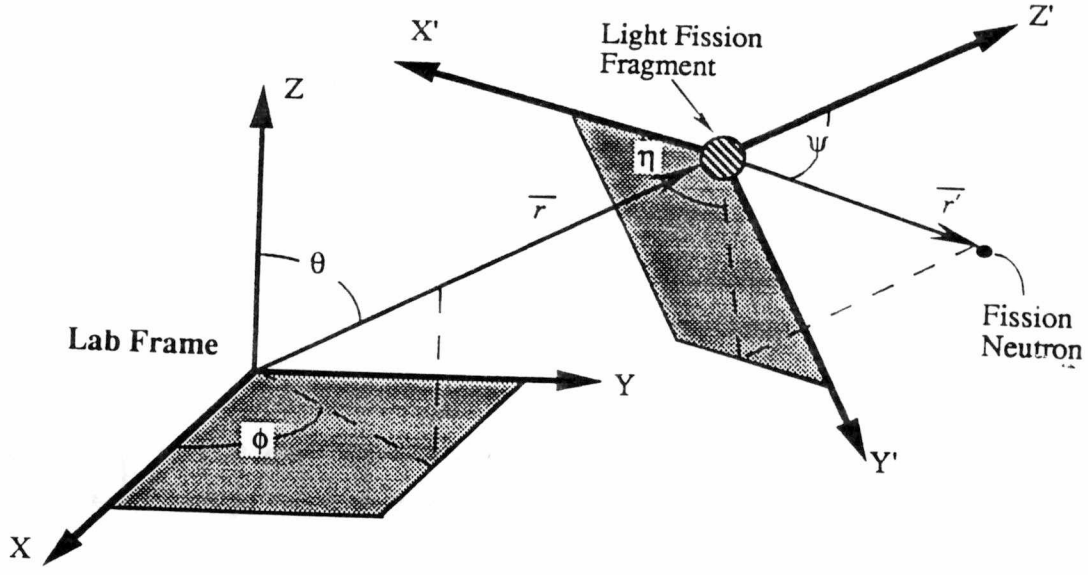

Figure C.1 Coordinate Transformation for Relating Neutron Direction to the Laboratory Reference Frame

$$\hat{e}_{z'}=\frac{\bar{r}}{|\bar{r}|}=\sin\theta\cos\phi\hat{e}_x+\sin\theta\sin\phi\hat{e}_y\cos\theta\hat{e}_z. \tag{C.3}$$

The unit direction vector $\hat{e}_{y'}$ must be at a right angle to $\hat{e}_{z'}$; therefore, the inner product of $\hat{e}_{y'}$ and $\hat{e}_{z'}$ must be zero. A vector that satisfies this criteria is

$$\hat{e}_{y'}=-\sin\phi\hat{e}_x+\cos\phi\hat{e}_y. \tag{C.4}$$

To construct a vector perpendicular to the plane formed by $\hat{e}_{y'}$ and $\hat{e}_{z'}$, the cross product of $\hat{e}_{y'}$ and $\hat{e}_{z'}$ is evaluated to obtain

$$\hat{e}_{x'}=\cos\theta\cos\phi\hat{e}_x+\cos\theta\sin\phi\hat{e}_y-\sin\theta\hat{e}_z. \tag{C.5}$$

Substitution of Eqs. C.3, C.4, and C.5 into Eq. C.2 yields the neutron direction in the lab frame

$$\begin{aligned}\bar{r}'=&(\alpha\frac{uw}{\sqrt{1-w^2}}-\beta\frac{v}{\sqrt{1-w^2}}+u\mu)\hat{e}_x\\&+(\alpha\frac{vw}{\sqrt{1-w^2}}+\beta\frac{u}{\sqrt{1-w^2}}+v\mu)\hat{e}_y\\&+(-\alpha\sqrt{1-w^2}+w\mu)\hat{e}_z\ ,\end{aligned} \tag{C.6}$$

where $u=\sin\theta\cos\phi$, $w=\sin\theta\sin\phi$, $w=\cos\theta$, $\alpha=\sin\psi\cos\eta$, $\beta=\sin\psi\sin\eta$, and $\mu=\cos\eta$.

APPENDIX D

^{252}Cf MODIFIED NEUTRON ENERGY SPECTRUM

Various measurements have been performed to determine the prompt neutron energy spectrum for ^{252}Cf. This spectrum is a standard for neutron detector calibration. The spectrum is typically represented as a Maxwellian with a nuclear temperature of 1.42 MeV. However, the Maxwellian differs from the measured spectrum. To correct for the discrepancy between the measured spectrum and the Maxwellian spectrum, Mannhart[26] developed an energy dependent correction factor, $R(E)$, which, when multiplied by the Maxwellian spectrum, would reproduce the measured spectrum. A least squares polynomial regression model was used to obtain a functional form for Mannhart's correction factor. For energies less than 5.0 MeV, the correction factor is represented as

$$R(E)=9.55\cdot10^{-1}+7.07\cdot10^{-1}E-4.44\cdot10^{-2}E^2 +2.00\cdot10^{-2}E^3-4.51\cdot10^{-3}E^4+3.68\cdot10^{-4}E^5. \quad \text{(D.1)}$$

For energies greater than 5.0 MeV, the correction factor is

$$R(E)=1.16-4.32\cdot10^{-1}\ E+1.85\cdot10^{-3}\ E^2-3.16\cdot10^{-5}\ E^3. \quad \text{(D.2)}$$

These energy ranges were chosen such that the functional representation adequately reproduces Mannhart's discrete points. Other fits could be applied to Mannhart's correction factor. These functional forms, when multiplied by the Maxwellian (Eq. 3.3), should adequately reproduce the measured spectra. The corrected Maxwellian spectrum, $N(E)$, is shown in Fig. D.1. The corrected spectrum is used to calculate the average energy of neutrons for the spontaneous fission of ^{252}Cf. The average energy of neutrons

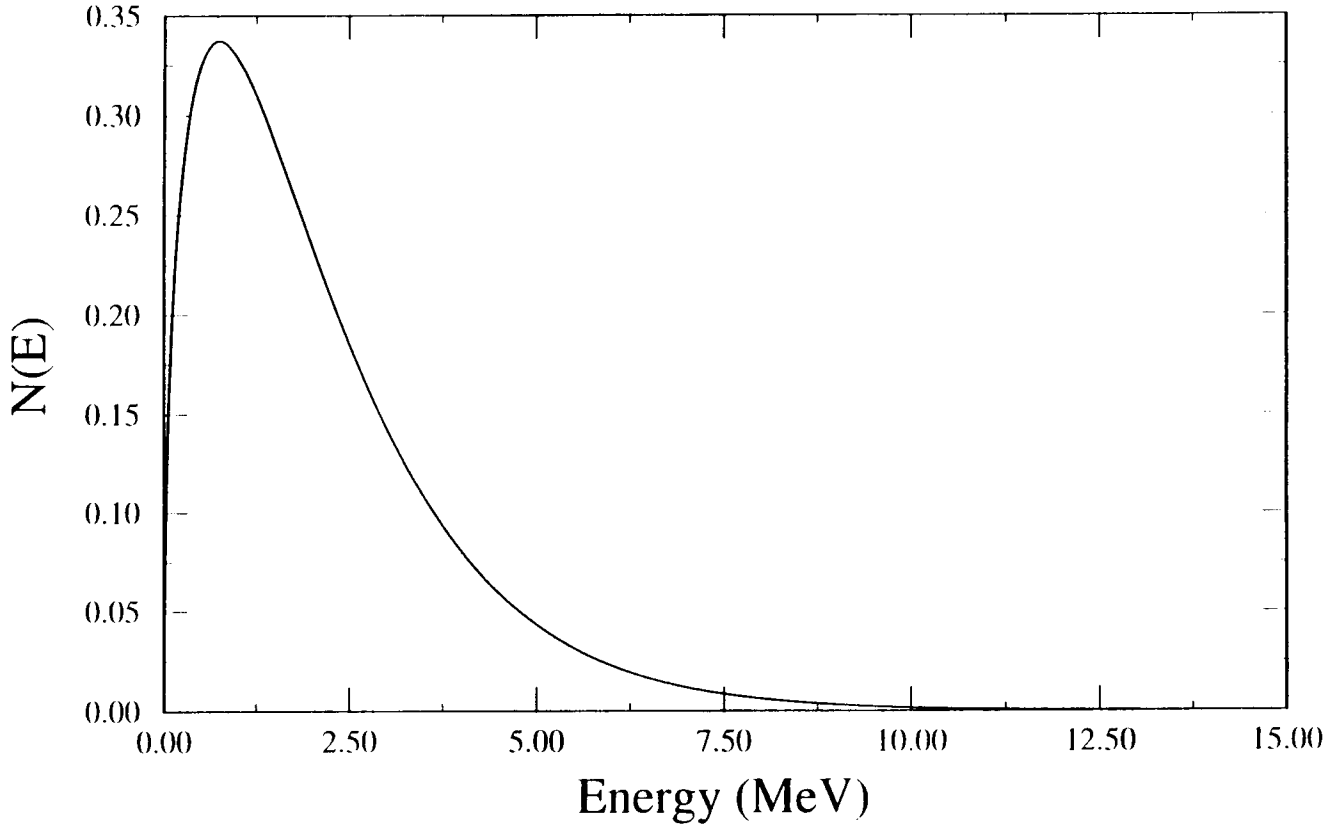

Figure D.1 Corrected Maxwellian Neutron Energy Spectrum

for the spontaneous fission of ^{252}Cf is calculated from

$$\langle E \rangle = \frac{\int_0^\infty E\, N(E)\, dE}{\int_0^\infty N(E)\, dE}. \qquad \text{(D.3)}$$

The value obtained for the average energy is 2.13 MeV. This value agrees well with the measured value.[26] This integral of the corrected spectrum was calculated as a function of energy and normalized to unity. The selection of the neutron energy in the Monte Carlo calculation is typically determined by sampling a random number and determining at which energy the normalized integral is equal to the random number. However, in the MCNP-DSP code, a least squares polynomial regression was used to fit the energy as a function of the normalized integral, that is, making the energy a polynomial function of the random variable.

APPENDIX E

INPUT AND OUTPUT SUMMARY

Examples of the input files and an example output file are presented for a 9.14-cm-high uranium metal cylinder. There are two input files. The first is the standard MCNP input files. The second input files contains data necessary for the noise analysis calculation. The output file contains a limited amount of information about the particle histories.

Figure E.1 is a listing of the MCNP input file to execute the noise analysis calculation for the 91.4-mm-high uranium metal cylinder. Figure E.2 is the extra data file for this problem. Only an overview of this input file is presented. For a more detailed description of the MCNP input file , consult ref 12.

Description of Input File

Line 1: The first line is the title line. Typically, a general description of the system is used as the title line.

Lines 2-9: These lines contain the cell descriptions for the problem. The cell cards are used to describe the material's density and the surfaces that bound the particular cell. In this example, the first cell is the uranium metal cylinder. Comment cards can be used along with the cell cards.

Lines 11-21: These lines contain the surface description for the problem. The surfaces typically consist of planes, cylinders, spheres, and cones. In this simple example, the system can easily be described by planes and cylinders.

Lines 23-35: These lines are referred to as the data cards because the necessary data needed to perform the calculation are presented in these lines. Line 23 states that this particular problem is a dual neutron-photon calculation. Lines 24 and 25 contain the cell importances for these neutrons and photons. Lines 26 through 31 contain the material descriptions for the problem. Line 32 is the debug control card. In this example, the debug control card is used to specify the starting random number seed along with the length of the random number stride. Line 33 is important since this line is used to control the execution of the noise analysis calculation. If the first input on

```
1       Uranium Metal Cylinder: 91.4 mm high, source top,ENDF/B-IV&5
2       1     1 0.04802913  1 -2 -10      $ Uranium Metal Cylinder
3       2     0 2 -9 -10                 $ Void Above Cylinder for Source
4       3     0 1 -9  10 -3 4 -5 6       $ Void Around Cylinder
5       4     2 0.081338  3 -7 -11       $ Right Detector
6       5     3 0.081338 -4  8 -11       $ Left Detector
7       6     0  3 -7 11 -5 6 1 -9       $ Void Around Right Detector
8       7     0 -4  8 11 -5 6 1 -9       $ Void Around Left Detector
9       8     0 -1:9:7:-8:5:-6
10
11      1     pz    0.0
12      2     pz    9.14
13      3     px    8.8855
14      4     px   -8.8855
15      5     py    8.8855
16      6     py   -8.8855
17      7     px   11.4255
18      8     px  -11.4255
19      9     pz    9.141
20      10    cz    8.8855
21      11    c/x   0.0   4.57   1.905
22
23      mode n p
24      imp:n 1 1 1 1 1 1 1 0
25      imp:p 1 1 1 1 1 1 1 0
26       m1   92234.50c 0.002411985   92235.11c 0.9321931
27            92236.50c 0.009665840   92238.12c 0.05572903
28       m2   3006.04c  0.215791 3007.05c  0.009885 8016.04c  0.529568
29            12000.50c 0.001820 13027.04c 0.017433 14000.50c 0.223942
30       m3   3006.04c  0.215791 3007.05c  0.009885 8016.04c  0.529568
31            12000.50c 0.001820 13027.04c 0.017433 14000.50c 0.223942
32      dbcn  19533486377795 11j 725525
33      idum  1
34      files 21 metin9 s f 0 22 umiv92 s f 0
35      ctme  1200
```

Figure E.1 Example MCNP-DSP Input File

```
1       scd=32.
2       bks=500000
3       scc=2
4       scx=0.0
5       scy=0.0
6       scz=9.1405
7       tbn=512  10000000.
8       fil=0 win=0 smo=no
9       det=2 2 2 0.0  0.3 2
10      det=3 3 2 0.0  0.3 2
11      stp=0
12      cng=0
13      end
```

Figure E.2 Extra Data File for MCNP-DSP Calculation

the idum card is a 1, the noise analysis calculation is performed. If the first number on the idum card is a 2 and the kcode card is included in the data cards, the analog criticality calculation will be performed. If the idum card is omitted, MCNP-DSP will execute the same as MCNP4A. Line 34 contains the file's card data. If the noise calculation is to be performed, this line must also be included in the problem specification. The first entry is the unit number for the following file. The second entry is the file name. This is the file that contains the data necessary for the noise analysis calculation. Data are read from this file to set up the calculation. The seventh entry is the output file name. This is name is also used as the first part of the files that contain the frequency and time spectra. For this particular problem, there will be three files created that contain the frequency data. These are: umiv92.123.fft.n, umiv92.123.fft.p, and umiv92.123.fft.np for the neutron data, the photon data, and the combined data. The last line is the time card and can be used to specify a time limit for the calculation.

An example of the extra data file is provided in Fig. E.2. The data in the extra data file can be ordered in any fashion.

Description of Extra Data File

Line 1: In the first line *scd* is the number of source events per block. This is the number of fissions per block for the ^{252}Cf source and is the number of DT reactions per block for the 14 MeV source.

Line 2: The second entry, *bks*, is the number of blocks to calculate.

Line 3: The cell location of the source is specified by *scc*.

Lines 4-6: These parameters *scx*, *scy*, and *scz* specify the source's x-, y-, and z-coordinates respectively.

Line 7: This line specifies the number of points per block and the sampling rate. The entries must be in that order. The number of points can be 128, 256, 512, or 1024 points.

Line 8: There are three important entries on this line. The first is the filter option flag, *fil*. The following are allowed filter options:

fil=0 no filter (default)
=1 Rockland filter
=2 Precision filter

The second option is the window flag, *win*. The following are allowed window options that are applied to the detector time response:

win=0 no window (default)
=1 Bartlett window
=2 Hanning window
=3 Hamming window

The third option, *smo*, is to use a Hanning window on the frequency spectra to smooth the frequency data. The choices are yes or no smoothing, with no being the default.

Lines 9 and 10: These lines contain the information concerning the detector options. The detector data are described in the following order:

detector number	allowed values are 2,3,4,or 5
detector material	the material in the MCNP that is the detector
detector type	2 is a neutron capture detector 3 is a neutron scattering detector 4 is a fission detector
neutron threshold	this entry is entered in units of MeV
photon threshold	this entry is entered in units of MeV
pulse generation time	this entry is entered in nanoseconds

Line 11: The parameter *stp* determines the source type. If *stp*=0 the ^{252}Cf source is used. If *stp*=1, the 14 MeV source is used.

Line 12: The parameter *cng* determines if the angular distribution data are to be used for the ^{252}Cf neutrons.

cng=0 isotropic distribution
=1 angular distribution determined relative to light fission fragment

Options that are not included in this example file are described below.

snu This card is used to specify the neutron emission probability for the source if the default values wish to be changed. Ten entries must be given since the neutron emission from ^{252}Cf ranges from 0 to 9 neutrons.

spu This card is used to specify the photon emission probability for the source if the default values wish to be changed. Twenty-one entries are required for the photon emission probabilities.

ltm This parameter is used to specify a time domain calculation to obtain the detector counts after the source event. The possible values are yes and no with no being the default.

ang If *ang* is equal to 1, the angular distribution data of Budtz-Jorgensen and Knitter are used to specify the neutron direction from fission. Otherwise, the default description from the cross data file is used to describe the neutron's direction.

pro This parameter is used to specify which data processing mode to process the detector response. If $pro=0$, the frequency spectra are obtained by direct fast Fourier transformation of the detector response. The default value is 0. If $pro=1$, the autocorrelation and cross-correlation functions are calculated and the frequency spectra are obtained from the Fourier transformation of the correlation functions.

sfs This parameter is the spontaneous fission source option. Several parameters must be specified for this option and in the following order:

sftyp = 1 ^{238}U spontaneous fission source.

= 2 ^{240}Pu or ^{242}Pu spontaneous fission source. Since $\bar{\nu}$ is the essentially the same for these two isotopes and since the prompt neutron fission spectrum is essentially the same for these two isotopes, one distribution can be used to characterize either of these inherent fission sources.

sfsc This is the cell that contains the inherent fission source.

sfpb This is the number of spontaneous fissions per block.

sfvol = 0 The inherent fission source is bounded by 6 planes, which are the +x, -x, +y, -y, +z, and -z for the given cell.

= 1 The inherent fission source is bounded by a cylinder on the x-axis. Four entries are then required. These are the inner radius and outer radius of the cylinder and the +x and -x planes, which determine the cylinder length.

= 2 The inherent fission source is bounded by a cylinder on the y-axis. Four entries are then required. These are the inner radius and outer radius of the cylinder and the +y and -y planes, which determine the cylinder length.

= 3 The inherent fission source is bounded by a cylinder on the z-axis. Four entries are then required. These are the inner radius and outer radius of the cylinder and the +z and -z planes, which determine the cylinder length.

= 4 The inherent fission source is bounded by a spherical volume. Two entries are required to specify the inner radius and the outer radius of the spherical volume.

An example of the output file is provided in Fig. E.3. The information is this file is self-explanatory.

```
*****************************************************************************
*                          Source Information                               *
*****************************************************************************
Number of Source Events/ Data Block=                          32.
Number of Data Blocks=                                     500000
Source Cell=                                                    2
Source Surface=                                                 0
Source Coordinates
Source X-Coordinate=                                       0.0000
Source Y-Coordinate=                                       0.0000
Source Z-Coordinate=                                       9.1405
*****************************************************************************
*****************************************************************************
*                         Detector Information                              *
*****************************************************************************
Det. Id.    Det. Mat.    Det. Type    N Cutoff     P Cutoff      Gen. Time
    2           2            2        0.00000      0.30000    2.000000000000
    3           3            2        0.00000      0.30000    2.000000000000
*****************************************************************************
*****************************************************************************
*                     Neutron Tracking Information                          *
*****************************************************************************
          Neutrons Followed:                                      12745823
          Number of Fissions:                                      4052135
          Number of Captures:                                       449253
          Number of Leakages:                                      8244435
          Cf Neutrons Followed:                                    2185312
          Number of Fissions (Cf)                                   466150
          Number of Captures (Cf)                                    48012
          Number of Leakages (Cf)                                  1671150
*****************************************************************************
*                          Calculated Parameters                            *
*****************************************************************************
          Average Cf Nu-Bar:                 3.77587 +/- 0.00000
          Average Cf Nu-Sq-Bar:             15.83813
          Source Diven Factor:               0.84605
          Average Cf Energy (MeV)            2.1277 +/- 0.00000
          Average Nu-Bar:                    2.60616 +/- 0.00000
          Average Nu-Sq-Bar:                 8.13286
          Diven Factor:                      0.81370
          Average Energy (MeV)               2.0129 +/- 0.00000
*****************************************************************************
*                         Detector Information                              *
*****************************************************************************
Det. Id.    Det. Mat    Det. Type          No. Detects          No. Cf Detects
    2           2            2                1815                    106
    3           3            2                1896                    104

*****************************************************************************
*                      Photon Tracking Information                          *
*****************************************************************************
          Cf Photons Followed:                                    4513197
          Number of Cf Leakages                                   2465349
*****************************************************************************
*                          Calculated Parameters                            *
*****************************************************************************
          Average Cf G-Bar:                  7.79809 +/- 0.00001
          Average Cf G-Sq-Bar:              70.785362
          Source Photon Diven Factor:        1.03580
          Average Cf Energy (MeV)            0.8986 +/- 0.00000
*****************************************************************************
*                         Detector Information                              *
*****************************************************************************
Det. Id.    Det. Mat    Det. Type          No. Detects          No. Cf Detects
    2           2            2                2338                      3
    3           3            2                2396                      0
```

Figure E.3 Output File from MCNP-DSP Calculation

APPENDIX F

COMPARISON OF DIRECT AND INDIRECT FOURIER PROCESSING

A detailed comparison of the frequency spectra obtained by taking the fast Fourier transforms of the detector responses and the spectra obtained by taking the Fourier transforms of the autocorrelation and cross-correlation functions of the detector responses is presented in this appendix. Figure F.1 shows γ_{12}^2 and γ_{23}^2 as a function of frequency for the 50.8-mm-OD detectors. Figure F.2 shows γ_{12}^2 and γ_{23}^2 as a function of frequency for the 25.4-mm-OD detectors. Figure F.3 shows γ_{12}^2 and γ_{23}^2 as a function of frequency for the 10.37-mm-OD detectors. Figure F.4 shows γ_{12}^2 and γ_{23}^2 as a function of frequency for the 4.234-mm-OD detectors. From this analysis, it is obvious that the indirect Fourier processing method produces the same results as the direct Fourier processing method.

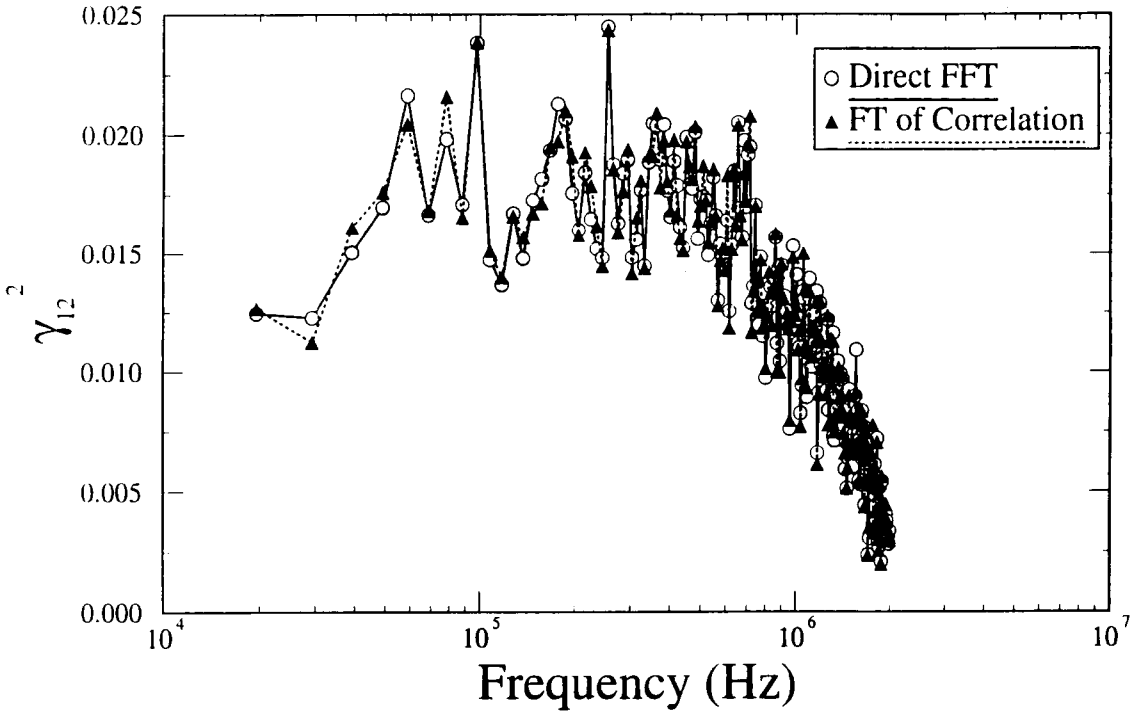

(a)

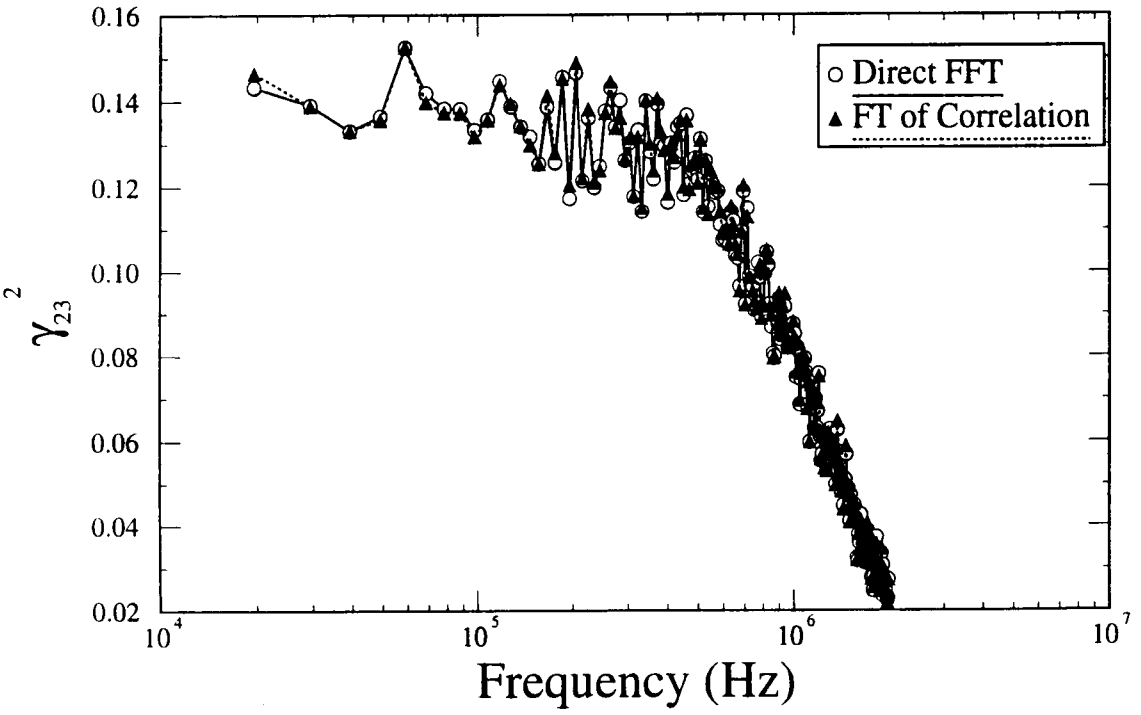

(b)

Figure F.1 Comparison of (a) γ_{12}^2 and (b) γ_{23}^2 from the Direct and Indirect Fourier Processing for the 50.8-mm-OD Detectors

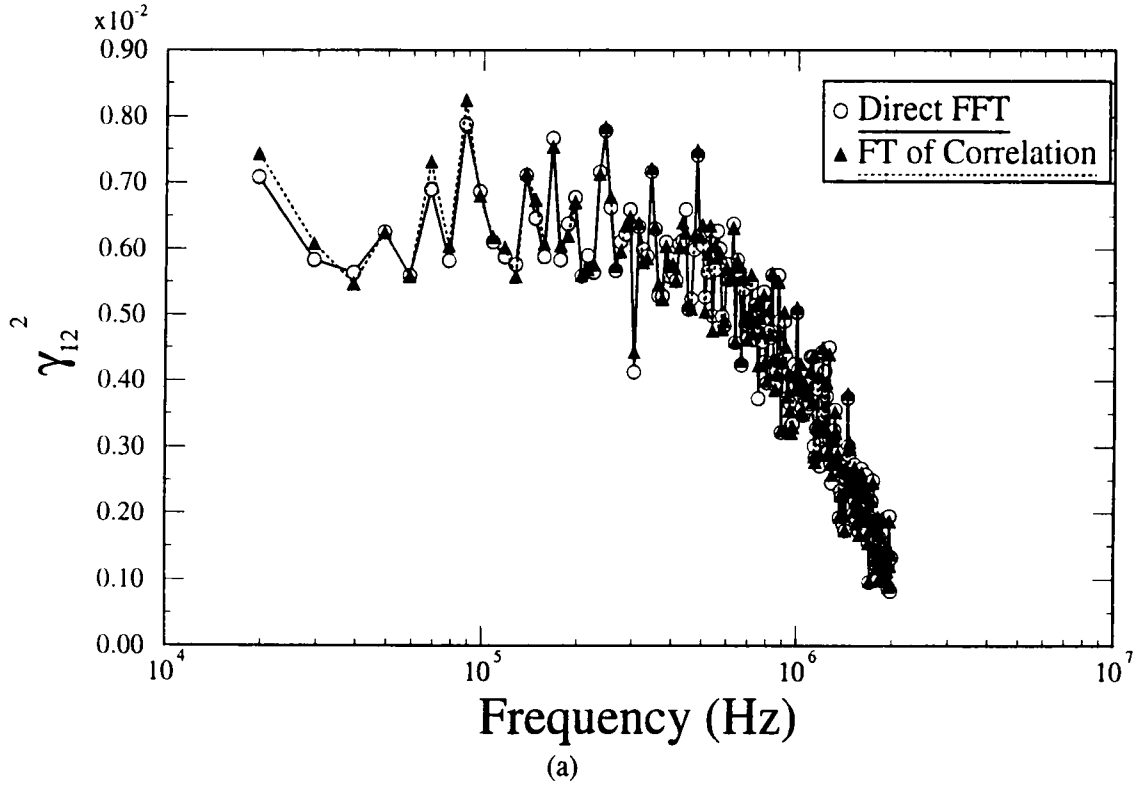

(a)

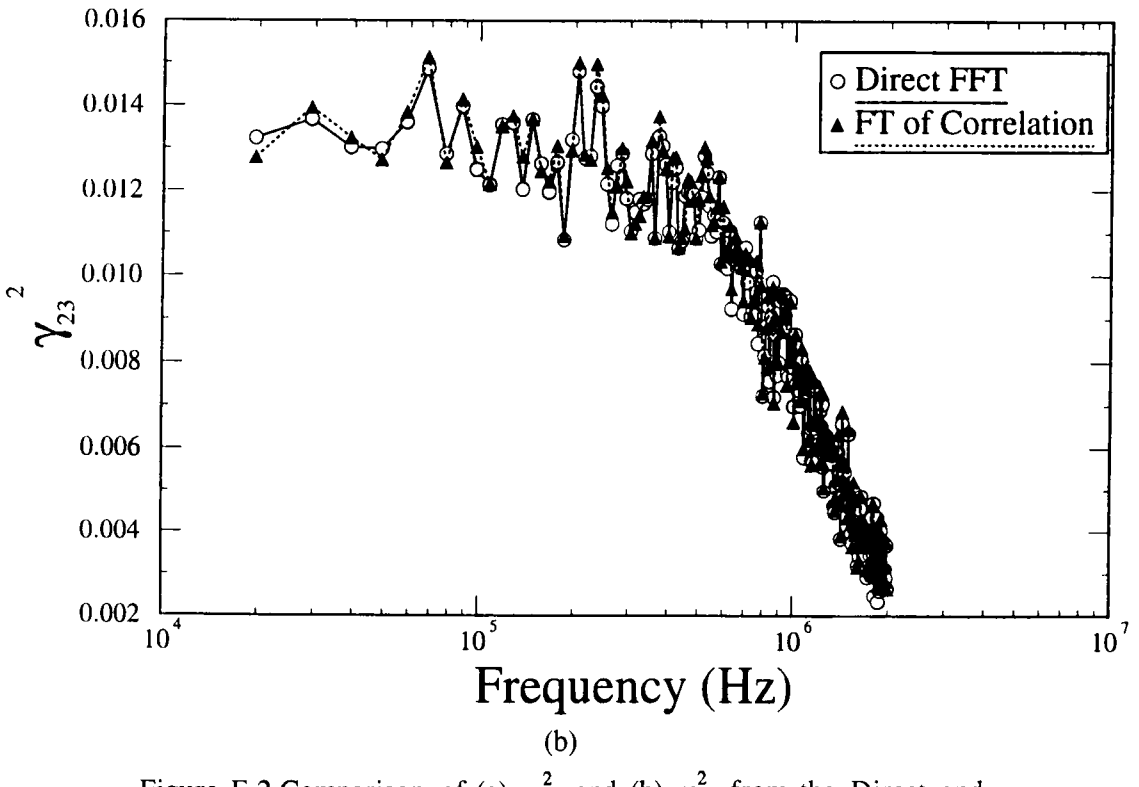

(b)

Figure F.2 Comparison of (a) γ_{12}^2 and (b) γ_{23}^2 from the Direct and Indirect Fourier Processing for the 25.4-mm-OD Detectors

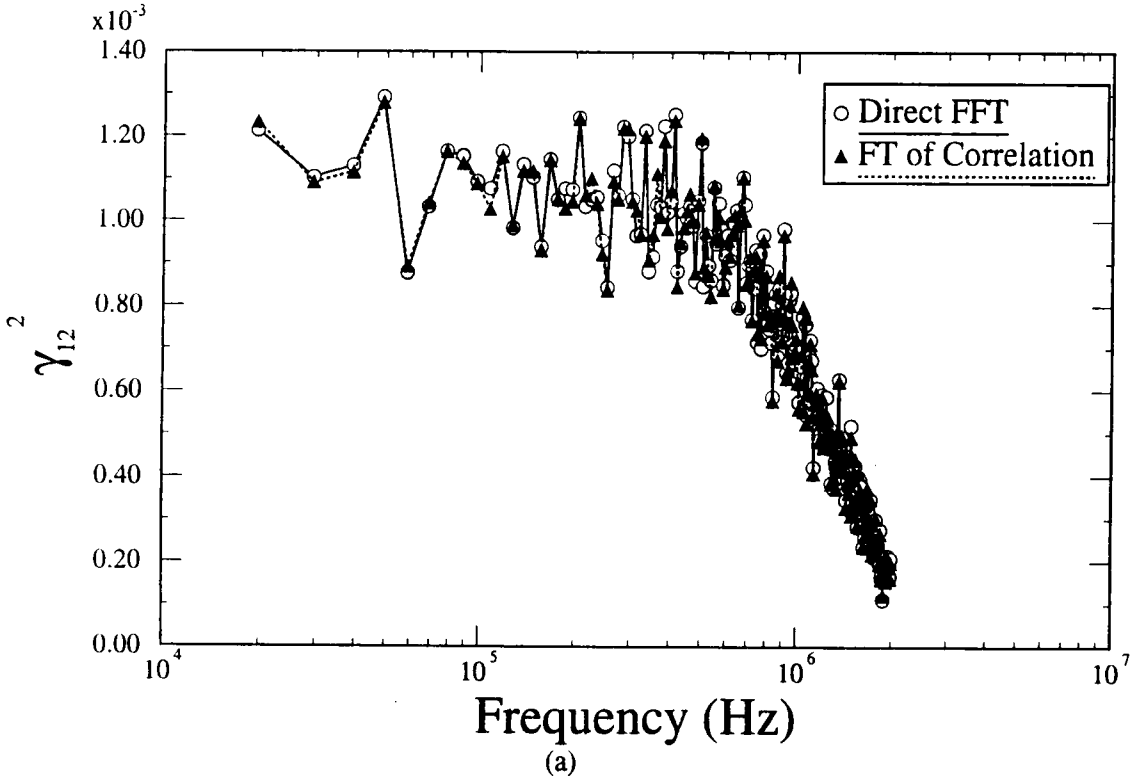

(a)

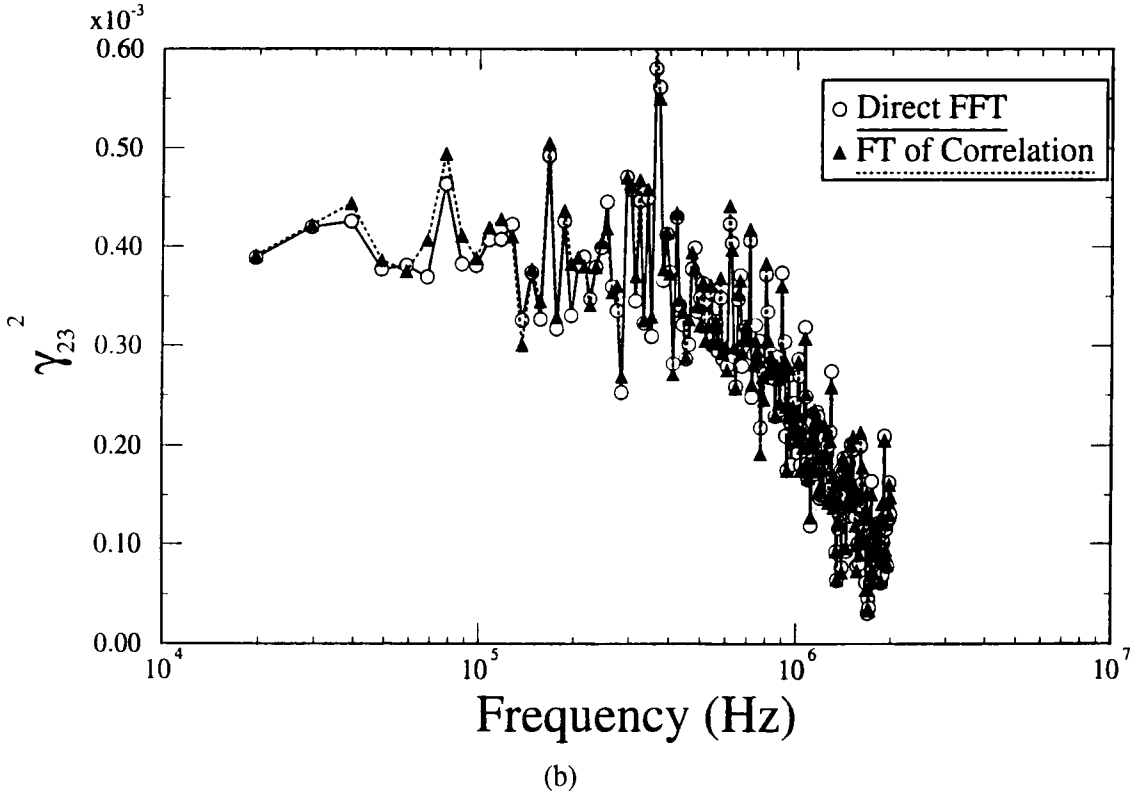

(b)

Figure F.3 Comparison of (a) γ_{12}^2 and (b) γ_{23}^2 from the Direct and Indirect Fourier Processing for the 10.37-mm-OD Detectors

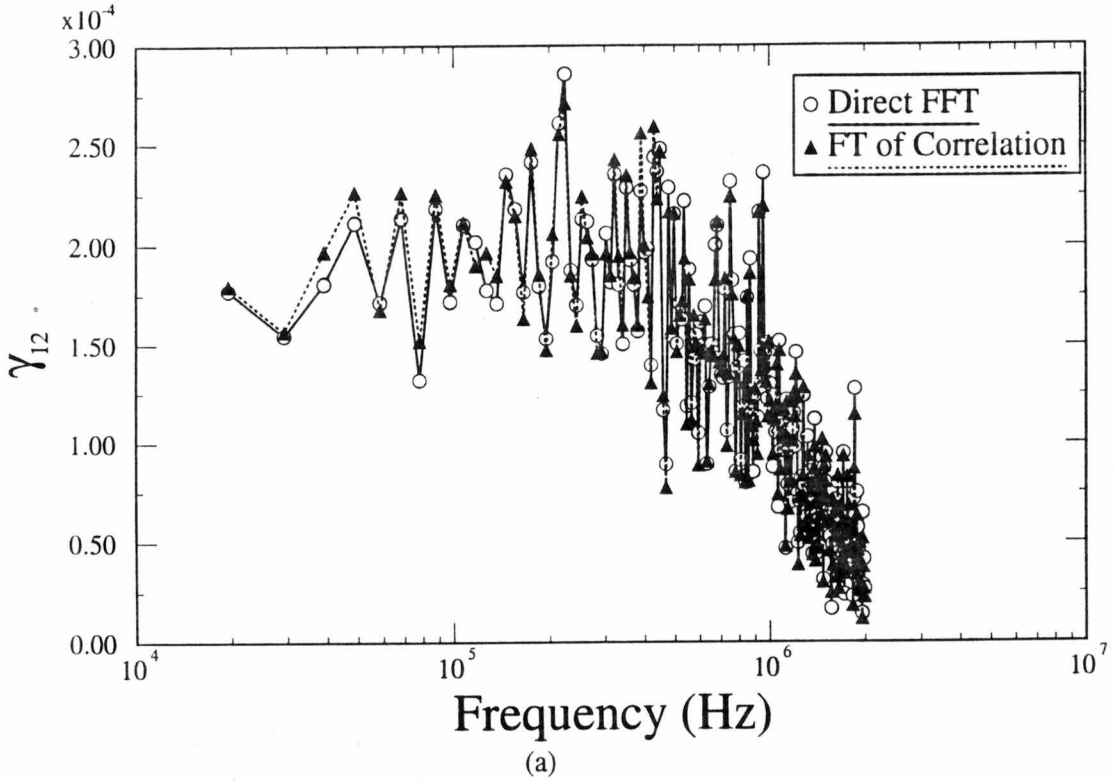

(a)

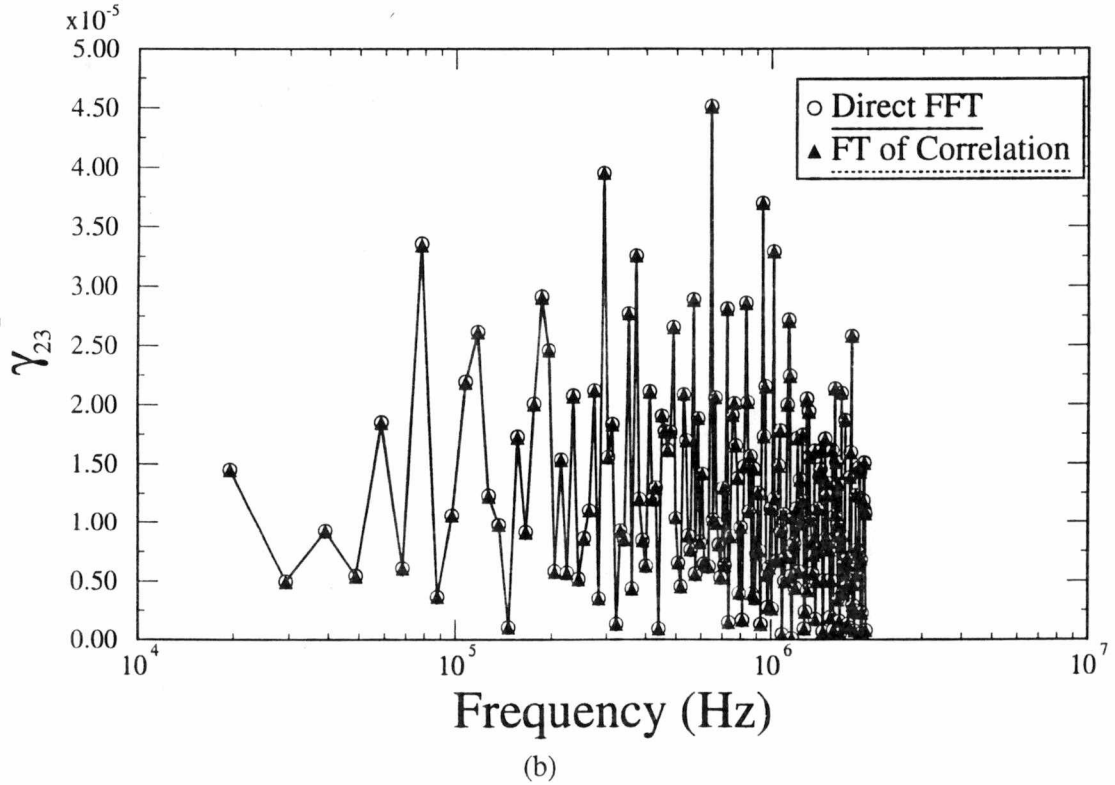

(b)

Figure F.4 Comparison of (a) γ_{12}^2 and (b) γ_{23}^2 from the Direct and Indirect Fourier Processing for the 4.234-mm-OD Detectors

VITA

Timothy Eugene Valentine was born in Knoxville, Tennessee, on September 26, 1969. He attended Gibbs High School and graduated in June 1987. In August 1987, he enrolled in The University of Tennessee, Knoxville. In February 1990, he married Jennifer Suzanne Mash. In May 1991, he received his Bachelor of Science degree in Nuclear Engineering from The University of Tennessee. In August 1992, he received his Master of Science degree in Nuclear Engineering from The University of Tennessee, Knoxville. After completing his Master of Science degree, he obtained a post graduate research fellowship at the Oak Ridge National Laboratory, where he worked on applications of neutron noise analysis techniques. In May 1995, he expects to receive a Doctor of Philosophy degree in Nuclear Engineering.